Decomposition of Phosphine-Stabilized Metathesis Catalysts by Lewis Donors

William McClennan

Thesis submitted to the
Faculty of Graduate and Postdoctoral Studies
University of Ottawa
in partial fulfillment of the requirements for the degree of

Master of Science

Center for Catalysis Research and Innovation
Department of Chemistry and Biomolecular Science
Ottawa-Carleton Chemistry Institute
Faculty of Science
University of Ottawa

Table of contents

List of figures

Chapter 1

Chapter 3

Chapter 4

List of Schemes

Chapter 1

Chapter 3

List of tables

Abstract

Olefin metathesis has had tremendous impact on synthetic approaches to the formation of new carbon-carbon bonds. Heterogeneous metathesis catalysts have been used in industry for decades, to effect redistribution of olefin chain lengths in petrochemicals processing. Only recently, however, has olefin metathesis emerged in pharmaceutical and specialty chemical manufacturing. The nearly 20-year gap between the discovery of easily-handled ruthenium catalysts and industrial implementation in these sectors is a result of many factors. One key contributor is the limited understanding of decomposition mechanisms that limit the reliability of olefin metathesis. Poor catalyst selectivities and yields remain a challenge for industrial uptake of olefin metathesis. Much academic effort focuses on designing methods and new catalysts for catalyst separation and reuse. Exploration of catalyst decomposition pathways has seen much less study in comparison. The limited recognition of decomposition as a problem in academia is undoubtedly due to the tendency to use high catalyst loadings, which mask catalyst decomposition problems. The catalyst loadings commonly reported in academia need to be decreased by a factor of 100–1000 for industrial viability in many processes.

This thesis explores the decomposition of metathesis catalysts bearing a phosphine ligand. Such Grubbs-type catalysts, particularly second-generation versions containing an *N*-heterocyclic carbene ligand, are the most widely used metathesis catalysts in current use. This study follows up on an earlier discovery from the Fogg group, which showed that pyridine and amine donors drastically accelerate decomposition of the Grubbs catalysts. For the first-generation Grubbs catalyst, decomposition of the resting-state methylidene complex $RuCl_2(PCy_3)_2(=CH_2)$ **Ru-6** was shown to proceed via nucleophilic attack of PCy_3 on the $Ru=CH_2$ bond, forming a σ-alkyl complex that was intercepted and characterized crystallographically. Further reaction led to liberation of the methyl phosphonium salt $[MePCy_3]Cl$ **2**. Under the same conditions, the second-generation methylidene complex **Ru-4a** decomposes rapidly without any detectable σ-alkyl intermediate.

In this thesis, decomposition of the important second-generation catalysts is shown to proceed via the methylidene-abstraction pathway. These studies centered on the methylidene complex $RuCl_2(NHC)(PCy_3)(=CH_2)$, where the NHC ligand is H_2IMes (**Ru-4a**) or IMes (**Ru-4b**). The short lifetime of the σ-alkyl complex was tentatively attributed to the ease of activation of a C–H bond on the NHC ligand (specifically, those on the mesityl *o*-methyl group). This intermediate could not be observed for **Ru-4a**, but could be observed for the IMes system **Ru-4b**. This is suggested to reflect the slower rotation of the H_2IMes ligand about the Ru–NHC bond, which promotes C–H activation.

Also examined is the ability of other Lewis donors to trigger this methylidene abstraction pathway during catalysis. Lewis donors are shown to greatly accelerate decomposition of a wide range of phosphine-stabilized metathesis catalysts. Remarkably, even weak donors such as water, ethers, alcohols, and nitriles (i.e. functionalities that are widespread among contaminants, functional groups, and "green solvents") are shown to promote this pathway. Phosphine-stabilized catalysts are generally regarded as more robust towards such donor functionalities, and the detrimental impact of such weak donors has gone widely unrecognized. These findings have profound implications for catalyst choice and use.

Finally, a deuterium-labelling study was undertaken, in which the mesityl substituents on the NHC ligand were fully deuterated, to confirm that the proton in the phosphonium salt **2** indeed originates in the mesityl methyl group. Of note, the energies of the PCy_3 dissociation and C–H activation steps were found to be closely similar. This was unexpected, given prior evidence that PCy_3 loss is rate-determining in the **Ru-2** precatalysts, and the much stronger Ru–PCy_3 bonding known to be present in the methylidene complexes. This finding highlights the need to impede C-H activation for phosphine-stabilized metathesis catalysts. More broadly, it underscores the risks inherent in the use of phosphine-stabilized catalysts, or indeed of catalysts that are stabilized by a donor group that can function as both a Lewis base, and a nucleophile.

Acknowledgements

To my supervisor, Deryn Fogg, I would like to thank you for all of the valuable training, expertise, and opportunities you have given to me. I would also like to thank you for the many tough, yet engaging scientific discussions and writing sessions we have been through. These last two years have allowed me to transition and grow into the scientist and person I am today. I would also like to sincerely thank my undergraduate supervisor Prof. Jason Masuda (Saint Mary's University) for giving me the opportunity to conduct research early on in my undergraduate studies. Your guidance and training has had a tremendous impact on my development as a graduate student and individual. Thank you Prof. Jason Clyburne and Prof. Robert Singer (Saint Mary's University) for all of the support you have given me.

I would like to thank the staff of the University of Ottawa NMR facility, Dr. Glenn Facey and Dr. Gang Ye, for all of their help in carrying out the work in this thesis.

To my current and past labmates, it has been a pleasure working with all of you. Justin, Emma, Carolyn, and Stephanie: thank you for all your support throughout my time in the Fogg lab. Adrian and Nikita, thank you for your friendship, and for the countless coffee runs.

To my parents: thank you for your endless love and support. I appreciate everything you have done for me, more than words can describe.

List of compounds

Organic and main group compounds

1a	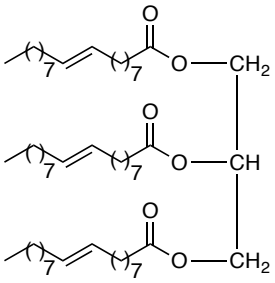	**1b**	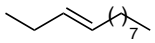
1c		**1d**	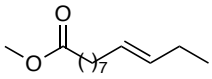
1e	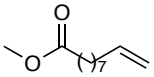	**2**	[MePCy$_3$]Cl
3	[MePPh$_3$]Cl	**4**	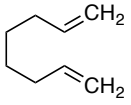
5	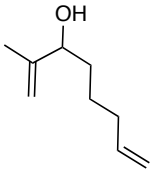	**6**	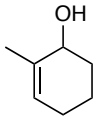
7	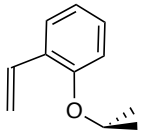	**8**	MeNH^{n}Bu
9	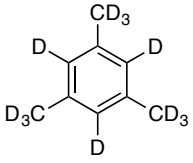	**10**	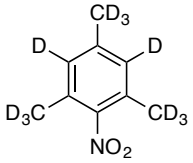
11	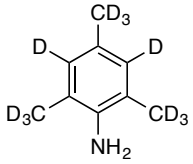	**12**	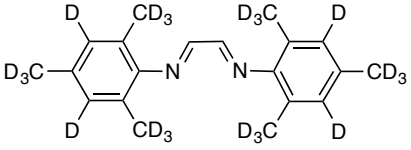
13	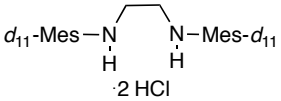	**14**	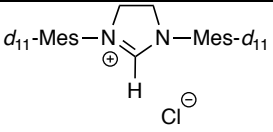

15	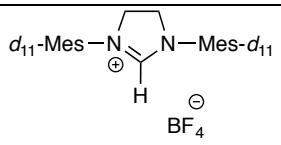	**16**	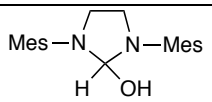
17	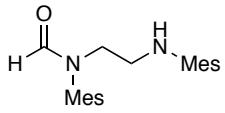	**18**	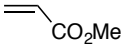
19	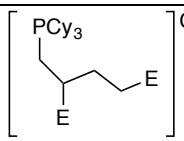	**20**	
***d*$_{22}$-H$_2$IMes**	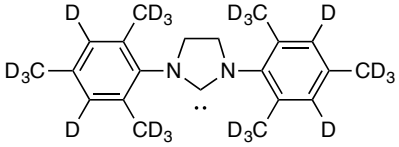	**H$_2$IMes**	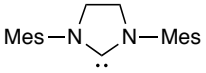
H$_2$IPr	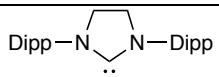	**H$_2$ITol**	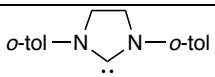
IPr	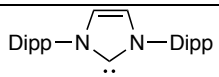	**IMes**	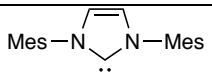
DDM	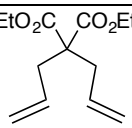	**TMB**	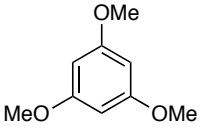

Metal complexes

Ta-1	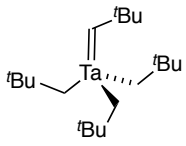	**W-1**	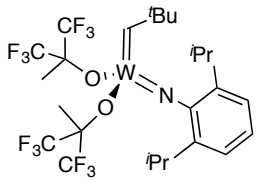
Mo-1	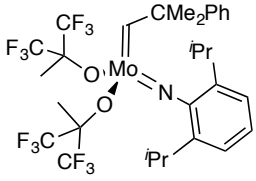	**Ru-1**	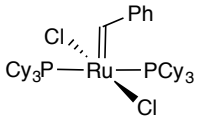
Ru-2	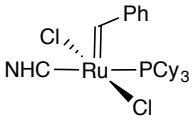	**Ru-2a**	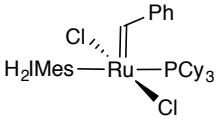

Ru-2b	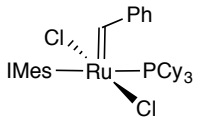	**Ru-2c**	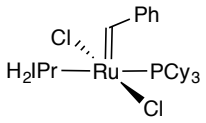
Ru-2d	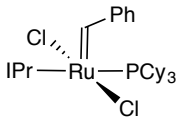	**Ru-2e**	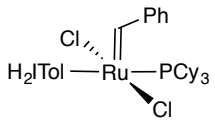
Ru-2f	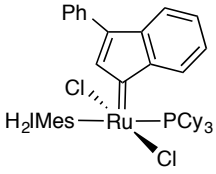	**Ru-2g**	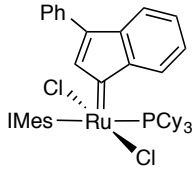
Ru-3	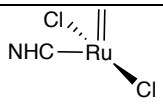	**Ru-4**	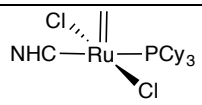
Ru-4a	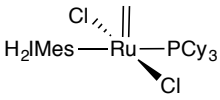	**Ru-4b**	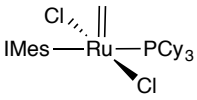
Ru-5	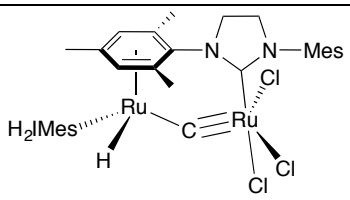	**Ru-6**	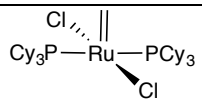
Ru-7	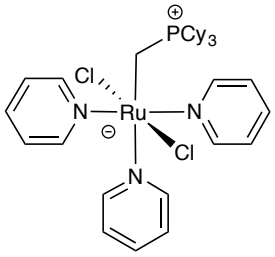	**Ru-8**	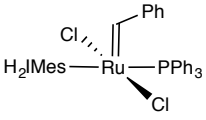
Ru-9	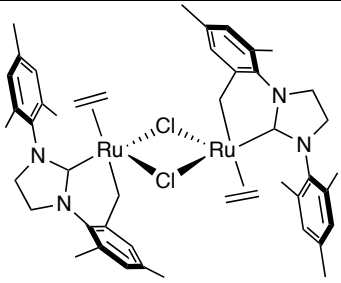	**Ru-10**	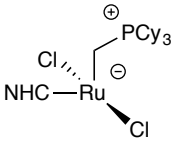
Ru-11a	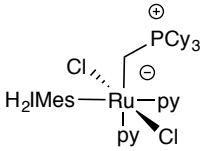	**Ru-11b**	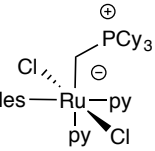

Ru-12	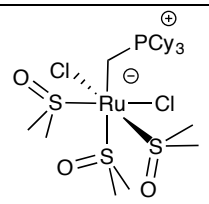	**Ru-13**	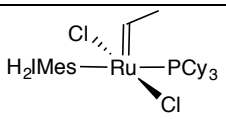
Ru-14	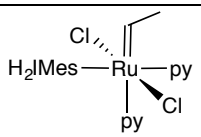	**Ru-15**	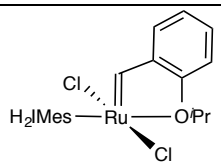
Ru-16	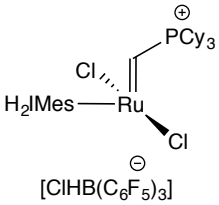	**Ru-17**	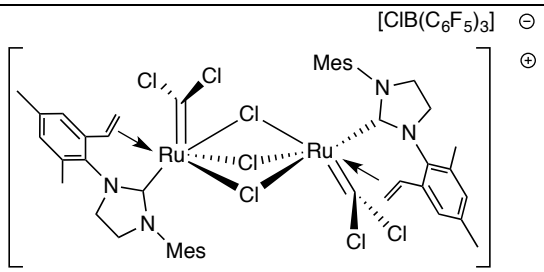
Ru-18	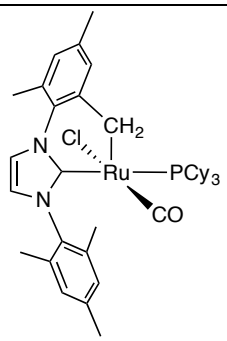	**Ru-19a**	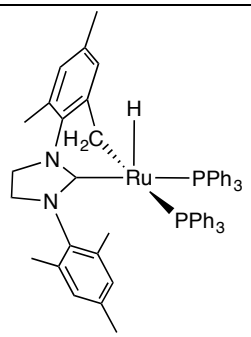
Ru-19b	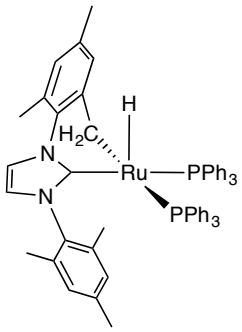	**Ru-20**	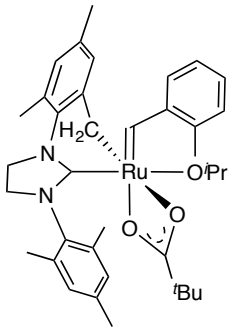

Ru-21	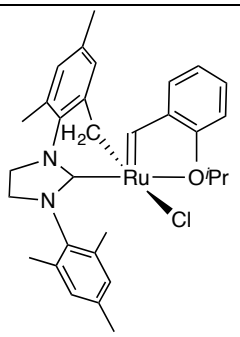		

Abbreviations

ADMET	Acyclic diene metathesis
ATR-IR	Attenuated total reflectance infrared spectroscopy
BI	Boehringer Ingelheim
CM	Cross-metathesis
COSY	Correlation spectroscopy
CT	Charge-transfer
DAD	Donor-accelerated decomposition
DBU	1,8-Diazabicycloundec-7-ene
DDM	Diethyl diallylmalonate
Dipp	2,6-Diisopropylphenyl
DMSO	Dimethyl sulfoxide
Equiv	Equivalent
EtOH	Ethanol
FID	Flame ionization detector
GC	Gas chromatography
GSK	GlaxoSmithKline
H_2IMes	1,3-Bis-(2,4,6-trimethylphenyl)imidazolin-2-ylidene
H_2IPr	1,3-Bis-(2,6-diisopropylphenyl)imidazolin-2-ylidene
H_2ITol	1,3-Bis-(2,6-*o*-methylphenyl)imidazolin-2-ylidene
HCV	Hepatitis C virus
HMQC	Heteronuclear multiple quantum coherence

IMes	1,3-Bis-(2,4,6-trimethylphenyl)imidazol-2-ylidene
IPr	1,3-Bis-(2,6-diisopropylphenyl)imidazol-2-ylidene
KHMDS	Potassium bis(trimethylsilyl)amide
KIE	Kinetic isotope effect
KTp	Hydrotris(1-pyrazolyl)borate
MALDI-TOF	Matrix-assisted laser desorption/ionization time-of-flight
MCB	Metallacyclobutane
MeCN	Acetonirile
MeOH	Methanol
Mes	2,4,6-trimethylphenyl
NHC	*N*-heterocyclic carbene
NMR	Nuclear magnetic resonance
$O=C(NMe_2)_2$	Tetramethyl urea
$O=P(NMe_2)_3$	Hexamethylphosphoramide
Py	Pyridine
RCM	Ring-closing metathesis
ROMP	Ring-opening metathesis polymerization
RT	Room temperature
SHOP	Shell higher olefin process
TCE	Tetrachloroethane
THF	Tetrahydrofuran
TLC	Thin-layer chromatography
TMB	1,3,5-Trimethoxybenzene
TMS	Tetramethylsilane
TON	Turnover number

Chapter 1. Introduction

1.1 Catalysis

A key objective in chemical synthesis is designing processes that minimize use and generation of hazardous substances.[1] Further, a sustainable society needs to meet the needs of the current generation without sacrificing the ability to meet needs of future generations.[1] Increasing pressure on energy and natural resources have driven significant advances in catalytic chemical transformations.[2] A catalyst is a substance that facilitates a chemical reaction without being consumed.[1] That is, it can "turn over" multiple times generating more product each time. Catalysis enables essential chemical transformations while reducing the need for stoichiometric reagents that lead to higher amounts of hazardous waste.[3,4] The impact of catalysis in advancing sustainable chemical transformations has been recognized with 15 Nobel Prizes since 1901.[5]

Advances in the assembly of carbon-carbon bond formation and in homogeneous catalysis have been recognized with multiple Nobel Prize awards over the past 15 years. William Knowles,[6] Ryoji Noyori,[7] and Barry Sharpless[8] were awarded the Nobel Prize in 2001 for their work on asymmetric catalysis; Yves Chauvin,[9] Robert Grubbs,[10] and Richard Schrock[11] for their development of olefin metathesis (Figure 1.1); Richard Heck, Ei-ichi Negishi,[12] and Akira Suzuki[13] for their development of Pd-catalyzed cross-coupling reactions. These awards underscore the impact of catalytic carbon-carbon bond formation in fundamental science, and their potential in chemical manufacturing.

References begin on page 18

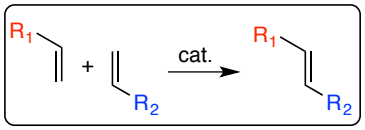

Chauvin, Grubbs, Schrock

Figure 1.1 Simplified representation of the olefin metathesis reaction.

This thesis focuses on catalyst decomposition pathways in olefin metathesis. Academic uptake of olefin metathesis expanded tremendously as a result of Grubbs' discovery of readily handled ruthenium catalysts, coupled with the discovery and synthetic potential of ring-closing metathesis. Uptake of these catalysts in industrial processes (specifically, pharmaceutical and specialty chemical manufacturing) is just beginning. Outlined below are some of the major advances to date, as well as some key challenges.

1.2 Olefin metathesis

1.2.1 Olefin metathesis: early days and development

Olefin metathesis has transformed how synthetic chemists think about constructing carbon-carbon double bonds. The reaction is used to synthesize molecular targets, via ring-closing metathesis (RCM) and cross-metathesis (CM), as well as polymer materials, via ring-opening metathesis polymerization (ROMP) and acyclic diene metathesis (ADMET) (Figure 1.2).

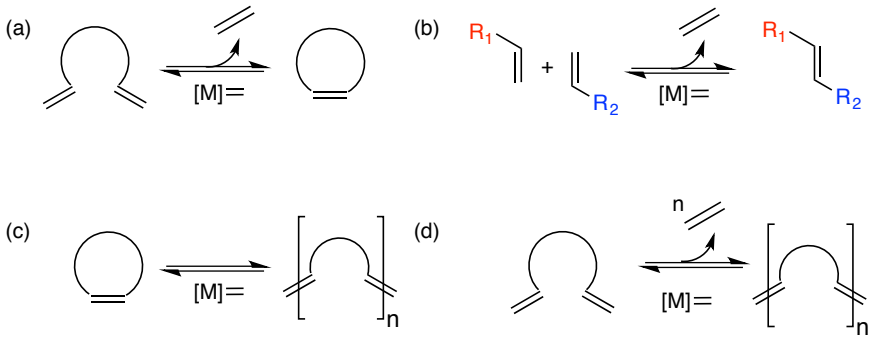

Figure 1.2 Olefin metathesis reactions. (a) Ring-closing metathesis. (b) Cross-metathesis. (c) Ring-opening metathesis polymerization. (d) Acyclic diene metathesis.

References begin on page 18

Olefin metathesis has been known for decades, with the first reports dating back to the 1950s. An unexpected observation during oligomerization of ethylene by Ziegler, showed the formation of 1-butene instead of the expected long-chain hydrocarbons.[10] DuPont scientists first described a process in a patent for ROMP of olefin norbornene catalyzed by titanium tetrachloride ($TiCl_4$).[14] These were two of the first-reported instances of olefin metathesis. Two major technological advances, the largest-scale metathesis processes to date, were achieved by scientists at Royal Dutch Shell and Phillips Petroleum in the 1960s.[15-17] In the Shell Higher Olefin Process (SHOP), metathesis is an enabling step in the production of linear α-olefins in the C12-C18 chain length regime.[16,17] Such "detergent range" olefins are highly desirable for detergents, fatty esters, lubricants, etc. The SHOP process involves successive steps of ethylene oligomerization, isomerization and metathesis. The metathesis catalyst is supported molybdate. The Phillips Triolefin Process, in contrast, used a heterogeneous WO_3/SiO_2 catalyst to convert propylene to ethylene and 2-butene.[15] It is now run in reverse, to take advantage of the higher price of propylene, and is known as Olefins Conversion Technology.

At the end of the 1960's, the mechanism of the metathesis reaction was very mysterious. Various mechanistic proposals had appeared (Figure 1.3), but none matched the results of all metathesis experiments.[9]

References begin on page 18

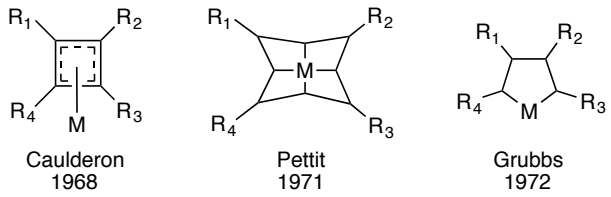

Figure 1.3 Representative examples of proposed olefin metathesis intermediates.

In a seminal 1971 study, Chauvin proposed that metathesis involves metal alkylidene and metallacyclobutene **MCB** intermediates, operating via [2+2] cycloaddition and cycloreversion steps (Scheme 1.1).[18] Key evidence was the observation of a mixture of C9, C10, and C11 products from the cross metathesis of cyclopentene and 2-pentene in a 1:2:1 ratio. Subsequent labelling studies provided further support for the Chauvin mechanism.[19-21]

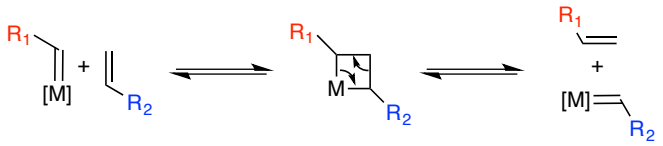

Scheme 1.1 The Chauvin mechanism showing [2+2] cycloaddition and cycloreversion for olefin metathesis.

The identification of a metal alkylidene and **MCB** intermediate led to an intense research effort directed at the synthesis of well-defined metathesis catalysts (Figure 1.4a). Pioneering work by Schrock, reported in 1974, described the synthesis of the groundbreaking tantalum alkylidene catalyst **Ta-1**,[22] followed shortly thereafter by the tungsten **W-1** and molybdenum **Mo-1** catalysts.[23-25] All of these complexes were shown to be metathesis-active, important support for the Chauvin mechanism. Despite the major opportunities revealed by these catalysts, they were not embraced in synthetic organic practice for two reasons. Most fundamentally, the synthetic opportunities of RCM were little recognized until the early 1990s. Related to this were the difficulties in handling

References begin on page 18

these catalysts. Specifically, they are readily decomposed by air, moisture, and protic functional groups, because of their high oxophilicity and susceptibility to protonolysis.[26] Grubbs' development of more robust, easily handled ruthenium metathesis catalysts was the breakthrough that put metathesis into the hands of organic chemists (Figure 1.4b).[27-30]

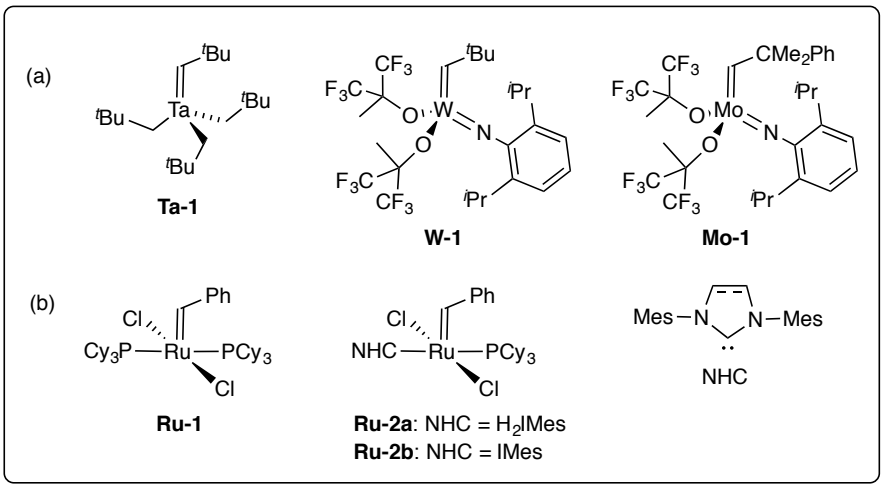

Figure 1.4 Key developments in the synthesis of metathesis catalysts containing (a) Group 5 and 6. (b) Group 8 transition metals.

In 2005, Boehringer Ingelheim Pharma (BI) began a pilot program directed at scaling up the synthesis of a potential antiviral drug, the hepatitis C virus (HCV) protease inhibitor Ciluprevir.[31] A key step involved the RCM assembly of a 15-membered macrocycle (Scheme 1.2). This was the first large-scale implementation of RCM. The key macrocyclization step was performed on 20 kg scale, to produce a total of 400 kg of the macrocyclic precursor to Ciluprevir. Refinements continued over the next decade to improve the macrocyclization step.[32,33] While Ciluprevir ultimately failed in Phase I clinical trials due to its cardiac toxicity,[34] this campaign demonstrated the feasibility of using RCM macrocyclization to assemble complex, biologically active molecules on large scale.

References begin on page 18

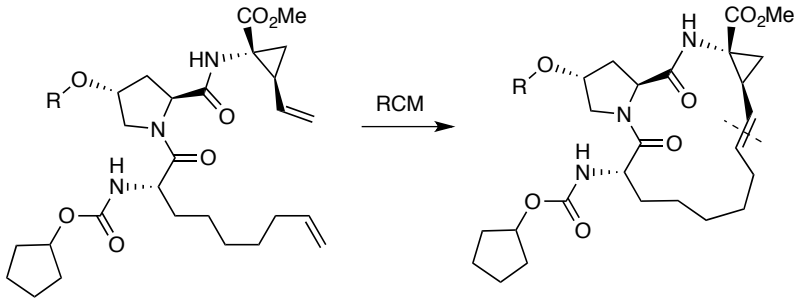

Scheme 1.2 Macrocyclization step in Boehringer-Ingelheim synthesis of Ciluprevir.

Since then, other examples of RCM in process chemistry directed at macrocyclic drug candidates have been reported. Simeprevir, a HCV protease inhibitor developed by Janssen Pharma (Figure 1.5), commenced production in 2014.[35] Shortly after, AbbVie and Merck reported the use of RCM in HCV drug candidates Paritaprevir[36] and Vaniprevir[37] respectively.

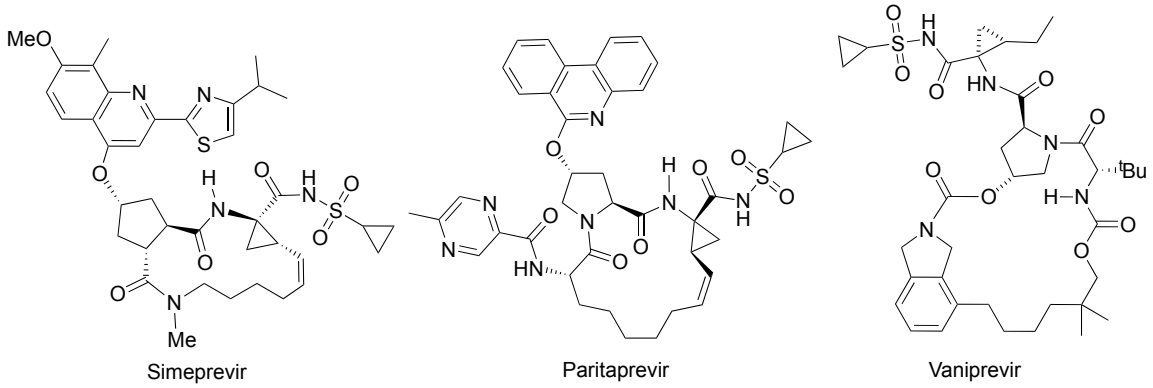

Figure 1.5 Approved HCV drugs prepared via RCM.

Use of molecular metathesis catalysts for commercial CM processes is also recent. The first report of implementation in industry was in 2013 by Elevance Renewable Sciences. In this process, renewable triglycerides **1a** from vegetable oils are subjected to sequential CM and transesterification (Scheme 1.3). The products formed **1b-e** have potential applications as lubricants, synthetic oils, fuels, waxes, and precursors to other specialty chemicals.[38-40]

References begin on page 18

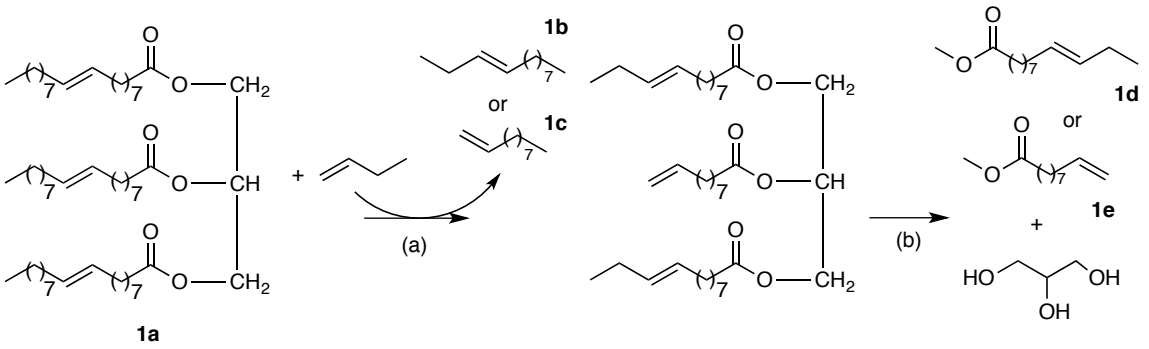

Scheme 1.3 Conversion of triglycerides by sequential (a) CM and (b) transesterification to specialty chemicals.

Within the context of olefin metathesis in industry, the general consensus is that ruthenium catalysts are highly robust and tolerant towards functional groups and impurities.[41] Countering this, the authors of the BI study showed that morpholine (a contaminant in the reaction solvent) had a deleterious impact on metathesis. They also needed to rigorously degas and dry solvents to achieve maximum yields. Thus, implementation into large-scale synthesis highlights challenges associated with catalyst deactivation, These problems are masked in academic practice by the use of high catalyst loadings, which have led to the belief that ruthenium catalysts are broadly functional-group tolerant. The issue of impurities and deactivation pathways will be discussed below following an overview of ruthenium catalyzed olefin metathesis.

1.2.2 Olefin metathesis using the Grubbs catalysts: catalytic cycle

The catalytic cycle in metathesis by phosphine-stabilized **Ru-2** begins with displacement of the phosphine ligand via a dissociative pathway (Scheme 1.4).[42] Certain phosphine-free catalysts, in contrast, initiate via an associative pathway.[43] Loss of the phosphine ligand generates the four-coordinate active species **Ru-3**. Reaction with olefin results in an **MCB** intermediate, which on retro-addition enables loss of the benzylidene moiety,

References begin on page 18

generating the key methylidene intermediate **Ru-3**. The latter can react with olefin to continue metathesis. However, free phosphine can compete with olefin for binding, thus generating the resting-state species **Ru-4**. This off-cycle species is much slower to re-enter the catalytic cycle owing to the inverse trans effect exerted by the *N*-heterocyclic carbene (NHC) ligand,[44] as well as the very limited steric pressure exerted by the methylidene moiety.[45] It is also much more prone to catalyst deactivation, as discussed below.

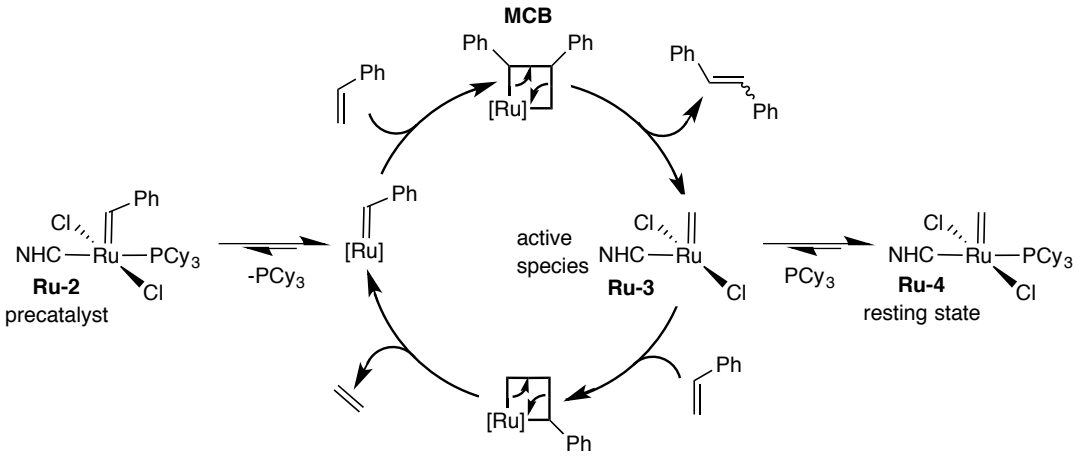

Scheme 1.4 Catalytic cycle for productive metathesis illustrated by CM of a terminal alkene with phosphine-stabilized catalysts Ru-2.

1.2.3 Phosphine-stabilized Grubbs catalysts

There are two dominant structures for ruthenium metathesis catalysts. Grubbs-type catalysts bear a phosphine ligand, while Hoveyda-type catalysts are phosphine-free. The latter complexes contain a chelating *o*-isopropxy benzylidene (Figure 1.6). The Grubbs catalysts dominate use in synthetic organic chemistry. This thesis focuses on their decomposition pathways, and the Hoveyda-type catalysts are thus not treated in any detail in the discussion below.

References begin on page 18

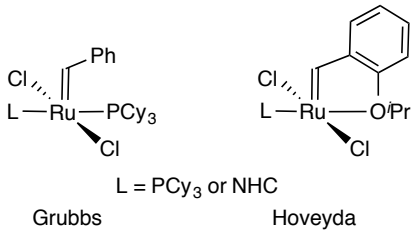

Figure 1.6 Structures of the most commonly used ruthenium metathesis catalysts.

The first-generation Grubbs catalyst **Ru-1** was first prepared in 1996.[27] This five-coordinate complex bears two tricyclohexylphosphine (PCy_3) ligands. In the second-generation Grubbs catalyst **Ru-2a**, reported in 1999,[28] one of the PCy_3 ligands is replaced by an NHC, resulting in much higher activity. Grubbs originally proposed that this is due to strong σ-donation from the NHC and consequent labilizing of the trans-PCy_3 ligand via the trans effect.[28,30,46-48] However, PCy_3 is in fact less labile in **Ru-2a** and its IMes analog **Ru-2b**, by 100 times and 640 times, respectively.[42] The higher activity of the second-generation catalysts is attributed to the higher "commitment" of the four-coordinate intermediate (i.e. its selectivity for reaction with olefins in preference to re-coordination of phosphine),[49] and strong σ-donation from the NHC ligand.[44]

While the NHC ligand confers high activity *within* the active cycle for metathesis, the much stronger Ru-PCy_3 binding in the second-generation systems impedes entry into the cycle. Yang, Truhlar and co-workers have proposed that alkylidene rotation contributes to the barrier to phosphine loss.[50] Dr. Justin Lummiss of this research group demonstrated that NHC binding greatly reinforces Ru-PCy_3 backbonding.[44] This accounts for the slower initiation of the precatalyst, and the even slower re-entry of the resting-state methylidene **Ru-4** into the catalytic cycle.[44] The difference in rate constants, normalized to **Ru-1**, is shown in Table 1.1.

References begin on page 18

Table 1.1 Rate constants for loss of PCy_3 from Grubbs precatalysts and the corresponding methylidene derivatives

System	k (s^{-1})	Lability vs. **Ru-1** (x times slower)
Ru=CHPh[42]		
Ru-1	9.6*	1
Ru-2a	0.13	148
Ru-2b	0.03	640
$Ru=CH_2$[44]		
Ru-4a	4.7×10^{-4}	41 000
Ru-4b	6.7×10^{-6}	287 000

*Values reported per coordinated PCy_3 ligand.

This inverse trans effect is enhanced for the unsaturated IMes ligand (consistent with the rate constants in Table 1.1) because its poor π-acceptor ability results in even stronger backbonding onto the PCy_3 ligand[44] (Figure 1.7).

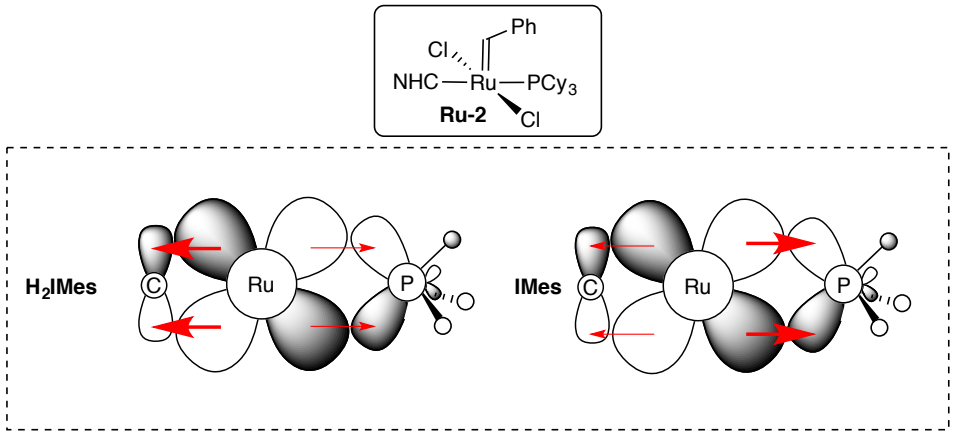

Figure 1.7 Inverse trans effect in second-generation Grubbs catalysts.

There has been much modification of the Grubbs catalysts, mainly of the NHC ligand. A recent review reported more than 400 ruthenium metathesis catalysts, with 46 being commercially available.[51] Despite this, **Ru-2a** remains the dominant catalyst choice.[51] Of

importance is the fact that many of these catalysts converge on the same methylidene resting state **Ru-4** (Figure 1.8). This is important because it implies that all of these catalysts will be vulnerable to the same deactivation pathways during catalysis.

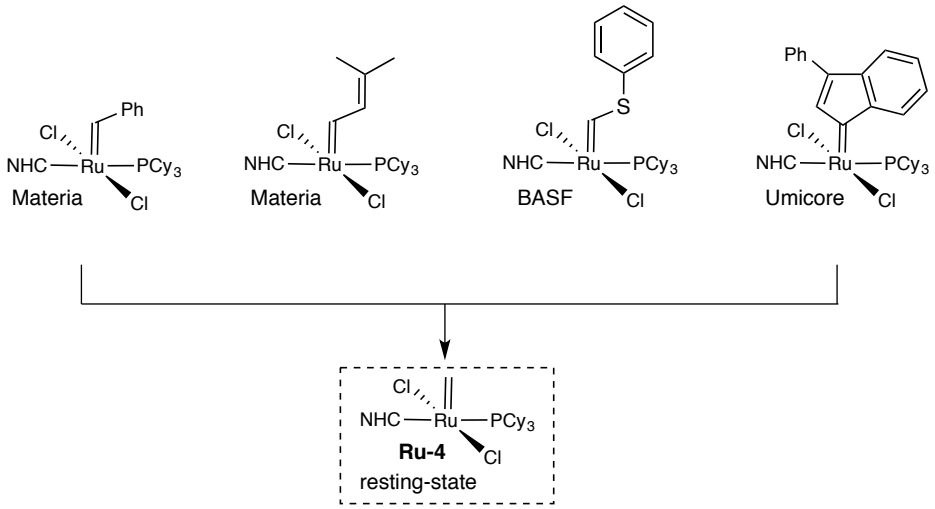

Figure 1.8 Metathesis catalysts that converge on methylidene Ru-4 as the resting state in metathesis of terminal olefins.

1.2.4 Impact of impurities on metathesis

Ruthenium metathesis catalysts are generally less stable toward impurities than reports from academia tend to suggest. Problems with impurities are revealed at low catalyst loadings. In a recent study with an in situ-generated Ru alkylidene, even organic halides were shown to be detrimental.[52] An economic necessity in industry is high turnover numbers (TONs) using technical-grade solvents. As noted above, Boehringer-Ingelheim scientists found that trace amounts of morpholine (<20 ppm) in the toluene solvent impaired reproducibility and led to undesired side reactions.[31] GlaxoSmithKline (GSK) reported similar issues during the synthesis of a cathepsin K inhibitor Relacatib, with residual base from prior steps and with secondary amines or ureas formed by undesired side reactions (Figure 1.9).[53]

References begin on page 18

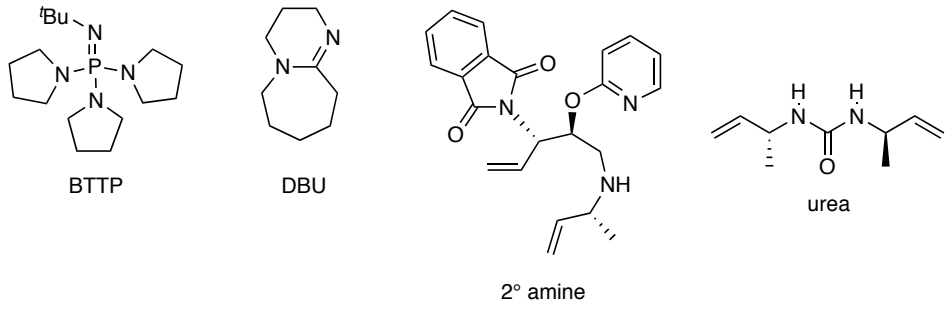

Figure 1.9 Impurities reported by GSK causing reproducibility issues in metathesis yields.

Various other impurities in industrial applications have also been reported to be detrimental towards reproducibility and metathesis yields. A recent review from our group reports examples of contaminants identified as detrimental to metathesis in industrial applications either as residues from prior steps or contaminants in solvents or feedstocks (Figure 1.10).[44] In most cases the reported impurities contain either a Brønsted or Lewis basic functionality.

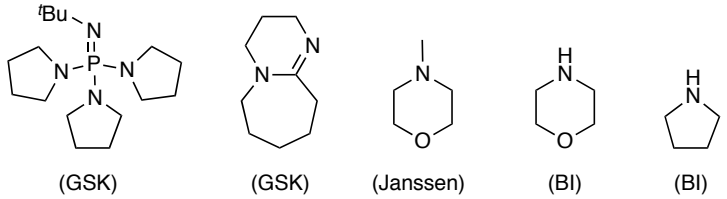

Figure 1.10 Selected contaminants identified as detrimental to metathesis in industry (See ref. 43 for a comprehensive list).

Of even greater significance is decomposition by water, a ubiquitous contaminant in organic solvents. While the Ru catalysts are widely viewed as water-tolerant, and have been used to effect metathesis in water,[54,55] such reactions involve facile RCM or ROMP reactions (typically of DDM or norbornenes, respectively), at high catalyst loadings. The limitations with respect to ROMP have been discussed.[56] In a recent study, Cazin[57] showed that added water was detrimental toward RCM yields in reactions promoted by commercially available phosphine-stabilized (**Ru-2a**, **Ru-2f)** as well as Hoveyda-type

catalysts. Within these studies, the mechanisms responsible for the deleterious impact on metathesis yields were not explored.

The foregoing highlights the importance of understanding catalyst decomposition by impurities, including water. This is often ignored in academic research, where the problem is masked by high catalyst loadings.

1.2.5 Decomposition of metathesis catalysts

Much research focuses on improving methods of catalyst separation and reuse with less emphasis on understanding catalyst deactivation pathways.[58] With industrial applications beginning to emerge for olefin metathesis, specifically in the pharmaceutical and specialty chemical sectors (as discussed above), increased understanding of deactivation pathways is of crucial importance.[59] There are several reports that describe decomposition of precatalysts by solvent,[31,60-62] adventitious oxygen,[63,64] or thermolysis.[47] Of more importance is focusing on the decomposition of species formed during catalysis since the precatalyst is lost after just a single turnover in the Grubbs system. This thesis is highly focused on decomposition of the resting-state methylidene, however pathways that decompose the **MCB** intermediate will also briefly be discussed.

Hong and Grubbs showed that thermolysis of the resting-state methylidene **Ru-4a** at 55 °C over 3 days resulted in the formation of a dinuclear ruthenium bridged dimer **Ru-5**.[65,66] Based on the observation of **Ru-5** (isolated in 46% yield) and the phosphonium salt [$MePCy_3$]Cl **2** (amounts not measured), the mechanism of Scheme 1.5 was proposed. Thus, nucleophilic attack by free PCy_3 ligand on **Ru-3a**, followed by liberation of a

phosphonium ylide and coupling of **Ru-4a** was suggested to yield **Ru-5**. The hydride **Ru-5** was suggested to be responsible for unwanted isomerization reported during catalysis. However, work by Dr. Carolyn Higman of this research group demonstrated that **Ru-5** is not kinetically competent to account for the rates and levels of isomerization seen during metathesis.[67] Finally, it should be noted that the decomposition of **Ru-4a** was carried out in the absence of substrate. The relevance of this chemistry to catalyst decomposition during metathesis is probably limited, given that it occurred over days, compared to a timescale of hours in metathesis.

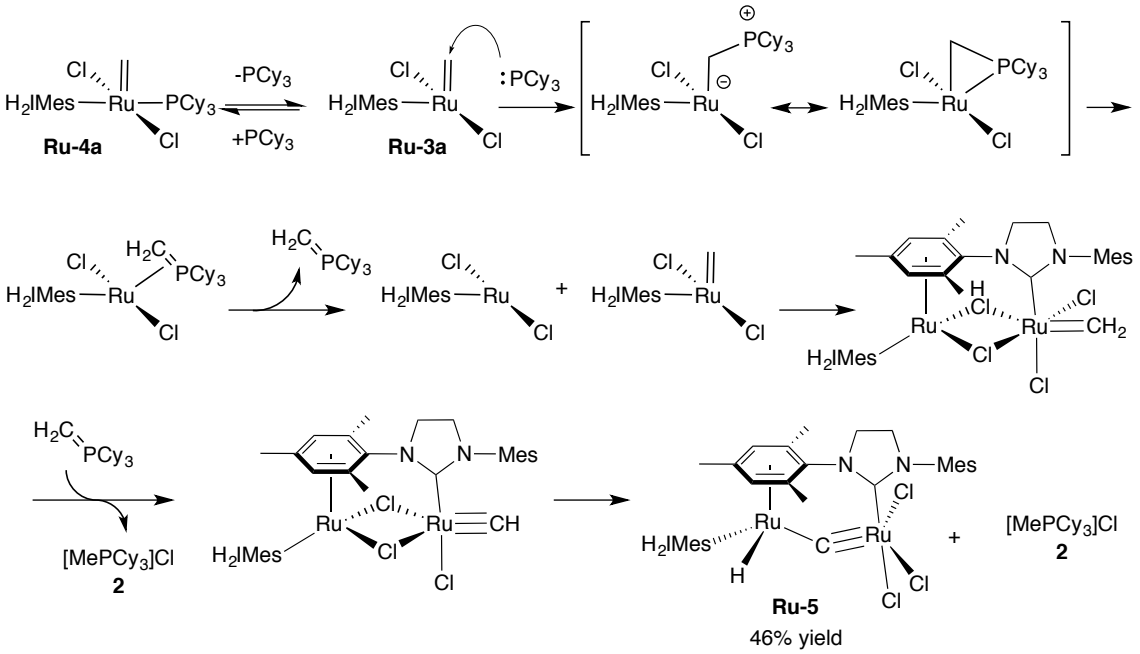

Scheme 1.5 Observation of Ru-5 and its proposed mechanism following thermolysis of Ru-4a over 3 days at 55 °C.

In our view, the key finding from this study was not the Ru product (which in our hands was formed in only 17%, accompanied by many unidentified by-products).[68] Much more important is the formation of the phosphonium salt. The latter is a marker for nucleophilic attack by the phosphine on the methylidene carbon, a reaction with multiple precedents.[69-71] Dr. Justin Lummiss of the Fogg group successfully intercepted the

otherwise transient σ-alkyl complex by moving to the first-generation system, and treating methylidene **Ru-6** with pyridine to displace *both* PCy3 groups (Scheme 1.6).[72] In the absence of an accessible, readily activated C-H bond,[64,73] the σ-alkyl species **Ru-7** was stable at RT and could be crystallographically analyzed. Upon full decomposition of **Ru-7**, liberation of phosphonium salt **2** was observed.

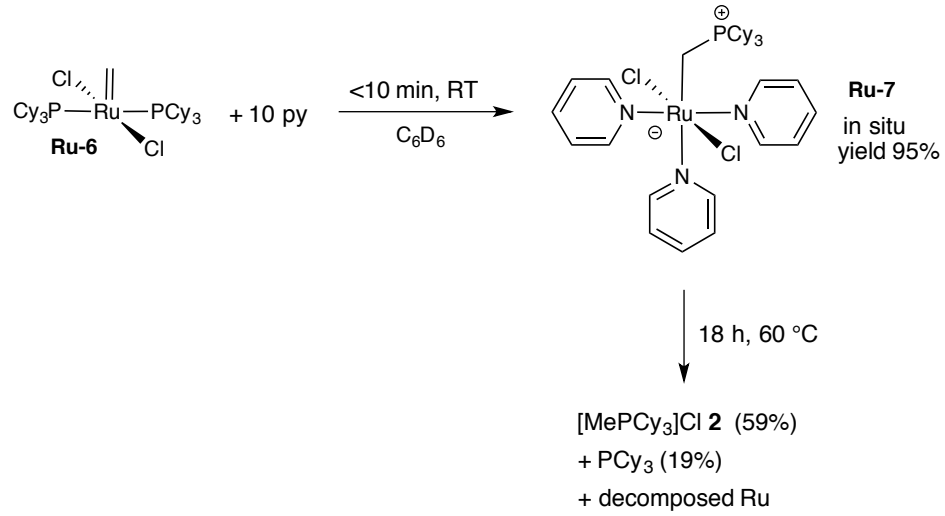

Scheme 1.6 Donor-accelerated deactivation of the first-generation Grubbs catalyst Ru-6 by pyridine.

Decomposition of the second-generation catalyst **Ru-4a** was originally reported to require days. Our group also showed that this process was significantly accelerated by pyridine and primary amines, causing full decomposition within minutes.[74,75] We termed this "donor-accelerated decomposition" and showed that liberation of phosphonium salt **2** is a key marker for this deactivation pathway.

Ethylene appears to promote an analogous pathway in decomposition of the PPh_3 complex **Ru-8**.[66] Hong and Grubbs reported that decomposition of **Ru-8** under ethylene liberated the phosphonium salt [$MePPh_3$]Cl **3**, and a C-H activated ruthenium dimer **Ru-9** (Scheme 1.7). However this was reported to occur over 5 days at room temperature.

References begin on page 18

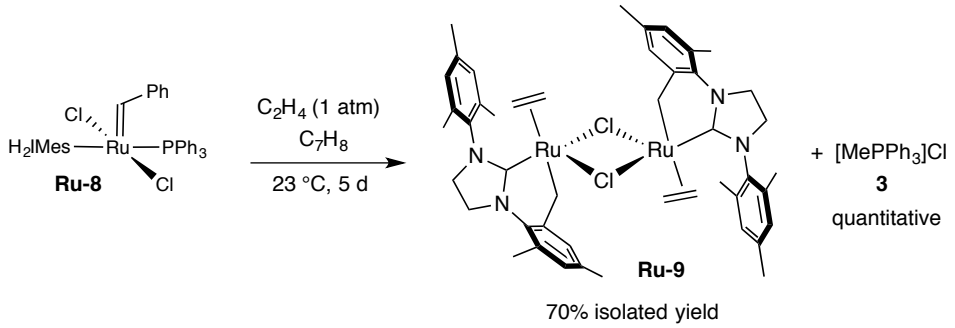

Scheme 1.7 Decomposition of in situ formed methylidene species from Ru-8 by ethylene.

The **MCB** intermediate formed during metathesis has also gained attention in deactivation studies. A 2005 report by van Rensberg and coworkers at Sasol reported decomposition of **Ru-2a** under ethylene to yield primarily propylene and unidentified ruthenium products.[76] This pathway was supported both computationally and experimentally. The proposed mechanism involved β-hydride transfer from the **MCB** intermediate, followed by reductive elimination of propylene (Scheme 1.8) Approximately 40% of **Ru-2a** was decomposed after 16 h °C at 40 °C. This is faster than decomposition in the absence of ethylene (**Ru-2a** has a half-life of 63 h at 40 °C)[44], although much slower than donor-accelerated decomposition. The observation of phosphonium salt was not reported.

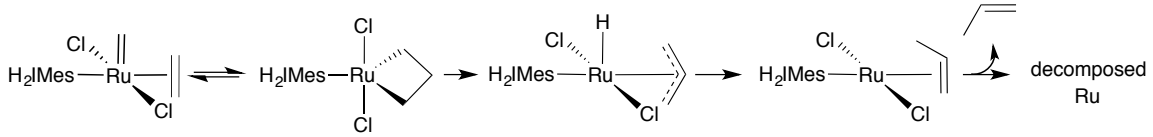

Scheme 1.8 Decomposition of MCB by β-H transfer.

Work by Dr. Ben Ireland and Ms. Gwendolyn Bailey within our own group has suggested that the negative impact of amines[77] and electron-deficient olefins[78] on metathesis productivity is due to attack on the **MCB**. In the presence of amines, decomposition of the **MCB** was proposed to occur by deprotonation of β-hydrogens on the **MCB** (Scheme

References begin on page 18

1.9). The basis for this suggestion was the observation of organic products containing the three carbons from the **MCB** ring. Given the low acidity of the **MCB** protons, however, the *o*-mesityl substituents on the NHC may offer a plausible alternative proton source.

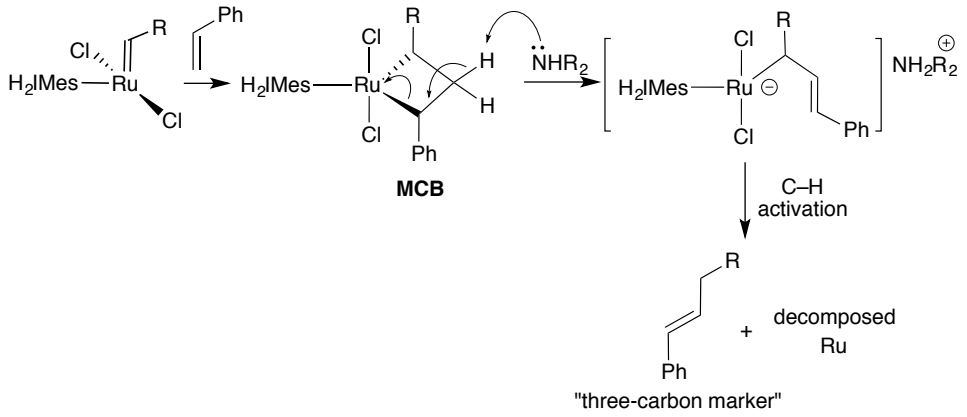

Scheme 1.9 Proposed pathway for deactivation of the MCB intermediate by amines.

The evidence for **MCB** deprotonation during acrylate metathesis is more unequivocal. In particular, isotopic labelling studies showed both negative evidence for NHC deprotonation, and positive evidence for deprotonation of the ester-functionalized **MCB**. In this case, however, the geminal **MCB** proton is substantially more acidic.

1.3 Scope of thesis work

Despite the transformative impact of olefin metathesis in organic synthesis, and the emergence of industrial applications in pharmaceutical manufacturing, product selectivities and isolated yields are adversely affected by catalyst decomposition. Within metathesis, loss of the alkylidene is typically irreversible which means complete loss of catalytic activity. Therefore, understanding deactivation pathways is critical and holds great value for catalyst redesign and in increasing overall productivity.

Uptake of the molecular metathesis catalysts in industry has been limited in part by their unreliability. This in turn can be seen as a function of our limited understanding of pathways by which ruthenium catalysts decompose. While the ruthenium catalysts are

References begin on page 18

widely viewed in academia as being typically relatively stable, findings from industry have reported that minor amounts of impurities result in lower catalyst productivity. The origin of decomposition for phosphine-stabilized catalysts is examined in this thesis. Chapter 2 presents all experimental details. Chapter 3 examines the scope of the donor-accelerated decomposition pathway described above. The impact of donors commonly present as impurities or solvents is examined with a range of phosphine-stabilized metathesis catalysts. The impact of these donors on catalyst productivity is examined, as well as potential ways to avoid accelerated decomposition in the presence of donors. Chapter 4 discusses the synthesis of an isotopologue of **Ru-4a** in which the mesityl groups are fully deuterated. This labelled catalyst is used to examine donor-accelerated decomposition to identify the origin of the proton that enables loss of the σ-alkyl ligand. Finally, Chapter 5 highlights the key advances and contributions of this thesis, and includes suggestions for future work.

1.4 References

(1) Rothenberg, G., *Catalysis*. Wiley-VCH: Weinheim, 2008.
(2) Federsel, H.-J. *Green Chem.* **2013**, *15*, 3105–3115.
(3) Sheldon, R. A., *Green Chemistry and Catalysis*. Wiley-VCH: Chichester, 2007.
(4) Anastas, P.; Eghbali, N. *Chem. Soc. Rev.* **2010**, *39*, 301–312.
(5) Thayer, A. M. *Chem. Eng. News,* **2013**, *91*, 68.
(6) Knowles, W. S. *Angew. Chem., Int. Ed.* **2002**, *41*, 1999–2007.
(7) Noyori, R. *Angew. Chem. Int. Ed.* **2002**, *41*, 2008–2022.
(8) Sharpless, K. B. *Angew. Chem., Int. Ed.* **2002**, *41*, 2024–2032.
(9) Chauvin, Y. *Angew. Chem. Int. Ed.* **2006**, *45*, 3741–3747.
(10) Grubbs, R. H. *Angew. Chem. Int. Ed.* **2006**, *45*, 3760–3765.
(11) Schrock, R. R.; *Angew. Chem.* **2006,** 3832-3844; *Angew. Chem. Int. Ed.* **2006**, *45*, 3748–3759.
(12) Negishi, E.-i. *Angew. Chem., Int. Ed.* **2011**, *50*, 6738–6764.
(13) Suzuki, A. *Angew. Chem., Int. Ed.* **2011**, *50*, 6722–6737.
(14) Anderson, A. W.; Merckling, N. G. Polymeric bicyclo[2.2.1]hept-2-ene. U.S. Patent No. 2721189, 1955.
(15) Banks, R. L.; Bailey, G. C. *Ind. Eng. Chem. Prod. Res. Dev.* **1964**, *3*, 170–173.
(16) Mol, J. C. *J. Mol. Catal. A* **2004**, *213*, 39–45.

(17) Keim, W. *Angew. Chem., Int. Ed.* **2013**, *52*, 12492–12496.
(18) Hérisson, J. L.; Chauvin, Y. *Makromol. Chem.* **1971**, *141*, 161–176.
(19) Katz, T. J.; McGinnis, J. *J. Am. Chem. Soc.* **1975**, *97*, 1592–1594.
(20) McGinnis, J.; Katz, T. J.; Hurwitz, S. *J. Am. Chem. Soc.* **1976**, *98*, 605-606.
(21) Grubbs, R. H.; Burk, P. L.; Carr, D. D. *J. Am. Chem. Soc.* **1975**, *97*, 3265-3267.
(22) Schrock, R. R. *J. Am. Chem. Soc.* **1974**, *96*, 6796–6797.
(23) Schrock, R. R.; DePue, R. T.; Feldman, J.; Schaverien, C. J.; Dewan, J. C.; Liu, A. H. *J. Am. Chem. Soc.* **1988**, *110*, 1423–1435.
(24) Schrock, R. R.; Murdzek, J. S.; Bazan, G. C.; Robbins, J.; DiMare, M.; O'Regan, M. *J. Am. Chem. Soc.* **1990**, *112*, 3875–3886.
(25) Fox, H. H.; Lee, J. K.; Park, L. Y.; Schrock, R. R. *Organometallics* **1993**, *12*, 759–768.
(26) Schrock, R. R. *Chem. Rev.* **2009**, *109*, 3211–3226.
(27) Schwab, P.; Grubbs, R. H.; Ziller, J. W. *J. Am. Chem. Soc.* **1996**, *118*, 100–110.
(28) Scholl, M.; Ding, S.; Lee, C. W.; Grubbs, R. H. *Org. Lett.* **1999**, *1*, 953–956.
(29) Nguyen, S. T.; Grubbs, R. H.; Ziller, J. W. *J. Am. Chem. Soc.* **1993**, *115*, 9858–9.
(30) Scholl, M.; Trnka, T. M.; Morgan, J. P.; Grubbs, R. H. *Tetrahedron Lett.* **1999**, *40*, 2247–2250.
(31) Nicola, T.; Brenner, M.; Donsbach, K.; Kreye, P. *Org. Process Res. Dev.* **2005**, *9*, 513–515.
(32) Yee, N. K.; Farina, V.; Houpis, I. N.; Haddad, N.; Frutos, R. P.; Gallou, F.; Wang, X.-J.; Wei, X.; Simpson, R. D.; Feng, X.; Fuchs, V.; Xu, Y.; Tan, J.; Zhang, L.; Xu, J.; Smith-Keenan, L. L.; Vitous, J.; Ridges, M. D.; Spinelli, E. M.; Johnson, M.; Donsbach, K.; Nicola, T.; Brenner, M.; Winter, E.; Kreye, P.; Samstag, W. *J. Org. Chem.* **2006**, *71*, 7133–7145.
(33) Farina, V.; Shu, C.; Zeng, X.; Wei, X.; Han, Z.; Yee, N. K.; Senanayake, C. H. *Org. Process Res. Dev.* **2009**, *13*, 250–254.
(34) Chatel-Chaix, L.; Baril, M.; Lamarre, D., Pharmacology and Mechanisms of Action of Antiviral Drugs: Protease Inhibitors. In *Advanced Therapy for Hepatitis C*, McCaughan, G. W.; McHutchison, J.; Pawlotsky, J.-M., Eds. Wiley-Blackwell: Toronto, 2011.
(35) Rosenquist, Å.; Samuelsson, B.; Johansson, P.-O.; Cummings, M. D.; Lenz, O.; Raboisson, P.; Simmen, K.; Vendeville, S.; de Kock, H.; Nilsson, M.; Horvath, A.; Kalmeijer, R.; de la Rosa, G.; Beumont-Mauviel, M. *J. Med. Chem.* **2014**, *57*, 1673–1693.
(36) Niu, D.; Liu, D.; Moore, J. D.; Xu, G.; Sun, Y.; Gai, Y.; Tang, D.; Or, Y. S.; Wang, Z. Preparation of quinoxalinyl macrocycles, especially quinoxalinyloxyproline-containing cyclic peptides, as hepatitis C virus (HCV) NS3-NS4A protease inhibitors for use in pharmaceutical compositions containing a cytochrome P450 monooxygenase inhibitor. US20090005387A1, 2009.
(37) Kong, J.; Chen, C.-Y.; Balsells-Padros, J.; Cao, Y.; Dunn, R. F.; Dolman, S. J.; Janey, J.; Li, H.; Zacuto, M. J. *J. Org. Chem.* **2012**, *77*, 3820–3828.
(38) Higman, C. S.; Lummiss, J. A. M.; Fogg, D. E. *Angew. Chem., Int. Ed.* **2016**, *55*, 3552–3565.
(39) Chikkali, S.; Mecking, S. *Angew. Chem., Int. Ed.* **2012**, *51*, 5802–5808.

References begin on page 18

(40) Dubois, J.-L., Refinery of the future: Feedstock, process, products. In *Biorefinery: from Biomass to Chemicals and Fuels*, Aresta, M.; Dibenedetto, A.; Dumeignil, D., Eds. Walter de Gruyter: Berlin, 2013; Vol. 2.
(41) Żukowska, K.; Grela, K., Cross Metathesis. In *Olefin Metathesis-Theory and Practice*, Grela, K., Ed. Wiley: Hoboken, NJ, 2014; pp 39–84.
(42) Sanford, M. S.; Love, J. A.; Grubbs, R. H. *J. Am. Chem. Soc.* **2001**, *123*, 6543–6554.
(43) Bates, J. M.; Lummiss, J. A. M.; Bailey, G. A.; Fogg, D. E. *ACS Catal.* **2014**, *4*, 2387–2394.
(44) Lummiss, J. A. M.; Higman, C. S.; Fyson, D. L.; McDonald, R.; Fogg, D. E. *Chem. Sci.* **2015**, *6*, 6739–6746.
(45) Lummiss, J. A. M.; Perras, F. A.; Bryce, D. L.; Fogg, D. E. *Organometallics* **2016**, *35*, 691–698.
(46) Morgan, J. P.; Grubbs, R. H. *Org. Lett.* **2000**, *2*, 3153–3155.
(47) Huang, J.; Stevens, E. D.; Nolan, S. P.; Petersen, J. L. *J. Am. Chem. Soc.* **1999**, *121*, 2674–2678.
(48) Weskamp, T.; Kohl, F. J.; Hieringer, W.; Gleich, D.; Herrmann, W. A. *Angew. Chem. Int. Ed.* **1999**, *38*, 2416–2419.
(49) Adlhart, C.; Chen, P. *Helv. Chim. Acta* **2003**, *86*, 941–949.
(50) Yang, H.-C.; Huang, Y.-C.; Lan, Y.-K.; Luh, T.-Y.; Zhao, Y.; Truhlar, D. G. *Organometallics* **2011**, *30*, 4196–4200.
(51) Grela, K., *Olefin Metathesis-Theory and Practice*. Wiley: Hoboken, NJ, 2014.
(52) Lübbe, C.; Dumrath, A.; Neumann, H.; Schäffer, M.; Zimmermann, R.; Beller, M.; Kadyrov, R. *ChemCatChem* **2014**, *6*, 684–688.
(53) Wang, H.; Goodman, S. N.; Dai, Q.; Stockdale, G. W.; Clark, W. M. *Org. Process Res. Dev.* **2008**, *12*, 226–234.
(54) Tomasek, J.; Schatz, J. *Green Chem.* **2013**, *15*, 2317–2338.
(55) Grela, K.; Gulajski, L.; Skowerski, K., Alkene Metathesis in Water. In *Metal-Catalyzed Reactions in Water*, Dixneuf, P. H.; Cadierno, V., Eds. Wiley-VCH: Weinheim, 2013; pp 291–336.
(56) Camm, K. D.; Fogg, D. E., From Drug Cocktails to Tissue Engineering: Synthesis of ROMP Polymers for Biological Applications. In *NATO Sci. Ser. II*, Imamoglu, Y.; Dragutan, V., Eds. Springer Verlag: Berlin, 2007; Vol. 243, pp 285–303.
(57) Guidone, S.; Songis, O.; Nahra, F.; Cazin, C. S. J. *ACS Catal.* **2015**, *5*, 2697–2701.
(58) Hubner, S.; de Vries, J. G.; Farina, V. *Adv. Synth. Catal.* **2016**, *358*, 3–25.
(59) Chadwick, J. C.; Duchateau, R.; Freixa, Z.; van Leeuwen, P. W. N. M., Alkene Metathesis. In *Homogeneous Catalysts: Activity – Stability – Deactivation*, Wiley-VCH: Weinheim, 2011; pp 347-396.
(60) Dinger, M. B.; Mol, J. C. *Eur. J. Inorg. Chem.* **2003**, 2827–2833.
(61) Kim, M.; Eum, M. S.; Jin, M. Y.; Jun, K. W.; Lee, C. W.; Kuen, K. A.; Kim, C. H.; Chin, C. S. *J. Organomet. Chem.* **2004**, *689*, 3535–3540.
(62) Beach, N. J.; Camm, K. D.; Fogg, D. E. *Organometallics* **2010**, *29*, 5450–5455.
(63) Dinger, M. B.; Mol, J. C. *Organometallics* **2003**, *22*, 1089–1095.
(64) Trnka, T. M.; Morgan, J. P.; Sanford, M. S.; Wilhelm, T. E.; Scholl, M.; Choi, T.-L.; Ding, S.; Day, M. W.; Grubbs, R. H. *J. Am. Chem. Soc.* **2003**, *125*, 2546–2558.

References begin on page 18

(65) Hong, S. H.; Day, M. W.; Grubbs, R. H. *J. Am. Chem. Soc.* **2004**, *126*, 7414–7415.
(66) Hong, S. H.; Wenzel, A. G.; Salguero, T. T.; Day, M. W.; Grubbs, R. H. *J. Am. Chem. Soc.* **2007**, *129*, 7961–7968.
(67) Higman, C. S.; Plais, L.; Fogg, D. E. *ChemCatChem* **2013**, *5*, 3548-3551.
(68) Plais, L. *JCEMolChem internship Thesis* **2013**, 14–15.
(69) Werner, H.; Stuer, W.; Weberndorfer, B.; Wolf, J. *Eur. J. Inorg. Chem.* **1999**, 1707–1713.
(70) Hansen, S. M.; Rominger, F.; Metz, M.; Hofmann, P. *Chem. Eur. J.* **1999**, *5*, 557–566.
(71) Galan, B. R.; Pitak, M.; Keister, J. B.; Diver, S. T. *Organometallics* **2008**, *27*, 3630–3632.
(72) Lummiss, J. A. M.; McClennan, W. L.; McDonald, R.; Fogg, D. E. *Organometallics* **2014**, *33*, 6738–6741.
(73) Leitao, E. M.; Dubberley, S. R.; Piers, W. E.; Wu, Q.; McDonald, R. *Chem. Eur. J.* **2008**, *14*, 11565–11572.
(74) Lummiss, J. A. M.; Botti, A. G. G.; Fogg, D. E. *Catal. Sci. Technol.* **2014**, *4*, 4210–4218.
(75) Lummiss, J. A. M.; Ireland, B. J.; Sommers, J. M.; Fogg, D. E. *ChemCatChem* **2014**, *6*, 459–463.
(76) van Rensburg, W. J.; Steynberg, P. J.; Meyer, W. H.; Kirk, M. M.; Forman, G. S. *J. Am. Chem. Soc.* **2004**, *126*, 14332–14333.
(77) Ireland, B. J.; Dobigny, B. T.; Fogg, D. E. *ACS Catal.* **2015**, *5*, 4690–4698.
(78) Bailey, G. A.; Fogg, D. E. *J. Am. Chem. Soc.* **2015**, *137*, 7318–7321.

References begin on page 18

Chapter 2. Experimental methods

2.1 General procedures

2.1.1 Reaction conditions

Reactions were carried out under N_2 using standard glovebox and Schlenk techniques.[1] Reactions carried out in air are indicated in the individual procedures. Room temperature is ca. 25 °C for glovebox work, or 23 °C for Schlenk work. For all reactions, glassware was cleaned and heated to 110 °C in an oven prior to use.

2.1.2 Reagents, standards, and matrices

The following reagents were prepared according to literature procedures: $RuCl_2(PCy_3)_2(=CHPh)$ **Ru-1**,[3] $RuCl_2(H_2IMes)(PCy_3)(=CHPh)$ **Ru-2a**,[4] $RuCl_2(IMes)(=CHPh)$ **Ru-2b**,[5] $RuCl_2(IPr)(PCy_3)(=CHPh)$ **Ru-2d**,[7] $RuCl_2(PCy_3)_2(=CH_2)$ **Ru-6**,[8] $RuCl_2(H_2IMes)(PCy_3)(=CH_2)$ **Ru-4a**,[8] $RuCl_2(IMes)(PCy_3)(=^{13}CH_2)$ ***Ru-4b**,[9] $RuCl_2(IMes)(PCy_3)(=CH_2)$ **Ru-4b**[8] (an improved workup was used for the purification of **Ru-4a** and **Ru-4b**),[9] H_2IMes,[10] and IMes.[11] Structures for the NHC ligands in these complexes appear in Figure 3.1. Ruthenium catalysts $RuCl_2(H_2IPr)(PCy_3)(=CHPh)$ **Ru-2c** and $RuCl_2(H_2ITol)(PCy_3)(=CHPh)$ **Ru-2e** (Sigma-Aldrich), $RuCl_2(H_2IMes)(PCy_3)(=C_{15}H_{10})$ **Ru-2f** and $RuCl_2(IMes)(PCy_3)(=C_{15}H_{10})$ **Ru-2g** (Strem), the ligands IPr (Strem), PCy_3 (97%, Strem), PPh_3 (99%, Strem), and miscellaneous standards or reagents 1,3,5-trimethoxybenzene (TMB, Sigma-Aldrich), dodecane (>99%, Sigma-Aldrich), and potassium hydrotris(1-pyrazolyl)borate (KTp, >99%, Sigma-Aldrich), d_{12}-mesitylene **9** (98%, Cambridge Isotopes), zinc powder (99.9%, Sigma-Aldrich), glyoxal solution (40 wt% in H_2O, Sigma-Aldrich), $NaBH_4$ (Sigma-Aldrich),

HBF_4 (48 wt% in H_2O, Sigma-Aldrich), and NaH (95%, Sigma-Aldrich), ethylene (BOC Ultra-High Purity Grade 3.0, 99.9%, Linde), ^{13}C-labelled ethylene (99% ^{13}C, Sigma-Aldrich), cis-2-butene gas (>99%, GFS Chemicals), pyrene (98%, Sigma-Aldrich) and anthracene (97%, Sigma-Aldrich) were used as received. 1-Methylpyridinium chloride $[MeNC_6H_5]Cl$ (>98%, TCI Chemicals) was dried under vacuum prior to use in NMR analysis. Pyridine (>99%, Fisher), NEt_3 (99%, Alfa Aesar), DMSO (>99%, BDH), and MeCN (>99%, Fisher) were distilled from CaH_2 under N_2. Hexamethylphosphoramide, tetramethyl urea (both 99%, Sigma-Aldrich), diethyldiallylmalonate (DDM; 98%, Sigma-Aldrich), and deionized H_2O were degassed by five consecutive freeze/pump/thaw cycles and stored under N_2.

2.1.3 Solvents

Hexanes, C_6H_6, C_7H_8, CH_2Cl_2, Et_2O and THF were dried and degassed using a Glass Contour or Anhydrous Engineering solvent purification system (SPS), and stored in the glovebox. In a test of the SPS drying capacity by Dr. Emma Davy of this research group, the following water contents were found prior to sieve treatment, by Karl-Fisher titration: C_6H_6, 3.6 ppm; THF, 10 ppm; CH_2Cl_2, 5 ppm. Other solvents were purified and degassed by standard[12] distillation methods: methanol from I_2-activated magnesium turnings, acetone from Drierite (calcium sulfate). Pentane was pre-dried over $MgSO_4$ for 24 h, and then distilled from phosphorus pentoxide. All solvents were stored in the glovebox over 4 Å molecular sieves for 16 h prior to use with the exception of methanol (stored over 3 Å molecular sieves) and acetone, which was not stored over sieves because they cause self-condensation. Reactions in air were carried out in reagent-grade solvents used as received.

References begin on page 38

2.1.4 Deuterated solvents

Deuterated solvents (Cambridge Isotope Laboratories, or Sigma Aldrich) were used as received for NMR analysis of air-stable species. Those used for analysis of oxygen- or moisture-sensitive compounds were dried and degassed, except CD_2Cl_2, which was purchased in ampoules packed under N_2 and used as received. C_6D_6 was degassed by five freeze/pump/thaw cycles and stored under N_2 over 4 Å molecular sieves for at least 24 h before use. $CDCl_3$ was distilled over CaH_2 and stored over 4 Å sieves in the glovebox prior to use.

2.1.5 Instrumentation

2.1.5.1 NMR spectroscopy

Nuclear magnetic resonance (NMR) spectroscopy (^1H, ^2H, $^{31}P\{^1H\}$, $^{13}C\{^1H\}$, ^1H-^{13}C HMQC, ^1H-^{31}P HMQC, ^1H-^1H COSY) was performed on a Bruker Avance 300 or Avance 500 NMR spectrometer at RT (23 ±2 °C) unless otherwise indicated. Samples were referenced to the residual proton/deuteron or carbon signals of the deuterated solvent, or to external 85% H_3PO_4 (^{31}P). Signals are reported relative to TMS (^1H, ^{13}C) or 85% H_3PO_4 (^{31}P) at 0 ppm. All NMR spectra of air or moisture sensitive compounds were collected under anaerobic conditions using a sealed- or screw-cap NMR tube. All $^{31}P\{^1H\}$ values are reported as a percentage of total integration.

2.1.5.2 Gas chromatography

GC quantification was performed on samples diluted with CH_2Cl_2 (ACS reagent grade) on an Agilent 7890A Series autosampler and an Agilent HP-5 polysiloxane column (30 m length, 320 μm diameter), using an inlet split ratio of 10:1, an inlet temperature of 250 °C, and helium (UHP grade) as the carrier gas to maintain column pressure at 11.5 psi.

The FID response was maintained between 50-2000 ρA, using analyte concentrations of ca. 5 mM. Calibration curves (peak areas vs. concentration) were constructed in the relevant concentration regime for DDM and its RCM product. Conversions and yields in catalytic runs were determined from the integrated peak areas, relative to dodecane as internal standard, and compared to the initial integration ratio of substrate to dodecane.

2.1.5.3 MALDI-TOF mass spectrometry

Mass spectra were recorded on a Bruker Daltonics UltraFleXtreme MALDI time-of-flight spectrometer (MALDI-TOF). MALDI samples were prepared in a N_2-filled glovebox, using pyrene or anthracene as matrix. Matrix and analyte solutions were prepared at concnetrations of 100 mM and 5 mM respectively. Samples were mixed in a matrix:analyte ratio of 25:1 to deliver a final molar ratio of 500:1. Approximately 2 μL aliquots were spotted on the MALDI target plate and allowed to evaporate by the dried-droplet method. Spotted plates were transferred directly to the MALDI through a small chamber attached to the glovebox. Samples were analyzed immediately after inserting the MALDI plate to minimize premature matrix evaporation.

2.1.5.4 Infrared spectroscopy

IR data were collected on powder samples using a Nicolet 6700 FT-ATR IR spectrometer, access to which was kindly provided by Prof. Muralee Murugesu (uOttawa).

2.1.5.5 Elemental analysis

Elemental analyses of new compounds were carried out by MHW Laboratories (Phoenix, AZ).

2.2 Experimental data for Chapter 3

2.2.1 Synthesis of $RuCl_2(IMes)(PCy_3)(=^{13}CH_2)$, *Ru-4b

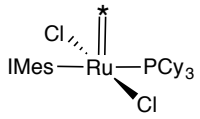

Prepared by the method established for ***Ru-4a***,[9] using IMes in place of H_2IMes. In the glovebox, light pink ***Ru-6*** (200 mg, 0.267 mmol) was dissolved in 12 mL C_6H_6 in a 100 mL Schlenk tube. White crystalline IMes (89 mg, 0.294 mmol, 1.1 equiv) was added. The flask was removed to a Schlenk line and immersed in an oil bath set at 60 °C. A color change from pink to yellow-brown occurred within 15 min. After heating for 45 min, the solvent was stripped off to leave a brown residue containing the desired product, contaminated with products from decomposition of ***Ru-6*** ($[^{13}CH_3PCy_3]Cl$ ***2**** and Ru decomposition products). In the glovebox, the residue was converted to a yellow powder by adding pentane, scratching with a spatula, and removing solvent (3 x 2 mL). The product was then washed with cold pentane (3 x 2 mL) and collected by filtration. Crude yield: 124 mg (62%). Phosphonium salt ***2**** was extracted with degassed H_2O (2 x 1 mL), after which the yellow powder was washed with cold acetone (1 mL) and cold pentane (3 x 1 mL). Yield of ***Ru-4b***: 102 mg (50%; 99.5% ^{13}C-enriched). Isolated yields are adversely affected by partial solubility in the solvents used to extract PCy_3 and ***2***. Chemical shifts are in excellent agreement with the values reported for the non-labelled isotopologue, with added ^{13}C coupling. $^{31}P\{^1H\}$ (121 MHz, C_6D_6): δ 40.9 (d, $^2J_{PC}$ = 9.5 Hz, *P*Cy_3). ^{1}H NMR (300 MHz, C_6D_6): δ 18.80 (d, $^1J_{HC}$ = 157.8 Hz, 2H, Ru=C*H*$_2$), 6.90 (s, 2H, Mes *m*-C*H*), 6.72 (s, 2H, Mes *m*-C*H*), 6.22 (br s, 1H, NC*H*), 6.13 (br s, 1H, NC*H*=), 2.60 (s, 6H, *o*-CH_3), 2.47-2.27 (br m, 9H, *o*-CH_3 and Cy), 2.19 (s, 3H, *p*-CH_3), 2.11 (s, 3H, *p*-CH_3), 1.78-1.47 (br m, 15H, Cy),

1.29-1.01 (br m, 15H, Cy). $^{13}C\{^{1}H\}$ (75 MHz, C_6D_6) (methylidene signal only): δ 295.4 (d, $^{2}J_{CP}$ = 9.5 Hz, Ru=*C*H_2). For spectra see Appendix 1, Figure A1.1.

2.2.2 Decomposition of Grubbs methylidene complexes by pyridine

In a representative procedure, a screw-cap NMR tube was charged with **Ru-4b** (230 μL of a 43 mM stock solution in C_6D_6; 0.012 mmol), TMB (ca. 1 mg), and C_6D_6 (350 μL), to obtain a final Ru concentration of 20 mM. A ^{1}H NMR spectrum was recorded to establish the initial integration ratio of **Ru-4b** vs. TMB. Pyridine (24 μL of a 1.3 M stock solution in C_6D_6; 3 equiv) was injected at the NMR instrument. An immediate colour change from yellow-brown to deep red resulted, with turbidity developing within minutes. The septum was covered with Parafilm, the tube shaken well, and ^{31}P NMR acquisition was immediately initiated. Spectra were collected at 5-min intervals for the first 50 min, then at 75 min. A transient signal assigned to **Ru-11b** (see section 2.2.3) was observed over the period 3–45 min. Complete loss of starting **Ru-4b** was evident at 75 min (See Figure 3.3, Chapter 3, and Appendix 1 for all spectra and data). $^{31}P\{^{1}H\}$ NMR values are reported as a percentage of total integration. $^{31}P\{^{1}H\}$ (121 MHz, C_6D_6): δ 34.2 (s, [$MePCy_3$]Cl **2**, 89%), 10.4 (s, PCy_3, 11%). With 10 equiv py, at 10 min, full decomposition is seen: $^{31}P\{^{1}H\}$ (121 MHz, C_6D_6): δ 34.2 (s, **2**, 81%), 10.4 (s, PCy_3, 19%).

2.2.3 Decomposition of IMes derivative *Ru-4b by pyridine: direct observation of σ-alkyl intermediate $RuCl_2(\sigma\text{-}^{13}CH_2PCy_3)(IMes)(py)_2$, *Ru-11b

Procedure as indicated for **Ru-4b** and pyridine. $^{13}C\{^{1}H\}$ (75 MHz, C_6D_6); collected over 2–16 min, 512 scans, key signals only, ***Ru-11b**: δ –27.4 (d, $^{1}J_{PC}$ = 11.6 Hz, Ru-*C*H_2PCy_3), 1.2 (d, $^{1}J_{PC}$ = 47.8 Hz, [$^{13}CH_3PCy_3$]Cl) ***2**, 295.4 (d, $^{2}J_{CP}$ = 9.5 Hz, Ru=*C*H_2,

Ru-4b). $^{31}P\{^{1}H\}$ (121 MHz, C_6D_6; collected over 16–22 min, 200 scans): δ 61.3 (d, $^{1}J_{PC}$ = 11.6 Hz, ***Ru-11b***, 6%), 40.9 (d, $^{2}J_{PC}$ = 9.5 Hz, ***Ru-4b***, 32%), 34.2 (d, $^{1}J_{PC}$ = 47.8 Hz, [$^{13}CH_3PCy_3$]Cl ***2***, 54%), 10.5 (s, free PCy_3, 8%). See Appendix 1, Figure A1.7. At 75 min: $^{31}P\{^{1}H\}$ (121 MHz, C_6D_6): δ 34.2 (d, $^{1}J_{PC}$ = 47.8 Hz, [$^{13}CH_3PCy_3$]Cl ***2***, 90%), 10.4 (s, PCy_3, 10%); no Ru-phosphine species apparent.

2.2.4 Decomposition of H_2IMes derivative $RuCl_2(H_2IMes)(PCy_3)(=^{13}CH_2)$ *Ru-4a by pyridine

As for **Ru-4b** above, using 10 equiv pyridine. No signal for **Ru-4a** was apparent after 5 min. $^{31}P\{^{1}H\}$ (121 MHz, C_6D_6): δ 34.2 (d, $^{1}J_{PC}$ = 47.8 Hz, [$^{13}CH_3PCy_3$]Cl ***2***, 87%), 10.4 (s, PCy_3, 13%).

2.2.5 Decomposition of in situ-generated methylidene complexes by pyridine

In a representative procedure, a 25 mL Schlenk tube equipped with a Kontes tap was loaded with **Ru-2b** (10 mg, 0.01 mmol) and 2 mL C_6H_6. The solution was freeze/pump/thaw degassed (3x) and allowed to thaw under ethylene. Pyridine (8 μL, 0.1 mmol, 10 equiv) was added via syringe against a positive pressure of ethylene. The flask was sealed, returned to the glovebox, and heated at 50 °C. A color change from pink to orange-red occurred within minutes. After 2 h, a C_6D_6 spike was added, and the $^{31}P\{^{1}H\}$ NMR spectrum was measured. $^{31}P\{^{1}H\}$ (121 MHz, C_6D_6): δ 34.2 (s, [$MePCy_3$]Cl **2**, 74%), 10.5 (s, PCy_3, 26%). See Appendix 1, Figure A1.8; Table A1.2. tabulates all data for catalysts studied.

2.2.6 Representative procedure for reaction of Ru-4a or Ru-4b* with Lewis donors

Experiments carried out as above, with the following modifications. The reaction was carried out in a sealed-cap NMR tube. The donor was added in the glovebox following measurement of the initial **Ru-4a**:TMB ratio by ^{1}H NMR analysis; the sample was shaken well and transferred to an oil bath set at 50 °C for 2 h. For DMSO (10 equiv): ^{31}P{^{1}H} (121 MHz, C_6D_6): δ 38.2 (s, **Ru-4a**, 65%), 34.2 (s, [MePCy$_3$]Cl **2**, 35%). ^{1}H NMR (300 MHz, C_6D_6): δ 18.42 (s, **Ru-4a**, 65%). For control experiment without donor see Appendix 1, Figure A1.9; for representative spectra for the DMSO experiment above, see Figure A1.10.

Variants: for H_2O and THF, repeated using 100 equiv R_2O; for MeCN, in neat MeCN. Kinetic studies carried out with 10, 33, 55, 78, and 100 equiv DMSO at RT and monitored for 27 h. See Appendix 1, Table A1.3 and Table A1.4.

2.2.7 Synthesis of RuCl$_2$(σ-CH$_2$PCy$_3$)(DMSO)$_3$, Ru-12

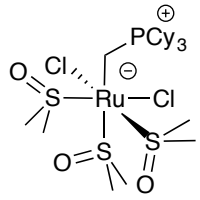

To a stirred solution of **Ru-6** (131 mg, 0.175 mmol) in C_6H_6 (8 mL) in a 25 mL Schlenk flask was added DMSO (1.24 mL, 1.37 g, 17.5 mmol, 100 equiv). A colour change from pink to yellow occurred over 2 h, but reaction was incomplete. After 4 h, no further **Ru-6** was present by ^{31}P NMR analysis. Pentane (20 mL) was added to precipitate pale yellow **Ru-12**, which was filtered off and washed with cold pentane (5 x 2 mL). Yield 74 mg (60%). ^{31}P{^{1}H} NMR (121 MHz, C_6D_6): δ 51.9 (s, *P*Cy$_3$). ^{1}H NMR (300 MHz, C_6D_6): δ 3.34 (overlapping s, 12H, ((C*H*$_3$)$_2$SO)$_2$, 3.19 (s, 6H, ((C*H*$_3$)$_2$SO)), 3.06-2.95 (m, 3H, Cy), 2.25-2.15 (m, 6H, Cy), 1.71-1.55 (m, 10H, Cy), 1.42-1.27 (m, 12H, Cy), 1.13-1.04 (m, 2H, Cy), 0.96 (d, 2H, $^{2}J_{HP}$

* The reaction with **Ru-4b** was carried out by Ms. Stephanie Rufh.

= 15.2 Hz, Ru-CH_2PCy$_3$). ^{13}C{^{1}H} (75 MHz, C_6D_6; selected): δ –8.8 (d, $^1J_{PC}$ = 22.2 Hz, Ru-*C*H$_2$PCy$_3$). Experiments supporting assignment of the σ-CH_2PCy$_3$ doublet at 0.96 ppm: ^{1}H-^{13}C HMQC correlation with ^{13}C{^{1}H} NMR doublet at –8.8 ppm; ^{1}H-^{31}P HMQC correlation with ^{31}P{^{1}H} NMR singlet at 51.9 ppm; ^{1}H-^{1}H COSY, no correlation. ATR-IR: ν(S=O) 1072, 1071 cm^{-1} (s, *S*-bonded DMSO). Anal. Calc'd. for $C_{25}H_{53}Cl_2O_3PRuS_3$: C, 42.85; H, 7.62. Found: C, 43.05; H, 7.75. For spectra, see Figure A1.2 to A1.5.

2.2.8 Impact of donors on RCM: representative procedure[†]

A Schlenk tube was loaded with DDM (48 mg, 0.2 mmol), dodecane (34 mg, 0.2 mmol; internal standard), DMSO (91 μL), and toluene (1.8 mL). An aliquot was removed for GC-FID analysis to establish the starting ratio of DDM to dodecane. To the flask was added catalyst **Ru-2a** from a stock solution in toluene (31 μL of a 3.0 mM solution containing 11 mg **Ru-2a** in 4.0 mL toluene; catalyst loading 0.05 mol%). The reaction was heated in an oil bath set to 50 °C. A sample was removed after 2 h, quenched with KTp (10 mg/mL in THF; 10 equiv vs. **Ru-2a**), and analyzed by GC-FID. See Appendix 1, Figure A1.13 for a representative GC-FID trace.

2.2.9 Reaction of $RuCl_2(H_2IMes)(PCy_3)(CHMe)$ Ru-13 (generated in situ) with pyridine

A solution of **Ru-2a** (10 mg, 0.012 mmol), 600 μL C_6D_6, and TMB (ca. 1 mg; internal standard) was made and analyzed (^{1}H NMR) to establish the initial integration ratio of **Ru-2a** vs. TMB. Pyridine (10 μL, 0.12 mmol, 10 equiv) was added, and the solution was freeze-pump-thaw degassed (3x) and allowed to thaw under an atmosphere of cis-2-

[†] These reactions were carried out by Ms. Stephanie Rufh of the Fogg group.

butene. The NMR tube was then sealed and heated at 50 °C in a thermostatted oil-bath. Decomposition rates were established by NMR analysis. Key signals at 1 h (see Appendix 1, Figure A1.14): ^{1}H NMR (300 MHz, C_6D_6) δ 19.67 (q, $^{3}J_{HH}$ = 6.4 Hz, $RuCl_2(H_2IMes)(py)_2$(=CHMe) **Ru-14**, 30%), 18.99 (q of d, $^{3}J_{HH}$ = 5.5 Hz, $^{2}J_{HP}$ = 0.7 Hz, **Ru-13**, 70%). $^{31}P\{^{1}H\}$ NMR (121 MHz, C_6D_6): δ 28.99 (s, **Ru-13**, 70%), 10.5 (s, free PCy_3, 30%). At 48 h (see Figure A1.15): $^{31}P\{^{1}H\}$ NMR (121 MHz, C_6D_6) δ 47.2 (s, O=PCy_3, 11%), 34.2 (s, [$MePCy_3$]Cl **2**, 56%), 10.5 (s, free PCy_3, 34%). MALDI-TOF-MS (*m/z*): 295.26, [$MePCy_3$]Cl **2** (Calc'd *m/z* for $[C_{19}H_{36}P]^{+}$: 295.26). No signal observed for [$EtPCy_3$]Cl (Calc'd *m/z* for $[C_{20}H_{38}P]^{+}$: 309.27).

2.2.10 Decomposition of $RuCl_2(H_2IMes)(PCy_3)$(CHMe) Ru-13 in the absence of pyridine

Complete decomposition was evident after 15 days. Key signals at 1 h: ^{1}H NMR (300 MHz, C_6D_6) δ 18.99 (q of d, $^{3}J_{HH}$ = 5.5 Hz, $^{2}J_{HP}$ = 0.7 Hz, **Ru-13**, 100%). $^{31}P\{^{1}H\}$ NMR (121 MHz, C_6D_6): δ 28.99 (s, **Ru-13**, 100%). After 15 days: $^{31}P\{^{1}H\}$ NMR (121 MHz, C_6D_6) δ 71.8 (s, unidentified, 5%), 71.2 (s, unidentified, 7%), 47.2 (s, unidentified, 12%), 34.2 (s, [$MePCy_3$]Cl **2**, 75%).

2.2.11 Evidence for water-accelerated methylidene abstraction during RCM macrocyclization[‡]

In the glovebox, a J. Young NMR tube was charged with **Ru-2a** (11.6 mg, 0.0137 mmol), prolactone (33.7 mg, 0.137 mmol, 10 equiv), 0.67 mL C_6D_6, and degassed H_2O (35 μL, 20:1 v/v vs C_6D_6 solvent). The sample was heated at 50 °C as for DDM. A color change from pink to orange occurred within the first 20 min. Phosphorus speciation at 2 h:

[‡] These reactions were carried out by Ms. Stephanie Rufh of the Fogg group.

$^{31}P\{^{1}H\}$ NMR (121 MHz, C_6D_6; as % of total integration): δ 38.2 (s, **Ru-4a**, 50%), 33.9 (s, [$MePCy_3$]Cl **2**, 38%), 31.1 (3%, unassigned), 29.1 (3%, unassigned), free PCy_3 (10.4 ppm, 6%). No **Ru-2a** (30.1 ppm) remained. The signal for **2** is broadened ($\omega_{1/2}$ 33 Hz) and its chemical shift ca. 0.3 ppm upfield relative to the values above, perhaps indicating H-bonding with water.

2.2.12 Supplementary data

All NMR spectra for isolated new compounds, in situ, and single time point reactions are in Appendix 1.

2.3 Experimental data for Chapter 4

2.3.1 Synthesis of d_{11}-2-nitromesitylene 10

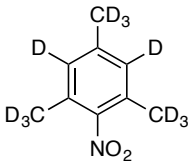

d_{11}-2-Nitromesitylene **10** was synthesized following a literature procedure.[13] Additional details beyond those in the published procedure are provided below. To a 100 mL round-bottom flask open to air, d_{12}-mesitylene **9** (5.1g, 38.5 mmol) was added followed by 10 mL of acetic anhydride. The flask was placed in an ice bath (0 ºC). In a separate flask 2.6 mL of nitric acid (1.05 equiv, 40.4 mmol) and 20 mL of acetic anhydride were combined slowly and cooled to 0 ºC. The nitric acid/acetic anhydride mixture was then added dropwise to the 100 mL round-bottom flask using a dropping funnel. The reaction mixture was stirred for 1.5 h at room temperature and the reaction was monitored by TLC (1:8 ethyl acetate/hexanes; product Rf value 0.7). Upon addition of 70 mL ice water the product precipitated out as a yellow oil. After 20 minutes the product crystallized, was then filtered, and washed with water resulting in yellow crystals that were dried under vacuum. Yield: 6.17 g (91%). ^{2}H

NMR chemical shifts agree with the literature values. ^{2}H NMR (46 MHz, $CHCl_3$) δ 6.20 (br s, 2D, C*D*), 1.52, 1.49 (overlapping br s, 9D, Mes CD_3).

2.3.2 Synthesis of d_{11}-2,4,6-trimethyl aniline 11

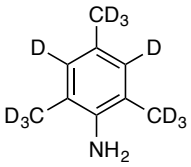

d_{11}-2,4,6-Trimethyl aniline **11** was synthesized following a literature procedure with slight modifications.[13] To a 250 mL round-bottom flask open to air, that was charged with a stir bar, d_{11}-2-nitromesitylene **10** (6.17g, 35 mmol) was added with 125 mL of ethanol. Zinc powder (11.4 g, 5 equiv, 35 mmol) was then added and the mixture was cooled to 0 ºC using an ice bath. Next, 14 mL of acetic acid was added dropwise using a dropping funnel (ca. 1 drop every 6 second) and left to slowly warm to room temperature over 5 h. Reaction completion was tested by TLC (1:4 ethyl aetate/hexanes) against starting material. After 5 h the reaction was complete. Next, 80 mL of a 2 M NaOH solution was added, causing precipitation of zinc salts forming a thick slurry. The slurry was filtered through Celite, and the filtrate was extracted with ether (3 x 85 mL), dried with $MgSO_4$, filtered again and the solvent was removed yielding an orange oil. Yield: 3.50 g (75%). ^{1}H and ^{2}H NMR chemical shifts agree with the literature values. ^{1}H NMR (300 MHz, $CDCl_3$) δ 3.46 (br s, 2H, NH_2). ^{2}H NMR (46 MHz, $CHCl_3$) δ 6.16 (br s, 2D, Mes C*D*), 1.41, 1.36 (overlapping s, 9D, Mes CD_3).

2.3.3 Synthesis of d_{22}-glyoxal-bis-(2,4,6-trimethylphenyl)imine 12

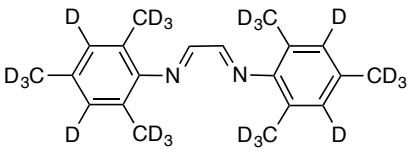

d_{22}-Glyoxal-bis-(2,4,6-trimethylphenyl)imine **12** was synthesized according to the method established for the non-labelled analog but using labelled starting material.[14] In a 50 mL Erlenmeyer flask open to air with a stir bar, d_{11}-2,4,6-trimethyl

aniline **11** (3.27 g, 22 mmol) was added with 25 mL of MeOH. Next, glyoxal (40% wt. in H_2O, 1.28 mL, 11 mmol, 0.5 equiv) and a drop of formic acid catalyst were added. A yellow precipitate formed and the reaction was left to stir at room temperature for 12 h. The yellow product was collected by filtration, washed with MeOH until colorless washings were obtained and dried under vacuum. Yield 2.40 g (68%). ^{1}H NMR shifts were consistent with literature values with exception of the d_{22}-mesityl deuterons. ^{1}H NMR (300 MHz, $CDCl_3$) δ 8.12 (s, 2H, NC*H*). ^{2}H NMR (46 MHz, $CHCl_3$) δ 6.92 (br s, 4D, Mes C*D*), 2.24, 2.11 (overlapping s, 18D, Mes C*D*$_3$).

2.3.4 Synthesis of d_{22}-N,N'-bis(2,4,6-trimethylphenyl)ethylenediamine dihydrochloride 13

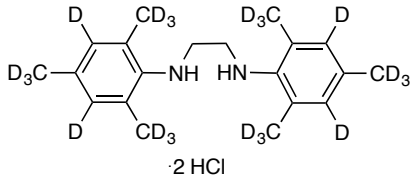

d_{22}-N,N'-Bis(2,4,6-trimethylphenyl)ethylenediamine dihydrochloride **13** was synthesized according to the method optimized for the non-labelled analog.[14] In a 125 mL Erlenmeyer flask open to air with a stir bar, d_{22}-glyoxal-bis-(2,4,6-trimethylphenyl)imine **12** (2.40g, 7.57 mmol) was added with 35 mL of THF and 14 mL of MeOH. The reaction mixture was cooled to 0 ºC in an ice bath, and $NaBH_4$ was added (2.22 g, 56.8 mmol, 7.50 equiv) in 4 portions over the course of 40 min. The reaction was allowed to warm to room temperature over 3.5 hours. As the solution was still slightly yellow after this time, it was warmed to 30 °C in a water-bath until no yellow colour remained (30 min). The reaction mixture was then cooled to 0 ºC and quenched by slow addition of distilled water (18 mL; vigorous evolution of H_2 gas occurs). Acidification to pH 1.0 with a 3M HCl solution caused the white product to precipitate. The product was collected via filtration, washed with distilled water and dried under vacuum overnight.

Yield: 1.8 g (60%). ^{1}H NMR shifts were consistent with literature values with the exception of the d_{22}-mesityl deuterons. ^{1}H NMR (300 MHz, DMSO-d_6) δ 3.55 (s, 4H, NCH_2CH_2N). ^{2}H NMR (46 MHz, DMSO) δ 6.90 (br s, 4D, Mes C*D*), 2.41, 2.24 (overlapping s, 18D, Mes CD_3).

2.3.5 Synthesis of d_{22}-1,3-bis(2,4,6-trimethylphenyl)imidazolium chloride 14

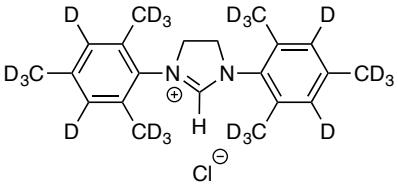

d_{22}-1,3-Bis(2,4,6-trimethylphenyl)imidazolium chloride **14** was synthesized according to the method optimized for the non-labelled analog.[14] In a 50 mL round-bottom flask open to air, d_{22}-N,N'-bis(2,4,6-trimethylphenyl)ethylenediamine dihydrochloride **13** (1.7 g, 4.25 mmol) was added with 15 mL triethylorthoformate and 1-2 drops of formic acid. The stirred suspension was heated at 135 ºC in a simple distillation apparatus for 6 h until evolution of ethanol ceased. To ensure all of the ethanol had been distilled off, the apparatus was put under a slight vacuum using a water aspirator. The solution was cooled in an ice bath to precipitate the product, which was filtered off, washed with cold ether (3 x 6 mL) and dried under vacuum. Yield: 1.25 g (81%). ^{1}H NMR shifts were consistent with literature values with the exception of the d_{22}-mesityl deuterons. ^{1}H NMR (300 MHz, DMSO-d_6) δ 9.02 (s, 1H, N=C*H*), 4.44 (s, 4H, NCH_2CH_2N). ^{2}H NMR (46 MHz, DMSO) δ 7.09 (br s, 4D, Mes C*D*), 2.36, 2.31 (overlapping s, 18D, Mes CD_3).

2.3.6 Synthesis of d_{22}-1,3-bis(2,4,6-trimethylphenyl)imidazolium tetrafluoroborate 15

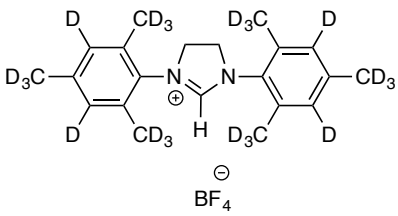

d_{22}-1,3-Bis(2,4,6-trimethylphenyl)imidazolium tetrafluoroborate **15** was synthesized according to the

method established for the non-labelled analog but using labelled starting material.[15] In a 250 mL Erlenmeyer flask open to air with a stir bar, d_{22}-1,3-bis(2,4,6-trimethylphenyl)imidazolium chloride **14** (1.25 g, 3.42 mmol) was added with 70 mL distilled water. The reaction was vigorously stirred for 20 minutes, and then filtered to remove residual salts. To the filtrate, HBF_4 (0.6 mL of a 48% wt solution in H_2O, 4.58 mmol, 1.3 equiv) was added dropwise forming a white precipitate. The solution was stirred for an additional 15 min, filtered, washed with hexanes (4 x 6 mL), and ether (1 x 7 mL), and dried under vacuum overnight at 30 ºC. Yield: 1.11 g (78%). ^{1}H NMR shifts were consistent with literature values with exception of the d_{22}-mesityl deuterons. ^{1}H NMR (300 MHz, $CDCl_3$) δ 7.90 (s, 1H, N=C*H*), 4.54, (s, 4H, NCH_2CH_2N). ^{2}H NMR (46 MHz, $CHCl_3$) δ 6.99, (br s, 4D, Mes C*D*), 2.36, 2.31 (overlapping s, 18D, Mes CD_3).

2.3.7 Synthesis of free d_{22}-H_2IMes

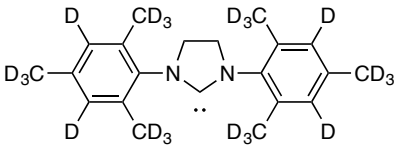

Free d_{22}-H_2IMes was synthesized according to the method established for the non-labelled analog but using labelled starting material.[14] In the glovebox, in a 100 mL round-bottom flask d_{22}-1,3-bis(2,4,6-trimethylphenyl)imidazolium tetrafluoroborate **15** (200 mg, 0.480 mmol) was added along with 8 mL of THF. Next, NaH (30 mg, 1.24 mmol, 2.6 equiv) was added slowly because of the evolution of H_2 gas. The reaction was then sealed with a rubber septum pierced with a needle. The reaction was left to stir for 16 h. The reaction mixture was then filtered through Celite and stripped to dryness leaving behind a white solid. The crude solid was dissolved in minimal amount of C_6H_6, filtered through Celite and stripped to dryness. The solid was washed with hexanes (3 x 1 mL) and dried under vacuum. Yield: 134 mg (85%). ^{1}H

NMR shifts were consistent with literature values with exception of the d_{22}-mesityl deuterons. ^{1}H NMR (300 MHz, C_6D_6) δ 3.27 (s, 4H, NC*H*$_2$C*H*$_2$N). ^{2}H NMR (46 MHz, C_6H_6) δ 6.91 (br s, 4D, Mes C*D*), 2.31, 2.17 (overlapping s, 18D, C*D*$_3$).

2.3.8 Synthesis of $RuCl_2(d_{22}\text{-}H_2IMes)(PCy_3)(=CH_2)$, d_{22}-Ru-4a

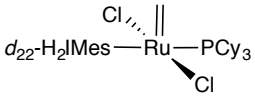

Prepared by the method established for **Ru-4a**,[9] using d_{22}-H_2IMes in place of H_2IMes. In the glovebox, light pink **Ru-11** (185 mg, 0.248 mmol) was dissolved in 12 mL C_6H_6 in a 100 mL Schlenk tube. White crystalline d_{22}-H_2IMes (100 mg, 0.304 mmol, 1.25 equiv) was added. The flask was removed to a Schlenk line and immersed in an oil bath set at 60 °C. A color change from pink to yellow-brown occurred within 15 min. After heating for 45 min, the solvent was stripped off to leave a brown residue containing the desired product and products from decomposition of **Ru-11** ([CH_3PCy_3]Cl **2** and Ru decomposition products). In the glovebox, the residue was converted to a yellow powder by adding pentane, scratching with a spatula, and removing solvent (3 x 2 mL). Phosphonium salt **2** was extracted with degassed H_2O (2 x 1 mL), after which the yellow powder was washed with cold acetone (1 mL) and cold pentane (3 x 1 mL). Yield 137 mg (70%). Chemical shifts are in excellent agreement with the values reported for the non-labelled isotopologue with exception of d_{22}-mesityl deuterons. ^{31}P{^{1}H} (121 MHz, C_6D_6): δ 38.2 (s, *P*Cy_3). ^{1}H NMR (300 MHz, C_6D_6): δ 18.42 (s, 2H, Ru=C*H*$_2$), 3.30-3.18 (m, 4H, NC*H*$_2$C*H*$_2$), 2.42-2.29 (m, 3H, Cy), 1.70-1.49 (m, 15H, Cy), 1.37-0.95 (m, 15H, Cy). ^{2}H NMR (46 MHz, C_6H_6) δ 6.93 (br s, 4D, Mes C*D*), 2.78 (br s, 6D, Mes *o*-*CD*$_3$), 2.56 (br s, 6D, Mes *o*-C*D*$_3$), 2.18, 2.11 (overlapping s, 6D, *p*-C*D*$_3$).

2.3.9 Representative decomposition of $RuCl_2(d_{22}\text{-}H_2IMes)(PCy_3)(=CH_2)$ d_{22}-Ru-4a

In the glovebox, yellow ***d*$_{22}$-Ru-4a** (12 mg, 0.015 mmol), was added to a sealed-cap NMR tube with 600 μL of C_6D_6. Next 12 μL of pyridine (0.15 mmol, 10 equiv) was added and the NMR tube was shaken. A color change from yellow to red was observed immediately. Full decomposition was evident by 15 min. Decomposition rates were established by NMR analysis. Key signals at 5 min: $^{31}P\{^1H\}$ (121 MHz, C_6D_6): δ 60.1 (s, **Ru-11a**, 29%), 34.1-34.2 (m, $\mathbf{2^{Dn}}$, 57%), 10.4 (s, PCy_3, 14%). See Appendix 2. At 10 min: $^{31}P\{^1H\}$ (121 MHz, C_6D_6): δ 34.2 (br m, $\mathbf{2^{Dn}}$, 87%), 10.5 (s, PCy_3, 13%).

2.3.10 Supplementary data

All NMR spectra for isolated new compounds, in situ, and single time point reactions are in Appendix 2.

2.4 References

(1) Shriver, D. F.; Drezdzon, M. A., *The Manipulation of Air-Sensitive Compounds*. 2nd Ed. ed.; John Wiley & Sons: New York, 1986.

(2) Stephenson, T. A.; Wilkinson, G. *J. Inorg. Nucl. Chem.* **1966**, *28*, 945–956.

(3) Schwab, P.; Grubbs, R. H.; Ziller, J. W. *J. Am. Chem. Soc.* **1996**, *118*, 100–110.

(4) van Lierop, B. J.; Reckling, A. M.; Lummiss, J. A. M.; Fogg, D. E. *ChemCatChem* **2012**, *4*, 2020–2025.

(5) Huang, J.; Stevens, E. D.; Nolan, S. P.; Petersen, J. L. *J. Am. Chem. Soc.* **1999**, *121*, 2674–2678.

(6) Love, J. A.; Morgan, J. P.; Trnka, T. M.; Grubbs, R. H. *Angew. Chem. Int. Ed.* **2002**, *41*, 4035–4037.

(7) Fürstner, A.; Ackermann, L.; Gabor, B.; Goddard, R.; Lehmann, C. W.; Mynott, R.; Stelzer, F.; Thiel, O. R. *Chem. Eur. J.* **2001**, *7*, 3236–3253.

(8) Lummiss, J. A. M.; Beach, N. J.; Smith, J. C.; Fogg, D. E. *Catal. Sci. Technol.* **2012**, *2*, 1630–1632.

(9) Lummiss, J. A. M.; Botti, A. G. G.; Fogg, D. E. *Catal. Sci. Technol.* **2014**, *4*, 4210–4218.

(10) Bates, J. M. Ruthenium Catalysts for Olefin Metathesis: Understanding the Boomerang Mechanism and Challenges Associated with Stereoselectivity. M.Sc. Dissertation, University of Ottawa, Ottawa, ON, 2014.

(11) Arduengo, A. J.; Dias, H. V. R.; Harlow, R. L.; Kline, M. *J. Am. Chem. Soc.* **1992**, *114*, 5530–5534.

(12) Armarego, W. L. F.; Perrin, D. D., *Purification of Common Laboratory Chemicals*. 4th Ed. ed.; Butterworth-Heinemann: Oxford, 1997.

(13) Leitao, E. M.; Dubberley, S. R.; Piers, W. E.; Wu, Q.; McDonald, R. *Chem. Eur. J.* **2008**, *14*, 11565–11572.

(14) Arduengo, A. J.; Krafczyk, R.; Schmutzler, R.; Craig, H. A.; Goerlich, J. R.; Marshall, W. J.; Unverzagt, M. *Tetrahedron* **1999**, *55*, 14523–14534.

(15) Bantreil, X.; Nolan, S. P. *Nature Protoc.* **2011**, *6*, 69–77

Chapter 3. A general decomposition pathway for phosphine-stabilized metathesis catalysts

Reprinted with permission from: Donor-Induced Decomposition of the Grubbs Catalysts: Lewis Donors Accelerate Methylidene Abstraction. William L. McClennan, Stephanie A. Rufh, Justin A. M. Lummiss, and Deryn E. Fogg.* *J. Am. Chem. Soc.* **2016**, 138, 14668-14677.

3.1 Introduction

Molecular metathesis catalysts have transformed organic synthesis in academia.[1,2] With pharmaceutical and speciality-chemicals manufacturing processes now emerging,[3-6] the demand for improved understanding of catalyst decomposition is increasing.[7,8] Catalyst lifetimes control metathesis productivity, and are also critical to product selectivity, because decomposed catalyst species can catalyze side-reactions such as C=C isomerization.[9,10] A central question is therefore the nature of the decomposition pathways operative during catalysis.[7,8] Examined here is the decomposition of phosphine-stabilized catalysts (Figure 3.1) by Lewis donors. Such donors may be present as unprotected functional groups on substrates or solvents, or as contaminants introduced with the solvent, a reagent, or prior synthetic steps.[9]

References begin on page 59

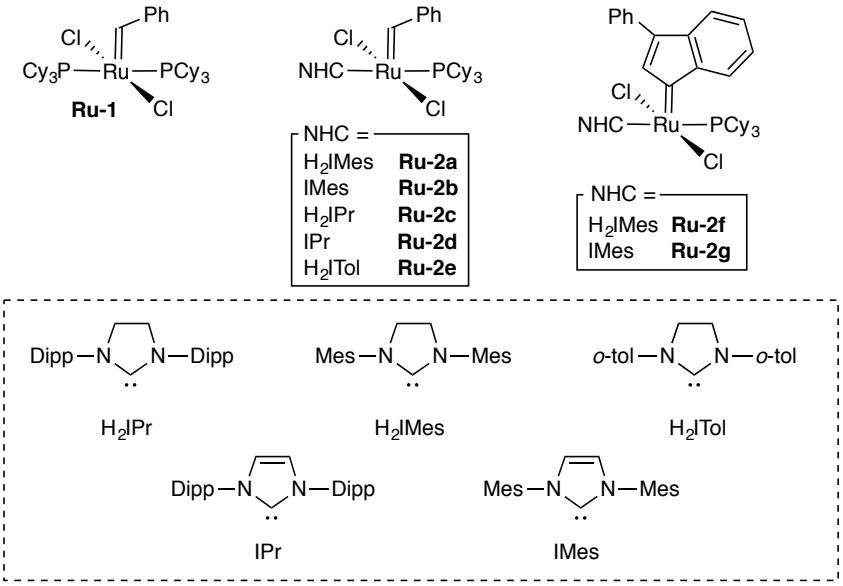

Figure 3.1 Metathesis catalysts examined.

In the hundreds of ruthenium metathesis catalysts developed to date,[1,11] a recurring structural feature is a stabilizing phosphine ligand that is lost during initiation. Reaction of the liberated phosphine with $RuCl_2(NHC)(=CH_2)$ **Ru-3**, a key catalytic intermediate formed in metathesis of terminal olefins, generates the catalyst resting state **Ru-4** (Scheme 3.1, top). The latter species is slow to re-enter the active cycle,[12] owing to the inverse trans effect exerted by the NHC ligand,[13] and the limited steric pressure exerted by the methylidene moiety, relative to the benzylidene group in the precatalyst.[14,15]

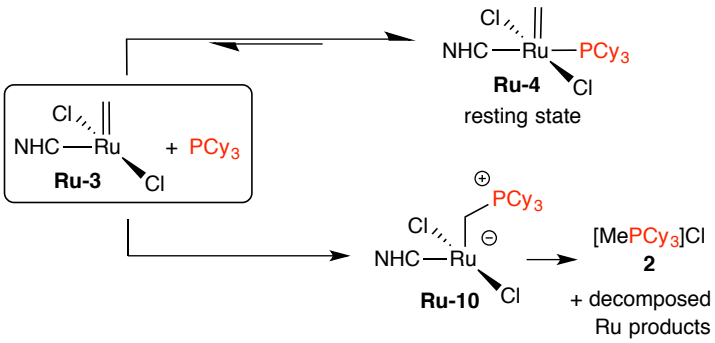

Scheme 3.1 Reactions of Ru-3 with free PCy_3: phosphine re-uptake vs. methylidene abstraction.

References begin on page 59

An alternative, more deleterious reaction pathway (Scheme 3.1, bottom) has been established[13,16] for the H_2IMes derivative **Ru-3a**. Here nucleophilic attack by free PCy_3 on the methylidene carbon[17] culminates in release of [$MePCy_3$]Cl **2**: that is, in loss of three ligands (methylidene, phosphine, and one chloride ligand, as well as a proton). This catalyst decomposition pathway, originally described as requiring 3 days at 55 °C,[16,18] was found to occur much more rapidly on coordination of amines.[19-21] In the present work, we demonstrate that "donor-accelerated decomposition" is general for phosphine-stabilized catalysts of the Grubbs class, including indenylidene catalysts, and that it is promoted by a range of weaker donors, including MeCN, DMSO, H_2O, THF, and methanol. We show that the mechanism is associative in donor, and that the rate of decomposition therefore increases with increasing concentration. Finally, we demonstrate that the ethylidene complex $RuCl_2(H_2IMes)(PCy_3)$(=CHMe) does not undergo alkylidene abstraction by PCy_3. Collectively, these findings have important implications for use of the large class of ruthenium metathesis catalysts based on the archetypal, phosphine-stabilized Grubbs catalyst **Ru-2a**.

3.2 Results and discussion

3.2.1 Observation of the σ-alkyl intermediate in the second-generation system

In a prior communication,[20] we described the near-quantitative formation and crystallographic characterization of a σ-alkyl intermediate (**Ru-7**, Scheme 3.2) generated by reaction of the first-generation Grubbs methylidene complex **Ru-6** with pyridine. In this system, *both* PCy_3 ligands were displaced by pyridine. The choice of pyridine in this system proved critical. Because the pyridine ligands contain no readily activated C–H bonds (in contrast to PCy_3), and because 1,2-hydrogen transfer is not possible (in contract

to the case with secondary amines as nucleophiles),[19] the stability of **Ru-7** was greatly increased. Indeed, elimination of the alkyl ligand took place only over days in solution at RT, or 18 h at 60 °C. ^{13}C-Labelling studies enabled location of the diagnostic $^{13}C\{^1H\}$ NMR doublet for the Ru–$^{13}CH_2PCy_3$ moiety, which appears unusually far upfield (δ_C – 12.3 ppm; $^1J_{PC}$ = 9.8 Hz) owing to shielding of the carbon nucleus by the formally anionic Ru center. The ^{31}P nucleus is correspondingly deshielded by its positive charge, and the $^{31}P\{^1H\}$ NMR doublet for ***Ru-7** is shifted ca. 20 ppm downfield relative to the value for **Ru-6**, to 55.7 ppm.

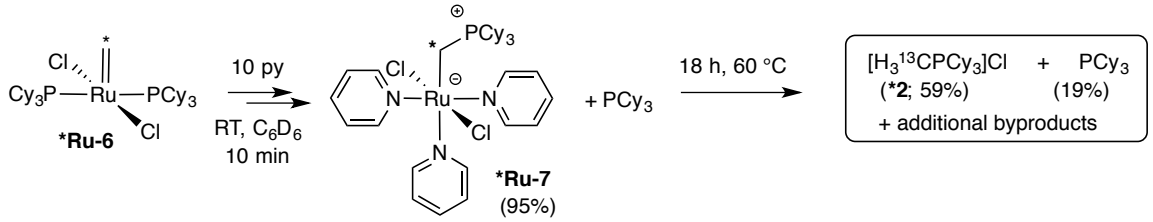

Scheme 3.2 Intercepted σ-alkylphosphonium species.

Under the same conditions, the labelled H_2IMes complex **Ru-4a** decomposed within minutes (87% ***2**, 13% free PCy_3), without observable intermediates. We hypothesized that a σ-alkyl intermediate is formed, but that it is very short-lived, because facile C–H activation of the mesityl *o*-methyl groups promotes the elimination step. Such C–H activation is a common feature for the H_2IMes and IMes ligands.[22] For H_2IMes complexes, this susceptibility may be enhanced by the significant double-bond character present in the Ru–H_2IMes bond, a consequence of π-back-donation from Ru onto the saturated Arduengo carbene.[23] Backbonding has been shown to retard rotation about the Ru–H_2IMes bond in **Ru-4a**.[13] The corresponding σ-alkyl intermediate **Ru-11a** may thus be locked into a conformation that favours the incipient interaction between the σ-alkyl

carbon and the mesityl group,[24,25] upon swivelling about the N–C_{Mes} bond (Figure 3.2a and inset).[26,27]

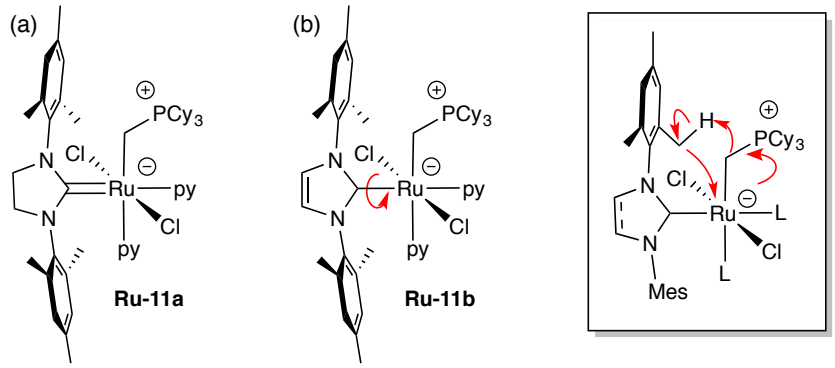

Figure 3.2 Ru–NHC rotation in second-generation σ-alkyl species, and impact on C-H activation (inset).

In seeking evidence for such a σ-alkyl intermediate in the second-generation systems, we turned to the "unlocked" complex **Ru-11b** (Figure 3.2b), in which we anticipated that free rotation of the IMes ligand should retard C–H activation. A ^{31}P NMR signal was indeed observed at ca. 61 ppm immediately after adding 10 equiv pyridine to a C_6D_6 solution of **Ru-4b**, but elimination of phosphonium salt [$MePCy_3$]Cl **2** was complete within 15 min. Injection of a smaller excess of pyridine (3 equiv) resulted in slower decomposition of **Ru-4b**: we will return to the mechanistic implications of this observation below. Under these conditions, **Ru-11b** decomposed at a rate slightly slower than the rate at which it formed (Figure 3.3). Thus, a singlet was observed at 61.3 ppm (maximum 13%), but was rapidly exceeded in intensity by the singlet due to **2** at 34.2 ppm. After 75 min, neither **Ru-4b** nor **Ru-11b** remained: the dominant ^{31}P-containing species was **2** (ca. 90%). A small proportion of free PCy_3 was also observed, indicating a minor contribution from an additional, unidentified pathway. Given the transience and low concentration of putative **Ru-11b**, we turned to ^{13}C labelling studies for unequivocal confirmation of its identity.

References begin on page 59

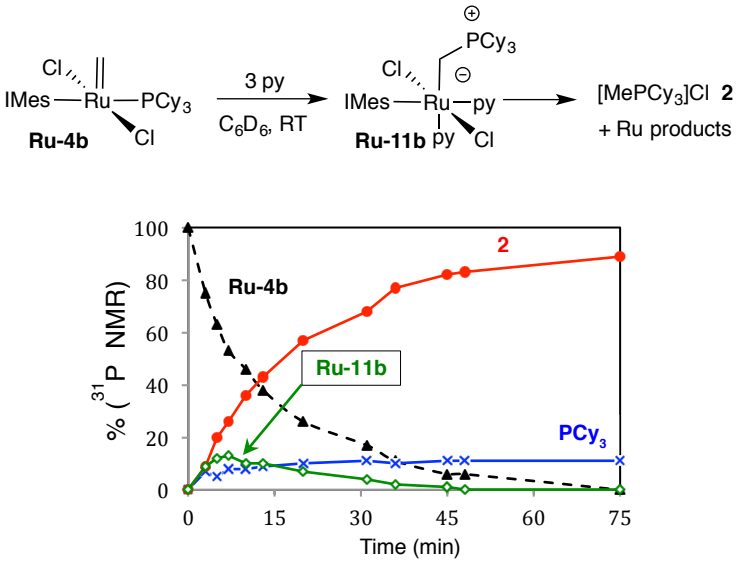

Figure 3.3 Direct observation of the short-lived σ-alkyl intermediate formed by IMes complex Ru-4b (20 mM [Ru], RT = 22 °C). See Table A1.1 and Figure A1.6.[*]

Accordingly, ^{13}C-labelled ***Ru-4b** was prepared by the method previously developed for its H_2IMes analogue ***Ru-4a**,[21] and treated with a threefold excess of pyridine at ambient temperature in C_6D_6. NMR analysis was initiated immediately after injecting pyridine. Diagnostic $^{13}C\{^1H\}$ and $^{31}P\{^1H\}$ NMR doublets for ***Ru-11b** were observed (δ_C –27.4 ppm, δ_P 61.3 ppm; $^1J_{PC}$ = 12 Hz). This multiplicity, and the magnitude of the J_{CP} coupling constant, offer strong evidence for the proposed assignment, comparing well with values for ***Ru-7** (Figure 3.4). The location of the Ru–*C* signal in ***Ru-11b**, ca. 15 ppm further upfield than that for ***Ru-7**, is consistent with shielding by the more strongly-donating IMes ligand, relative to the pyridine ligands in ***Ru-7**. A six-coordinate, bis(pyridine) structure is shown, by analogy to that established crystallographically for **Ru-7** and for the H_2IMes derivative of the benzylidene precatalyst.[28] However, all of these complexes are likely to exist in dynamic equilibrium with the five-coordinate mono-pyridine species.[29]

[*]For a discussion of the limitations of $^{31}P\{^1H\}$ NMR quantitation in these experiments, resulting from inequivalent NOE enhancement and relaxation times for the various ^{31}P nuclei present, see Section 3.4.

We conclude that the mechanism established for **Ru-6** is indeed also operative in the second-generation systems.[30] That is: (1) the incoming donor displaces the PCy_3 ligand[17d] and stabilizes the resulting methylidene species; (2) nucleophilic attack of the free phosphine on the methylidene carbon ensues, forming the σ-alkyl intermediate, and (3) the alkyl moiety is liberated as the phosphonium salt **2** by abstraction of a proton from the NHC ligand (confirmed by *d*-labelling studies, see below), as well as a chloride ligand. For sterically unencumbered amines of sufficiently high nucleophilicity, direct methylidene abstraction by amine has been shown to offer a competing pathway: $NH_2{}^nBu$, for example, abstracts the methylidene ligand as neutral $NHMe{}^nBu$.[19] No evidence of the corresponding methylpyridinium chloride was observed in the present work, however.

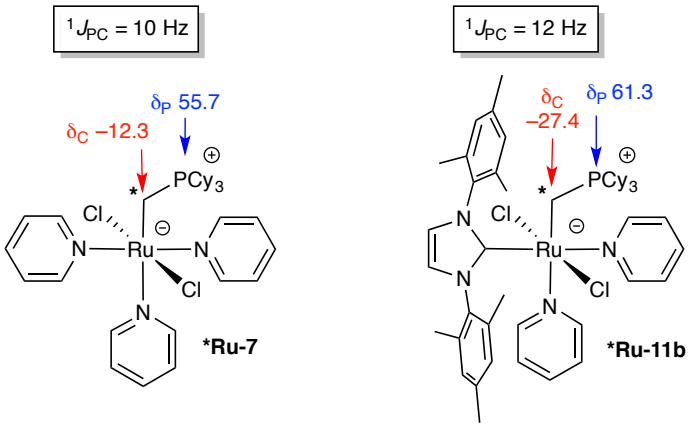

Figure 3.4 Key NMR shifts for first- and second-generation σ-alkyl complexes.

3.2.2 Scope with respect to catalyst

The broader relevance of this pathway was examined for an array of commercially-available catalysts (**2a**–**2g**; Figure 3.5), upon metathesis with ethylene at 50 °C. This treatment generates the methylidene species **Ru-3**/ **Ru-4** in situ, enabling us to assess the impact of added pyridine on the proportion of $[MePCy_3]Cl$ **2** present at 2 h. In all cases,

pyridine treatment accelerated catalyst decomposition, with the extent of of methylidene abstraction (as judged from % **2**) ranging from 80–100%: see Figure 3.5.

For the benchmark H_2IMes catalyst **Ru-2a**, the dominant species present after 2 h at 50 °C in the absence of py was the resting-state methylidene complex **Ru-4a** (62% of total $^{31}P\{^1H\}$ NMR integration), the balance of material being due to **2**. In the presence of 10 py, formation of **2** was quantitative. Similar behaviour was observed for the H_2IPr complex **Ru-2c** and IPr catalyst **Ru-2d**.

In the donor-free control experiments, the IPr and IMes systems (**Ru-2d** and **Ru-2b**, respectively) show a higher proportion of the methylidene species relative to their saturated analogues,[31] as expected given the stronger binding of phosphine ligands trans to an unsaturated NHC.[13] Importantly, however, the increased strength of the Ru–PCy_3 bond does not confer protection against donor-accelerated methylidene abstraction: like **Ru-2c**, the IPr complex **Ru-2d** undergoes complete decomposition to **2** within 2 h when ethylene and pyridine are simultaneously present, while the IMes derivative **Ru-2b** eliminates 74% **2**.[32] For the latter system, a minor contribution from an additional, unidentified pathway is implied by the observation of free PCy_3: 9% in the control experiment, and 26% in the presence of pyridine. As noted above, ^1H NMR analysis shows no evidence of the pyridinium salt $[MeNC_5H_5]Cl$,[33] ruling out the possibility that pyridine competes for attack on the methylidene site.

References begin on page 59

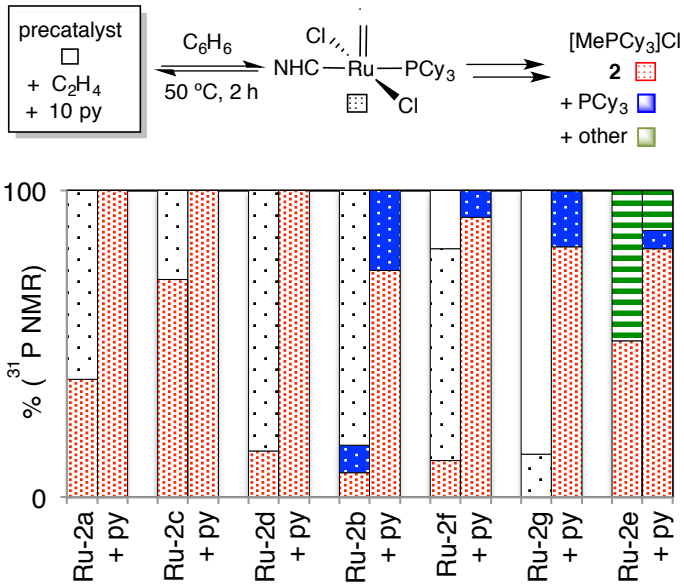

Figure 3.5 Accelerating effect of pyridine on decomposition of phosphine-stabilized catalysts under ethylene. Complexes grouped by behaviour; for codes, see Figure 3.1.

The indenylidene catalysts **Ru-2f** and **Ru-2g** (bearing H_2IMes and IMes ligands, respectively) are far less active than the other systems examined. In the absence of pyridine, catalyst initiation was incomplete in both cases, with 19% **Ru-2f**, and 86% **Ru-2g**, remaining unreacted even after 2 h at 50 °C under ethylene. (As expected, the balance was chiefly the resting-state methylidene complexes **Ru-4a** or **Ru-4b**). Again, however, poor turn-on efficiency does not protect against donor-accelerated methylidene abstraction. Both **Ru-2f** and **Ru-2g** show >80% decomposition to **2** in the presence of pyridine (91% for **Ru-2f**; 82% for **Ru-2g**). We infer that pyridine binding accelerates initiation for these species, but that methylidene abstraction is competitive with metathesis. As with **Ru-2b**, a small proportion of free PCy_3 was also observed.

The H_2ITol derivative **Ru-2e** likewise exhibited >80% elimination of **2** following treatment with ethylene and pyridine. Also present was ca. 10% of an as-yet unidentified species, observed as a $^{31}P\{^1H\}$ NMR singlet at 48.1 ppm. No alkylidene signal was

evident by ^{1}H NMR analysis, ruling out the possibility that this is simply a pyridine adduct of **Ru-2e** or its methylidene resting state. Complicating analysis is the presence of ca. 15% impurities in the commercial precatalyst (see Appendix 1).[34] Identification of the unknown species was therefore not pursued.

In all cases, the [$MePCy_3$]Cl marker **2** was the dominant ^{31}P-containing species present after 2 h exposure to ethylene at 50 °C. We conclude that abstraction of the methylidene ligand by phosphine is the major pathway operative, and that such abstraction is significantly accelerated by the Lewis donor pyridine.

3.2.3 Scope with respect to donor

Of keen interest is the extent to which Lewis bases other than pyridine and primary or secondary amines[19,21,35] accelerate methylidene abstraction. To examine this point, we treated **Ru-4a** and its less labile IMes analogue **Ru-4b** with a range of less potent donors at 50 °C. Shown in Table 3.1 is the proportion of **2** formed, vs. **Ru-4** remaining, after 2 h. These figures should be compared to a baseline value of 10% or 3% for **Ru-4a** or **Ru-4b**, respectively, in the base-free control experiments (entry 1). Values for pyridine are shown as the final table entry, for comparison. In all cases, the trend seen with the IMes complex **Ru-4b** parallels that with **Ru-4a**. While stronger Ru–PCy_3 binding lessens the impact on decomposition rates, it also limits entry into the active cycle for metathesis.

References begin on page 59

Table 3.1 Loss of Ru-4 and yield of [MePCy$_3$]Cl (2) on treatment with L-Donors (*n* Equiv) for 2 h at 50 °C[a]

entry	L-donor	n	% **Ru-4** lost (% **2** formed)	
			a: H_2IMes	**b**: IMes
1	None	0	10[d] (10)	3[d] (N.D.)
2	NEt_3	10	11 (11)	3 (N.D.)
3	$O{=}P(NMe_2)_3$	10	13 (13)	3 (N.D.)
4	$O{=}C(NMe_2)_2$	10	16 (16)	3 (N.D.)
5a	MeCN	10	11 (11)	3 (N.D.)
5b		neat	100 (100)	–
6a	THF	10	20 (20)	8 (8)
6b		100	30 (30)	–
7a	H_2O	10	25 (25)	10 (10)
7b		100	49 (49)	–
8a	DMSO	10	35 (35)	18 (16)
8b		100	93 (93)	–
9	MeOH	10	49 (49)	29 (29)
10	pyridine	10	100 (100)[b]	100 (90)[c]

[a] C_6D_6 solvent, [Ru] = 20 mM. % Loss of **Ru-4** determined by ^{1}H NMR analysis, by integration of the methylidene signal vs. internal standard (TMB); % **2** by ^{31}P{^{1}H} NMR analysis, as a percentage of total integration. N.D. = not determined; peak intensity insufficient for reliable ^{31}P NMR integration. **Ru-4** completes the mass balance, except where noted. [b] Complete in <10 min at RT. [c] For L = py, free PCy_3 accounts for the discrepancy between the proportion of **Ru-4b** lost vs. that of **2** formed. [d] The values of 10% and 3% decomposition for **Ru-4a** and **Ru-4b** are due to the background methylidene-abstraction reaction; Scheme 3.1.

The NEt_3, phosphoramide, and urea additives shown in entries 2-4 were chosen for the detrimental impact of these and related structures in other contexts, including in metathesis promoted by non-phosphine catalysts.[3,9,36-39] The absence of any significant impact for any of these indicates that the Lewis basicity of the donor is irrelevant, if steric

congestion precludes access to the metal center.[40] This is consistent with the prior finding that added DBU did not trigger decomposition of **Ru-2a** into **2** during catalysis.[19]

Of note, even relatively weak donors such as MeCN, THF, and H_2O accelerate decomposition (entries 5–7). Addition of MeCN had minimal impact in small amounts (10 equiv), but decomposition was quantitative at 2 h in neat MeCN (entries 5a, 5b; see also Figure 3.6a). Similarly, while 10 equiv THF and H_2O proved innocuous, a tenfold increase led to ca. 30% or 50% decomposition, respectively, notwithstanding the weak oxophilicity of these ruthenium complexes. The heightened effect of water and methanol, relative to THF (entries 7a and 9, vs. 6a), may be due to attractive hydrogen-bonding interactions with the chloride ligands. While additional decomposition pathways could be envisaged for these H-bond donors, **2** was the sole or dominant phosphorus product in all cases, indicating that methylidene abstraction is the principal vector for decomposition.

Accelerated methylidene abstraction by MeCN, THF, DMSO, H_2O, and MeOH helps to account for the sub-optimal metathesis performance of phosphine-functionalized catalysts in these solvents.[41-45] More generally, it provides the first clear explanation for low metathesis productivities in polar media, despite the correlation between solvent polarity and faster initiation (phosphine loss) established for **Ru-2a**.[46] This behaviour is of particular note given interest in metathesis in water and "green" solvents, often bearing ether donors.[43,44,47-49] The impact of water holds arguably even greater significance, given its ubiquity as a contaminant in synthetic and process chemistry.

References begin on page 59

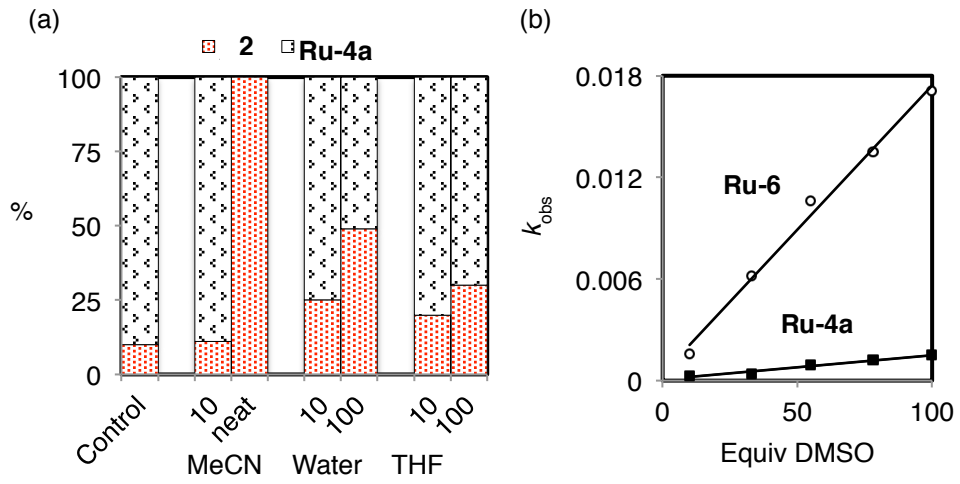

Figure 3.6 (a) Impact of donor stoichiometry on decomposition of $RuCl_2(H_2IMes)(PCy_3)(=CH_2)$ Ru-4a (C_6D_6, 50 °C, 2 h; data from Table 3.1). (b) First-order dependence of decomposition rates on [DMSO] for Ru-4a and Ru-6 at 25 °C. See Appendix 1.

3.2.4 Associative mechanism and implications

Rates of metathesis by **Ru-2a** and its analogues are independent of olefin concentration, because loss of PCy_3 is rate-limiting.[46] In the absence of donors, loss of PCy_3 likewise controls the rate of decomposition of the resting-state species **Ru-4a** and **Ru-4b**.[13,31] The rapidity with which these complexes decompose in the *presence* of donor ligands (see above) strongly suggests an associative pathway for the decomposition reaction, as does the impact of donor bulk and stoichiometry. For sterically accessible donors, coordination to the Ru center prior to PCy_3 loss would plausibly create a degree of steric pressure that promotes expulsion of the phosphine ligand.

To probe this point, **Ru-4a** was treated with varying concentrations of DMSO, with which decomposition is sufficiently slow to monitor at RT, and the rates of loss of **Ru-4a** (Figure 3.6b) and formation of **2** were measured. Both rates exhibit a first-order dependence on [DMSO]. Decomposition of the first-generation complex **Ru-6** was likewise first-order in [DMSO], but two notable differences emerged. First, the reaction

was five-fold faster (k_{obs} = 0.0003 and 0.0015 min^{-1} for **Ru-4a** and **Ru-6**, respectively). This is consistent with the reported[13] operation of the inverse trans effect in the NHC complex **Ru-4a**, which enhances the Ru–PCy_3 bond strength. Secondly, the rate of formation of **2** no longer corresponds to the rate of loss of **Ru-6**. This is consistent with displacement of both PCy_3 ligands from **Ru-6**, upon which the C-H activation step becomes rate-determining, as with the pyridine system shown in Scheme 3.2.[20]

While isolation of the σ-alkyl intermediate for the H_2IMes complex was precluded by facile C–H activation, as indicated above, the σ-alkyl complex $RuCl_2$(σ-CH_2PCy_3)$(DMSO)_3$ **Ru-12** decomposed slowly. Indeed, this complex could be isolated in ca. 60% yield following treatment of **Ru-6** with a 100-fold excess of DMSO (Scheme 3.3). Its molecular identity is supported by NMR and combustion analysis. The fac,*S*-coordination mode is proposed on the basis of the predominance of this binding mode in other Ru complexes.[50-52] IR evidence is consistent with *S*-binding (two strong ν(S=O) bands at 1072 and 1017 cm^{-1}, vs. an expected value of ca. 950 cm^{-1} for the *O*-bound linkage isomer). The chemical shifts and multiplicities for the Ru-CH_2PCy_3 moiety agree well with those for pyridine analogue **Ru-7** (see Figure 3.4 left).[20] The stability of these species reflects the absence of a readily-activated C-H bond, a consequence of the displacement of both PCy_3 ligands (see discussion above).

References begin on page 59

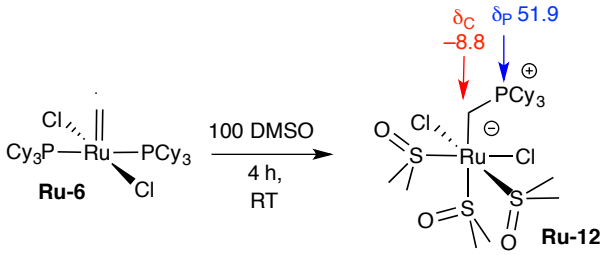

Scheme 3.3 σ-alkyl intermediates accessible by inhibiting C–H activation of ancillary ligands.

3.2.5 Impact on metathesis

The drastically inhibiting impact of amines in metathesis reactions catalyzed by **Ru-2a** has been described elsewhere.[19,21] The rapidity of decomposition, and the co-formation of **2**,[19] testify to the capacity of such donors to accelerate methylidene abstraction. To assess the impact of weaker donors, we examined the metathesis productivities attainable for the readily-cyclized diene diethyl diallylmalonate (DDM) in the presence of added water or methanol, or in neat THF, MeCN, or DMSO. The results are collected in Table 3.2. In the control experiment in anhydrous toluene, RCM was quantitative at 2 h at a catalyst loading of 0.05 mol%. This corresponds to a turnover number (TON) of 2,000. In neat THF at 50 °C, RCM activity dropped by more than 30%, to a TON of 1,440. The presence of 5% degassed H_2O in toluene caused a 65% drop in TON. With 5% MeOH, MeCN, and DMSO, the impact was even more detrimental: for the DMSO reaction, metathesis was essentially quenched. The ease with which DDM normally undergoes RCM underscores the severity of this degradation in metathesis performance.

Of note, reaction at 30 °C does not inhibit methylidene abstraction. Indeed, the impact of donors on total metathesis productivity is in general even more deleterious, in keeping with prior findings of faster increases in rates of metathesis as a function of temperature, relative to rates of decomposition.[9,57]

Table 3.2 Donor-accelerated decomposition: impact of weak donors on metathesis productivity[a]

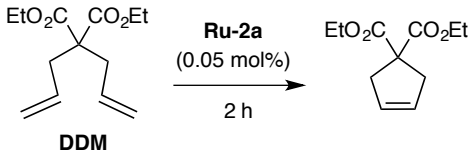

entry	solvent medium	% conv. (TON)[a]	
		50 °C	30 °C[58]
1	toluene	100 (2,000)[b]	100 (2,000)[c]
2	THF	72 (1,440)	13 (260)
3	20:1 toluene-H_2O	35 (700)	24 (480)
4	20:1 toluene-MeOH	18 (360)	5 (100)
5	20:1 toluene-MeCN	13 (260)	17 (340)
6	20:1 toluene-DMSO	1 (20)	1 (20)

[a] Calibrated GC-FID analysis; ±2% in replicate runs. [b] Quantitative within 10 min. [c] Quantitative within 60 min.

Of particular interest is the impact of the weak donor H_2O, which represents a ubiquitous contaminant in organic synthesis. To explicitly tie the presence of water to formation of **2** during catalysis, a related experiment was carried out with a pro-lactone (Scheme 3.4). Use of this substrate has the dual advantage of verifying the impact of water in an RCM reaction of broad interest, i.e. macrocyclization, while ensuring complete catalyst conscription at ruthenium loadings high enough to permit interrogation by NMR methods. Analysis after 2 h at 50 °C in 20:1 C_6D_6–H_2O indicates that **2** accounts for ca. 38% of the total $^{31}P\{^1H\}$ NMR integration, with ca. 50% being due to the resting-state methylidene complex **Ru-4a**. Also observed is a small amount of free PCy_3 (7%), and two minor, unidentified species. A control experiment confirmed that the proportion of **2** formed in the absence of water is substantially lower (7% **2**).

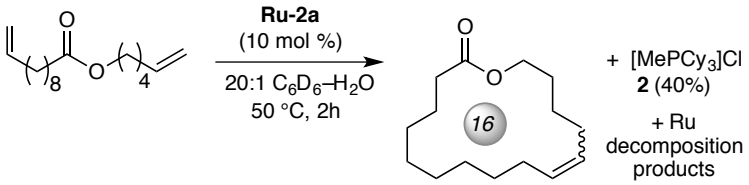

Scheme 3.4 Evidence for water-accelerated methylidene abstraction during RCM macrocyclization.

The Cazin group recently described the negative impact of water on RCM yields in the challenging cyclization of a derivative of diethyl diallylmalonate bearing geminally-disubstituted olefins.[59] The present study is only the second report of the severely deleterious impact of water on Ru-catalyzed olefin metathesis: it is the first to demonstrate that even facile metathesis reactions are affected, and to advance a mechanistic basis for this behaviour. While the present study does not rule out other, additional avenues for catalyst degradation, it clearly demonstrates that water significantly accelerates the methylidene-abstraction pathway.

3.2.6 Blocking methylidene abstraction

A final set of experiments examined the possibility that this decomposition pathway could be blocked by introducing a methyl substituent on the methylidene ligand. This question was inspired by reports of higher turnover numbers in metathesis when α-olefins were replaced by β-methyl olefins,[6,60-62] and by the trend in half-lives at 55 °C reported in the $RuCl_2(PCy_3)_2(=CHR)$ series: R = Ph, 8 days; R = Me, 8 h, R = H, 40 min.[55]

To test the resistance of the ethylidene moiety to abstraction by PCy_3, **Ru-13** was generated in situ in the presence of pyridine (Scheme 3.5). Complete conversion of **Ru-2a** into known[15] **Ru-13** and bis-pyridine adduct **Ru-14** (70:30) was evident after 1 h at 50

°C. Decomposition occurred over ca. 48 h, as compared to the timescale of minutes at RT for the methylidene complex **Ru-4a**. Unexpectedly, NMR analysis revealed that the major ^{31}P-containing product was [MePCy$_3$]Cl **2** (34.2 ppm; 56% of total integration) – despite the evidence for complete formation of the ethylidene complex – accompanied by PCy$_3$ (10.5 ppm, 34%) and O=PCy$_3$ (47.2 ppm, 10%). The identity of **2** was confirmed by MALDI-TOF mass spectrometry; no signal was observed for [EtPCy$_3$]Cl. We attribute liberation of **2** to isomerization of 2-butene into 1-butene (observed by ^{1}H NMR analysis), metathesis of which enables partial formation and decomposition of **Ru-4a**. These results indicate that use of 2-butene in cross-metathesis is an incomplete solution to the problem of catalyst decomposition. More fundamentally, they demonstrate that the ethylidene moiety indeed resists donor-accelerated decomposition, offering the first clear insight into the superior metathesis performance attainable with β-methyl olefins, vs. α-olefins.

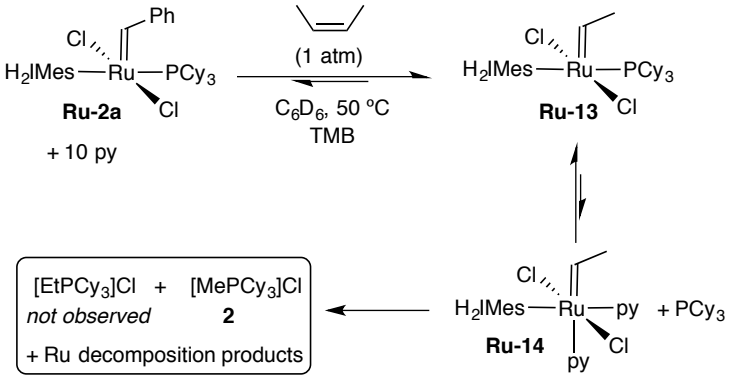

Scheme 3.5 Resistance of ethylidene ligand to nucleophilic abstraction by PCy$_3$.

3.3 Conclusions

The foregoing demonstrates that the resting-state methylidene complexes formed by phosphine-stabilized metathesis catalysts are subject to a common decomposition pathway: specifically, abstraction of the methylidene ligand as [MePCy$_3$]Cl **2**. Sterically

accessible Lewis donors are shown to accelerate this process, at rates that depend on donor concentration. Because of the associative nature of this pathway, even rather feeble donors such as THF, H_2O, and MeOH are able to promote decomposition when present in significant amounts, with drastic consequences even for metathesis of readily-cyclized substrates such as diethyl diallylmalonate. These results highlight the limited compatibility of phosphine-functionalized metathesis catalysts with substrates bearing a terminal olefin. Wherever sterically accessible donor functionalities are present (whether in the solvent, within the substrate structure, or in contaminants), they can trigger irreversible loss of the critical methylidene moiety from the active species. Installation of a β-methyl substituent is shown to circumvent this catalyst decomposition pathway.

3.4 Future work

The work in this chapter demonstrated that water can promote decomposition of phosphine-bearing metathesis catalysts via donor-accelerated decomposition. Of considerable interest is the possibility of additional, more general pathways involving O–H bond activation. In prior studies with primary and secondary amines, N–H activation resulted in facile loss of the [Ru]=CHR moiety, without NHC cyclometallation.[19] Thus, in the reaction of **Ru-4a** with secondary amines, liberation of $[MePCy_3]Cl$ **2** was mediated by proton transfer from the NH group of the coordinated amine.[20] In the corresponding reaction of **Ru-2** with $NH_2{}^nBu$, nucleophilic attack of the primary amine on the benzylidene carbon was followed by a 1,2-proton shift, as judged by the elimination of NH^nBuCH_2Ph.[19] Shuttling of protons by N-H activation is well established for Ru-amine chemistry.[70,71]

References begin on page 59

In the case of reactions with water, low nucleophilicity is likely to disfavor the second pathway, but proton transfer from bound water could plausibly contribute to liberation of [$MePCy_3$]Cl **2** via a low-energy pathway that circumvents NHC cyclometallation. By extension, H_2O could potentially reduce the barrier to methylidene / alkylidene loss, via activation of the O–H bond in bound water, following attack by PCy_3 or other nucleophiles at the [Ru]=CHR carbon. This could be probed by tracking incorporation of a deuterium label during decomposition of **Ru-4a** by D_2O.

An additional recommended study stemming from Chapter 3 is the re-examination of methods for NMR quantitation of phosphorus-containing species. The standard broad-band decoupled $^{31}P\{^1H\}$ NMR experiments used to quantify **Ru-4a** and [$MePCy_3$]Cl **2** in Chapter 3 are problematic because of the faster relaxation of ^{31}P nuclei that bear nearby protons, as well as disproportionate NOE enhancement. An alternative experiment that can be used to minimize NOE effects, and hence to achieve more accurate quantification, involves inverse gated decoupling; that is, applying ^1H decoupling during signal acquisition, but not during the recycle delay.

3.5 References

(1) Grela, K., *Olefin Metathesis-Theory and Practice*. Wiley: Hoboken, NJ, 2014.
(2) Grubbs, R. H.; Wenzel, A. G., *Handbook of Metathesis*. 2nd ed.; Wiley-VCH: Weinheim, 2015.
(3) Higman, C. S.; Lummiss, J. A. M.; Fogg, D. E. *Angew. Chem., Int. Ed.* **2016**, *55*, 3552–3565.
(4) Farina, V.; Horváth, A., Ring-Closing Metathesis in the Large-Scale Synthesis of Pharmaceuticals. In *Handbook of Metathesis*, Grubbs, R. H.; Wenzel, A. G., Eds. Wiley-VCH: Weinheim, 2015; Vol. 2, pp 633–658.
(5) Fandrick, K. R.; Savoie, J.; Jinhua, N. Y.; Song, J. J.; Senanayake, C. H., Challenges and Opportunities for Scaling the Ring-Closing Metathesis Reaction in the

Pharmaceutical Industry. In *Olefin Metathesis – Theory and Practice*, Grela, K., Ed. Wiley: Hoboken, 2014; pp 349-366.

(6) Pederson, R. L.; Nickel, A., Commercial Potential of Olefin Metathesis of Renewable Feedstocks. In *Olefin Metathesis-Theory and Practice*, Grela, K., Ed. Wiley: Hoboken, NJ, 2014; pp 335–348.

(7) Chadwick, J. C.; Duchateau, R.; Freixa, Z.; van Leeuwen, P. W. N. M., *Homogeneous Catalysts: Activity – Stability – Deactivation*. Wiley-VCH: Weinheim, 2011.

(8) Hubner, S.; de Vries, J. G.; Farina, V. *Adv. Synth. Catal.* **2016**, *358*, 3–25.

(9) van Lierop, B. J.; Lummiss, J. A. M.; Fogg, D. E., Ring-Closing Metathesis. In *Olefin Metathesis-Theory and Practice*, Grela, K., Ed. Wiley: Hoboken, NJ, 2014; pp 85–152.

(10) For the poor kinetic competence of molecular hydride species often cited as potential culprits, see: (a) Higman, C. S.; Plais, L.; Fogg, D. E. *ChemCatChem* **2013**, *5*, 3548-3551. For the involvement of Ru nanoparticles formed following loss of [$MePCy_3$]Cl from **Ru-2a**, see: (b) Higman, C. S.; Lanterna, A. E.; Marin, M. L.; Scaiano, J. C.; Fogg, D. E. *ChemCatChem* **2016**, *8*, 2446–2449.

(11) Hughes, D. L. *Org. Process Res. Dev.* **2016**, *20*, 1008−1015.

(12) Styrenyl ether-stabilized catalysts of the Hoveyda class, in contrast, readily enter the active cycle for metathesis, as indicated by experiments with a ^{13}C-labelled styrenyl ether. See: Bates, J. M.; Lummiss, J. A. M.; Bailey, G. A.; Fogg, D. E. *ACS Catal.* **2014**, *4*, 2387−2394.

(13) Lummiss, J. A. M.; Higman, C. S.; Fyson, D. L.; McDonald, R.; Fogg, D. E. *Chem. Sci.* **2015**, *6*, 6739–6746.

(14) Lummiss, J. A. M.; Perras, F. A.; Bryce, D. L.; Fogg, D. E. *Organometallics* **2016**, *35*, 691–698.

(15) Sponsler and co-workers pointed out the corresponding labilizing effect of alkylidene substituents on metathesis reactivity. See: Williams, J. E.; Harner, M. J.; Sponsler, M. B. *Organometallics* **2005**, *24*, 2013–2015.

(16) Hong, S. H.; Wenzel, A. G.; Salguero, T. T.; Day, M. W.; Grubbs, R. H. *J. Am. Chem. Soc.* **2007**, *129*, 7961–7968.

(17) For precedents for attack of phosphine on a [Ru]=CHR carbon in complexes related to **Ru-2a**, see: (a) Burrell, A. K.; Clark, G. R.; Rickard, C. E. F.; Roper, W. R.; Wright, A. H. *J. Chem. Soc., Dalton Trans.* **1991**, 609-614. (b) Werner, H.; Stuer, W.; Weberndorfer, B.; Wolf, J. *Eur. J. Inorg. Chem.* **1999**, 1707–1713. (c) Hansen, S. M.; Rominger, F.; Metz, M.; Hofmann, P. *Chem. Eur. J.* **1999**, *5*, 557–566. (d) Galan, B. R.; Pitak, M.; Keister, J. B.; Diver, S. T. *Organometallics* **2008**, *27*, 3630–3632. See below for evidence supporting the intermolecular pathway depicted in 3.1.

(18) Methylidene abstraction was reportedly slow for **Ru-4a** at 55 °C, requiring 3 days for complete decomposition. See: ref 16. In separate experiments, we measured a decomposition half-life of ca. 160 min at 60 °C (specifically, 53% loss of alkylidene signals, 45% **2** (ref 14), a figure in good agreement with the value of 144 min measured in ref 19.

(19) Lummiss, J. A. M.; Ireland, B. J.; Sommers, J. M.; Fogg, D. E. *ChemCatChem* **2014**, *6*, 459–463.

(20) Lummiss, J. A. M.; McClennan, W. L.; McDonald, R.; Fogg, D. E. *Organometallics* **2014**, *33*, 6738–6741.

(21) Lummiss, J. A. M.; Botti, A. G. G.; Fogg, D. E. *Catal. Sci. Technol.* **2014**, *4*, 4210–4218.

(22) For selected examples of the C–H activation of mesityl *o*-methyl groups in ruthenium complexes of H_2IMes and IMes, see ref 16 and: (a) Jazzar, R. F. R.; Macgregor, S. A.; Mahon, M. F.; Richards, S. P.; Whittlesey, M. K. *J. Am. Chem. Soc.* **2002**, *124*, 4944–4945. (b) Chilvers, M. J.; Jazzar, R. F. R.; Mahon, M. F.; Whittlesey, M. K. *Adv. Synth. Catal.* **2003**, *345*, 1111–1114. (c) Abdur–Rashid, K.; Fedorkiw, T.; Lough, A. J.; Morris, R. H. *Organometallics* **2004**, *23*, 86–94. (d) Leitao, E. M.; Dubberley, S. R.; Piers, W. E.; Wu, Q.; McDonald, R. *Chem. Eur. J.* **2008**, *14*, 11565–11572. (e) Endo, K.; Herbert, M. B.; Grubbs, R. H. *Organometallics* **2013**, *32*, 5128-5135.

(23) For leading references, see ref 13 and: (a) Comas-Vives, A.; Harvey, J. N. *Eur. J. Inorg. Chem.* **2011**, 5025-5035. (b) Vummaleti, S. V. C.; Nelson, D. J.; Poater, A.; Gomez-Suarez, A.; Cordes, D. B.; Slawin, A. M. Z.; Nolan, S. P.; Cavallo, L. *Chem. Sci.* **2015**, *8*, 1895–1904.

(24) Fernandez, I.; Lugan, N. l.; Lavigne, G. *Organometallics* **2012**, *31*, 1155−1160.

(25) Credendino, R.; Falivene, L.; Cavallo, L. *J. Am. Chem. Soc.* **2012**, *134*, 8127–8135.

(26) Gallagher, M. M.; Rooney, A. D.; Rooney, J. J. *J. Organomet. Chem.* **2008**, *693*, 1252–1260.

(27) Kotyk, M. W.; Gorelsky, S. I.; Conrad, J. C.; Carra, C.; Fogg, D. E. *Organometallics* **2009**, *28*, 5424–5431.

(28) Sanford, M. S.; Love, J. A.; Grubbs, R. H. *Organometallics* **2001**, *20*, 5314–5318.

(29) Conrad, J. C.; Yap, G. P. A.; Fogg, D. E. *Organometallics* **2003**, *22*, 1986–1988.

(30) Independent decomposition experiments with first-generation complex **Ru-6** likewise support an intermolecular pathway, even in the absence of added donors. Thus, a half-life of 67 ±3 h was measured for **Ru-6** at 22 °C in C_6D_6, but this figure dropped to 13.5 ±0.2 h when 10 equiv PCy_3 was present. The stability of this complex exhibits a non-linear dependence on temperature.

(31) The background reaction, i.e. methylidene abstraction in the absence of an added donor, was shown to be dissociative in PCy_3 in experiments carried out on the **Ru-4a** system. See: refs 13 and 16. For a detailed kinetics derivation, see Supporting Information for ref 13.

(32) A slight increase in the proportion of PCy_3 is observed under ethylene, relative to the experiments with the isolated methylidene complexes **Ru-4b**. This is consistent with the operation of additional elimination pathways in the presence of ethylene. See: van Rensburg, W. J.; Steynberg, P. J.; Meyer, W. H.; Kirk, M. M.; Forman, G. S. *J. Am. Chem. Soc.* **2004**, *126*, 14332–14333.

(33) The poor solubility of the pyridinium salt in non-polar solvents (confirmed with an authentic sample of $[MeNC_6H_5]Cl$) could mask its presence in this experiment. The benzene solvent was therefore evaporated, and the residue redissolved in $CDCl_3$. The ^1H NMR spectrum showed no evidence of the diagnostic methyl singlet seen for authentic samples at 4.79 ppm in $CDCl_3$ (see Appendix 1).

(34) These impurities may also contribute to elimination of **2** from the H_2ITol catalyst **Ru-2e**. However, the commercial availability of this catalyst has been discontinued owing to problems with decomposition on long-term storage. It has been replaced by its phosphine-free styrenyl ether analogue. Personal Communication, John Phillips, Catalyst R&D, Materia, Inc.

(35) Half-lives for decomposition of $RuCl_2(H_2IMes)(PCy_3)(=CH_2)$ **Ru-4a** on addition of 1 equiv L (20 mM Ru, C_6D_6). At RT: with H_2N^nBu, < 3 min; with pyrrolidine, 87 min; with morpholine, 14 h; with DBU, >24 h, as compared to >24 h in the absence of added L. At 60 °C: with H_2N^nBu, < 3 min; with pyrrolidine, 8 min; with morpholine, 35 min; with DBU, 127 min (ref 19). For values in the absence of added L, see: refs 18, 19.

(36) Wang, H.; Matsuhashi, H.; Doan, B. D.; Goodman, S. N.; Ouyang, X.; Clark, W. M. *Tetrahedron* **2009**, *65*, 6291–6303.

(37) Wang, H.; Goodman, S. N.; Dai, Q.; Stockdale, G. W.; Clark, W. M. *Org. Process Res. Dev.* **2008**, *12*, 226–234.

(38) Ireland, B. J.; Dobigny, B. T.; Fogg, D. E. *ACS Catal.* **2015**, *5*, 4690−4698.

(39) Nagarkar, A. A.; Crochet, A.; Fromm, K. M.; Kilbinger, A. F. M. *Macromolecules* **2012**, *45*, 4447–4453.

(40) While binding of tertiary amines such as NEt_3 to Ru centers has been established, the complexes involved are less sterically congested arylphosphine derivatives. For a discussion of such complexes and their degradation products, see: Fogg, D. E.; James, B. R. *Inorg. Chem*. **1995**, *34*, 2557–61.

(41) Zhao, Z.-X.; Wang, H.-Y.; Guo, Y.-L. *Rapid Commun. Mass Spectrom.* **2011**, *25*, 3401-3410.

(42) Donor-accelerated methylidene abstraction accounts for the observation of shorter lifetimes for **Ru-4** and related methylidene complexes in THF. See: refs 13, 21. For the methylidene derivative of **Ru-1**, for example, the half-life at 35 °C in THF was 1.1 h, vs. 2.5 h in CH_2Cl_2, and 6.6 h in C_6H_6. See: ref 21.

(43) Tomasek, J.; Schatz, J. *Green Chem.* **2013**, *15*, 2317–2338.

(44) Grela, K.; Gulajski, L.; Skowerski, K., Alkene Metathesis in Water. In *Metal-Catalyzed Reactions in Water*, Dixneuf, P. H.; Cadierno, V., Eds. Wiley-VCH: Weinheim, 2013; pp 291–336.

(45) Stark, A.; Ajam, M.; Green, M.; Raubenheimer, H. G.; Ranwell, A.; Ondruschka, B. *Adv. Synth. Catal.* **2006**, *348*, 1934–1941.

(46) Sanford, M. S.; Love, J. A.; Grubbs, R. H. *J. Am. Chem. Soc.* **2001**, *123*, 6543–6554.

(47) Bantreil, X.; Sidi-Ykhlef, M.; Aringhieri, L.; Colacino, E.; Martinez, J.; Lamaty, F. *J. Catal.* **2012**, *294*, 113–118.

(48) Bilel, H.; Hamdi, N.; Zagrouba, F.; Fischmeister, C.; Bruneau, C. *Green Chem.* **2011**, *13*, 1448–1452.

(49) Miao, X.; Fischmeister, C.; Bruneau, C.; Dixneuf, P. H. *ChemSusChem* **2008**, *1*, 813–816.

(50) Alessio, E. *Chem. Rev.* **2004**, *104*, 4203–4242.

(51) Evans, I. P.; Spencer, A.; Wilkinson, G. *J. C. S. Dalton Trans.* **1973**, 204.

(52) Seddon, E. A.; Seddon, K. R., *The Chemistry of Ruthenium*. Elsevier: Amsterdam, 1984.

(53) Measured rate constants (k_{obs}) for decomposition on reaction with 10 DMSO at 25 °C: for disappearance of **Ru-4a**: 0.003 min^{-1}; for disappearance of **Ru-4a^{D}**: 0.002 min^{-1} ($k_H/k_D = 1.5$).

(54) Gomez-Gallego, M.; Sierra, M. A. *Chem. Rev.* **2011**, *111*, 4857–4963.

(55) Ulman, M.; Grubbs, R. H. *J. Org. Chem.* **1999**, *64*, 7202–7207.

(56) Formation of non-labelled **A**, d_2-**A** and d_3-**A**, in addition to the expected d_1-**A**, may reflect scrambling between the mesityl *o*-CD_3 group, the Ru=CH_2 functionality, and the cyclohexyl rings. An early report described exchange between the methylidene and cyclohexyl sites in the *d*-labelled first-generation system $RuCl_2(PCy_3)(=CD_2)$. See: ref (55) An alternative, intriguing possibility raised by a referee is reversible C–H activation.

(57) Monfette, S.; Eyholzer, M.; Roberge, D. M.; Fogg, D. E. *Chem. Eur. J.* **2010**, *16*, 11720–11725.

(58) In comparison, use of the second-generation Hoveyda catalyst resulted in 100% conversion in neat toluene or 20:1 toluene-MeCN under the conditions of Table 3.2, but 31% in 20:1 toluene-H_2O, consistent with Cazin's finding (ref 59) of a more generally deleterious role for water than has hitherto been acknowledged.

(59) Guidone, S.; Songis, O.; Nahra, F.; Cazin, C. S. J. *ACS Catal.* **2015**, *5*, 2697–2701.

(60) Patel, J.; Mujcinovic, S.; Jackson, W. R.; Robinson, A. J.; Serelis, A. K.; Such, C. *Green Chem.* **2006**, *8*, 450–454.

(61) Nickel, A.; Ung, T.; Mkrtumyan, G.; Uy, J.; Lee, C. W.; Stoianova, D.; Papazian, J.; Wei, W.-H.; Mallari, A.; Schrodi, Y.; Pederson, R. L. *Top. Catal.* **2012**, *55*, 518–523.

(62) Vancompernolle, T.; Vignon, P.; Trivelli, X.; Mortreux, A.; Gauvin, R. M. *Cat. Commun.* **2016**, *77*, 75-78.

(63) Arduengo, A. J.; Dias, H. V. R.; Harlow, R. L.; Kline, M. *J. Am. Chem. Soc.* **1992**, *114*, 5530–5534.

(64) van Lierop, B. J.; Reckling, A. M.; Lummiss, J. A. M.; Fogg, D. E. *ChemCatChem* **2012**, *4*, 2020–2025.

(65) Fürstner, A.; Ackermann, L.; Gabor, B.; Goddard, R.; Lehmann, C. W.; Mynott, R.; Stelzer, F.; Thiel, O. R. *Chem. Eur. J.* **2001**, *7*, 3236–3253.

(66) Lummiss, J. A. M.; Beach, N. J.; Smith, J. C.; Fogg, D. E. *Catal. Sci. Technol.* **2012**, *2*, 1630–1632.

(67) Fürstner, A.; Langemann, K. *Synthesis* **1997**, 792–803.

(68) Arduengo, A. J.; Krafczyk, R.; Schmutzler, R.; Craig, H. A.; Goerlich, J. R.; Marshall, W. J.; Unverzagt, M. *Tetrahedron* **1999**, *55*, 14523–14534.

(69) Bailey, G. A.; Fogg, D. E. *ACS Catal.* **2016**, *6*, 4962–4971.

(70) O, W. W. N.; Morris, R. H. *ACS Catal.* **2013**, *3*, 32–40.

(71) Gunanathan, C.; Milstein, D. *Acc. Chem. Res.* **2011**, *44*, 588–602.

References begin on page 59

Chapter 4. Exploring the C-H activation step in donor-accelerated methylidene abstraction using a deuterium-labelled NHC

4.1 Introduction

Isotopic labelling, in conjunction with NMR and mass spectrometric analysis, has long been used to probe reaction mechanisms.[1-3] Incorporation of a label can be particularly useful where standard spectroscopic techniques are ineffective. Where rates of elementary steps are similar, for example, such methods can aid in identifying the rate-determining step.[4] Measurements of kinetic isotope effects (KIEs) are also valuable in eliciting details about the rate-determining step.[4] As well, labelling studies can reveal whether species observed during catalysis are intermediates, or simply kinetically inactive, off-cycle species (including decomposition products).

The use of isotopic labelling to clarify mechanistic questions in olefin metathesis has benefited greatly from recently developed synthetic routes to labelled ligands[5] and catalysts.[6-8] Shown in Figure 4.1 are key labelled catalysts, both phosphine-stabilized and phosphine-free, and the resting state species for the Grubbs catalysts. Also advantageous is the parallel development of mass spectrometric techniques suitable for observation of organometallic species.[2,9-12] Particularly important for the analysis of *neutral* complexes is the development of charge-transfer MALDI mass spectrometry (MALDI = matrix-assisted laser desorption-ionization), which enables detection of the radical molecular

cations.[9] Recent advances have improved the capacity to observe such species with minimal fragmentation.[13]

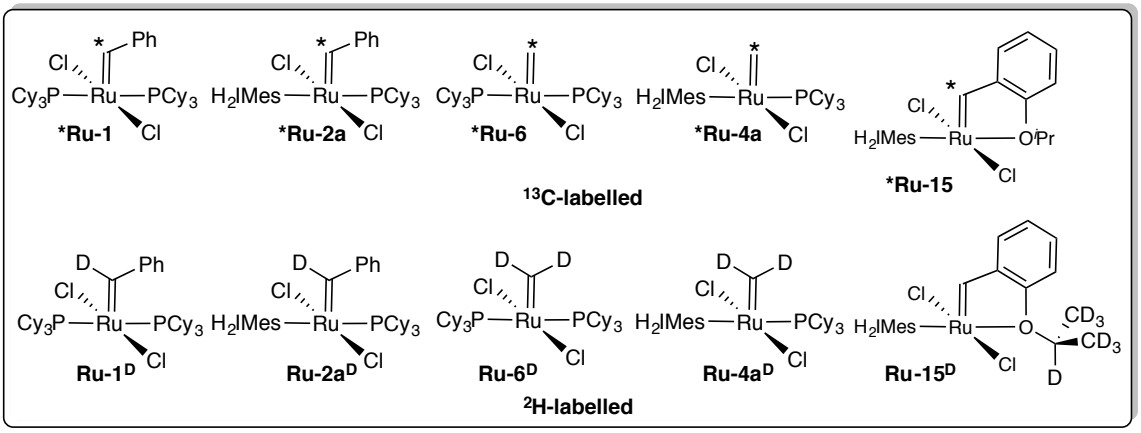

Figure 4.1 Selected ^{13}C-labelled and ^{2}H-labelled metathesis catalysts.

Among the most widely used isotopic labelling experiments are crossover experiments and H/D labelling.[4] Within the context of olefin metathesis, experiments with labelled olefins have afforded vital evidence for both the Chauvin mechanism,[14-16] and the long-debated "boomerang mechanism" for metathesis via the Hoveyda catalyst.[7,8] Thus, early studies by the Grubbs group examined the competitive RCM of labelled and non-labelled 1,7-octadiene **4** (Figure 4.2). A distribution of ethylene isotopomers was observed, consistent only with the Chauvin mechanism.

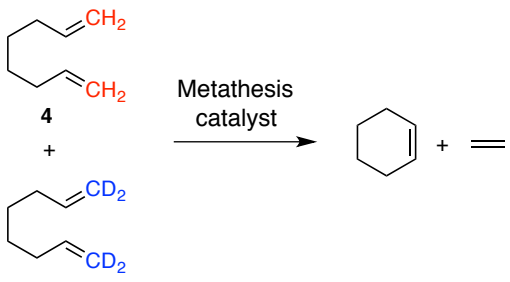

Predicted product ratios		
Isotopomers	Chauvin	Pairwise
$D_2C{=}CD_2$ + $H_2C{=}CD_2$ + $H_2C{=}CH_2$	1 : 2 : 1	1 : 0 : 1

Figure 4.2 Labelling study supporting the Chauvin mechanism for olefin metathesis.

Evidence for the "boomerang" re-uptake of styrenyl ether in metathesis[8,17-20] using the Hoveyda catalyst **Ru-15** was reported by the Grela and Fogg groups, using a ^{2}H- or ^{13}C-

labelled styrenyl ether ***7***, respectively.[7,8] The ^{13}C-labelled work is described here, as it eliminates the risk of Ru-promoted H/D exchange, an ever-present hazard when carrying out labelling experiments with Ru species. Thus, uptake of ***7*** was assessed during RCM of diene **5** (Figure 4.3), from the emergence of a ^{1}H NMR doublet for the alkylidene proton in ***Ru-15*** (16.71 ppm; $^{1}J_{CH}$ = 167.1 Hz). The ratio of labelled vs. unlabelled catalyst reached near-equilibrium values (45% ***Ru-15***) in just 10 min, providing clear evidence that the boomerang pathway is operative.

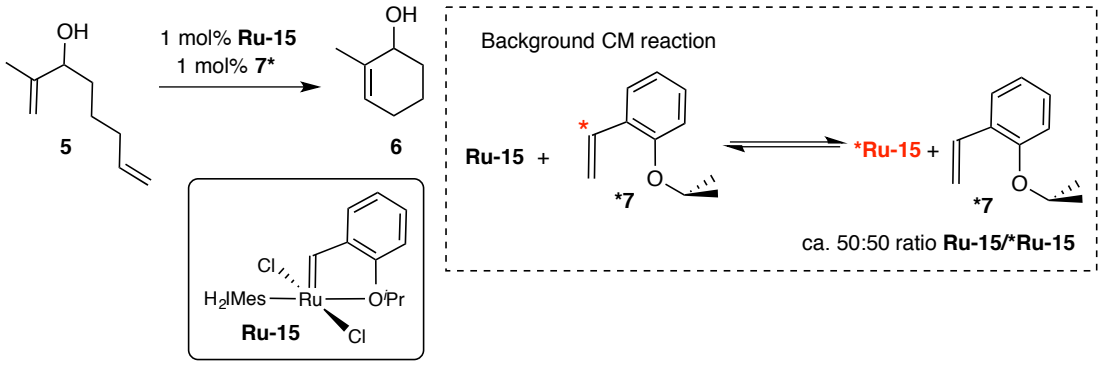

Figure 4.3 Labelling study supporting the boomerang mechanism for the Hoveyda catalyst Ru-15.

Leitao and Piers used *d*-labelling to explore thermal decomposition of the four-coordinate Piers catalyst, phosphonium-alkylidene **Ru-16** (Scheme 4.1).[21] The authors synthesized three isotopomers in which the methyl groups of the H_2IMes ligand were fully or partially deuterated. These were used to measure KIEs for decomposition to **Ru-17**. Large KIEs were observed (4.4 and 6.9 for inter- and intramolecular KIEs respectively), consistent with a primary kinetic isotope effect. Activation of a C-H bond in the *o*-methyl position of the H_2IMes ligand was hence proposed as the rate-determining step in decomposition.

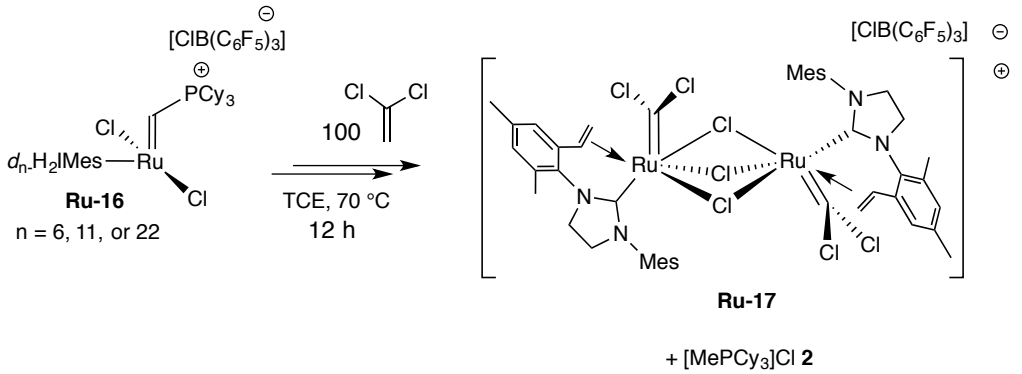

Scheme 4.1 Thermal decomposition of ruthenium phosphonium alkylidene Ru-16.

Courchay and Wagener also used a deuterium-labelled *N*-heterocyclic carbene (NHC) to probe the role of C-H activation on isomerization during catalyst deactivation.[28] They showed the formation of a deuteride complex during metathesis with various substrates and a competitive H/D exchange process between the CD_3 groups on the NHC and the C-H bond of the substrates. It was proposed that the exchange is promoted by a ruthenium dihydride intermediate.

Other notable examples of the mechanistic value of isotopic labelling in metathesis include evidence for the chain-carrying role of metal alkylidene intermediates,[22] and the competence of ring-closing[23-25] or cross-metathesis[26,27] relative to non-productive metathesis, and to characterize or track the release and return of solid-supported catalysts.[18,29]

Noted above was the importance of developing robust synthetic routes to labelled species. A breakthrough in the context of metathesis was the development by Justin Lummiss of the Fogg group of a high-yield route to methylidene complex **Ru-4a** (the catalyst resting state in metathesis of terminal olefins; see Chapter 1), bearing a ^{13}C label

at the key Ru=CH_2 site.[6] This proved invaluable in tracking the fate of the methylidene ligand. Abstraction of the methylidene moiety by both phosphine and amine was demonstrated, with the former being the dominant pathway (Scheme 4.2).[6]

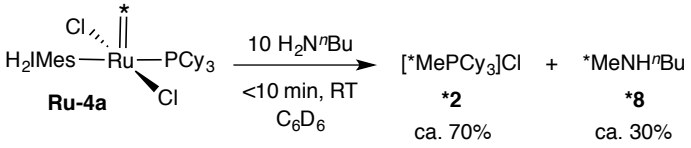

Scheme 4.2 Decomposition of Ru-4a by H_2N^nBu: competing methylidene abstraction by the amine and PCy_3 ligand.

The present Chapter describes the use of isotopic labelling to gain deeper mechanistic insight into the donor-accelerated deactivation (DAD) pathway presented in Chapter 3. A key question is the origin of the proton required to liberate [$MePCy_3$]Cl **2** from **Ru-11a**, the zwitterionic intermediate generated by nucleophilic attack of PCy_3 on the methylidene ligand. One plausible site of deprotonation is the mesityl *o*-methyl group of the H_2IMes ligand. Such benzylic C-H activation, resulting in cyclometallated ruthenium products (Figure 4.4) has been established as a recurring feature for the H_2IMes and IMes ligands,[30-33] including in the Piers catalyst decomposition study described above. To examine whether methylidene abstraction is completed by such a step, a deuterium-labelling study was undertaken.

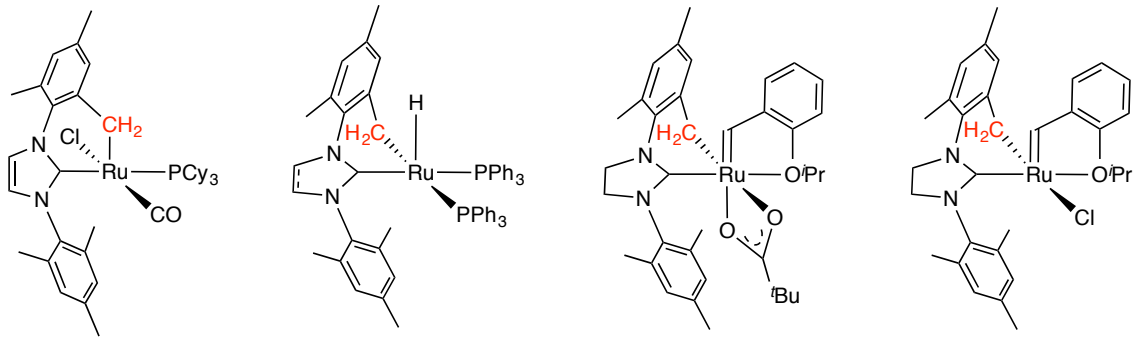

Ru-18
Grubbs 2003[30]
δ_H 3.29 and 2.17

Ru-19a (NHC = H_2IMes)
Ru-19b (NHC = (IMes)
Morris 2004[31]
δ_H 3.38 and 2.25
d_H 3.80 and 2.20

Ru-20
Grubbs 2011[32]
δ_H 3.44 and 3.30

Ru-21
Grubbs 2013[33]
δ_H 3.15 and 2.18

Figure 4.4 Literature examples of C-H activated H_2IMes and IMes ligands. Chemical shifts are in ppm.

4.2. Results and discussion

The goal of this project was synthesis of the methylidene complex ***d*$_{22}$-Ru-4a**, and determination of whether decomposition resulted in deuterium uptake into the [MePCy3]Cl **2** product. Accordingly, a synthetic route to ***d*$_{22}$-Ru-4a** was developed, building on Piers' report of the synthesis of the deuterated imidazolinium chloride d_{22}-[H_2IMes]•HCl,[21] and the Lummiss-Fogg route to the second-generation methylidene complexes.[34]

4.2.1 Synthesis of *d*$_{22}$-glyoxal-bis(2,4,6-trimethylphenyl)imine 12

The Piers synthesis of the labelled imidazolium salt requires five steps from commercially available d_{12}-mesitylene **9** (98% isotopic enrichment).[21] The first two steps, culminating in the labelled aniline, are shown in Scheme 4.3. Addition of nitric acid/acetic anhydride to a solution of **9** in acetic anhydride led to complete reaction after 1.5 h (assessed by TLC monitoring), as expected from the literature report. After 1.5 h, the nitrated product **10** was precipitated from ice water. Some difficulties were encountered on isolation, however. The product **10** initially formed a yellow oil, and

attempts at filtration resulted in a significant reduction of yield. However, cooling for 20 min or more resulted in solid crystals suitable for filtration, and the product **10** was isolated in 91% yield.

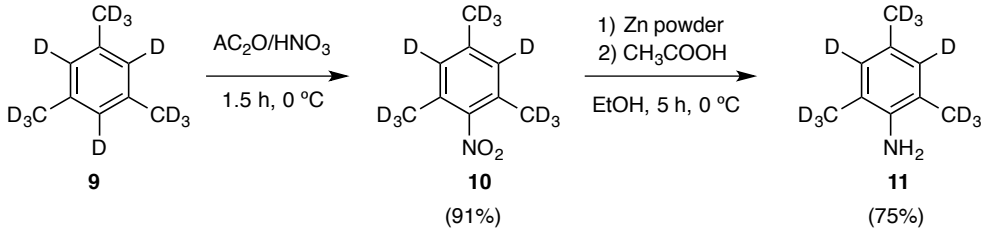

Scheme 4.3 Synthetic route to d_{11}-2,4,6-trimethyl aniline 11.

Reduction of **10** to form aniline **11** involved treatment with zinc powder and acetic acid. Additional details are provided here, to supplement those provided in the literature report. Activation of the zinc reagent (by stirring in 2% HCl, and successive washing with water, 95% ethanol, and diethyl ether) was essential, as reaction times otherwise varied between 5 and 24 h. In the original procedure, once the reaction was complete (again, as judged by TLC analysis), the product was isolated by quenching with aqueous NaOH (1 M) and extracting with petroleum ether. In our hands, addition of the NaOH solution resulted in a thick slurry, presumably of ZnO, which resisted extraction. The slurry was therefore diluted with petroleum ether before filtering through Celite, and the Celite was extracted repeatedly with further petroleum ether. The ultimate yield of 75% compares with 82% in the literature report. To simplify workup, an alternative procedure was attempted, involving reduction of unlabelled material with Pd/C under H_2 pressure. However, conversions were incomplete even after stirring for 24 hours at RT under 3 atm in THF.

With **11** in hand, synthesis of the labelled imine **12** was undertaken (Scheme 4.4).[35] Accordingly, a solution of **11** in glyoxal and methanol was stirred with a catalytic amount

of formic acid for 12 h at room temperature. A yellow-brown solid precipitated overnight, which was collected by filtration and washed with methanol to remove brown impurities. This treatment afforded **12** as a yellow solid in 68% yield.

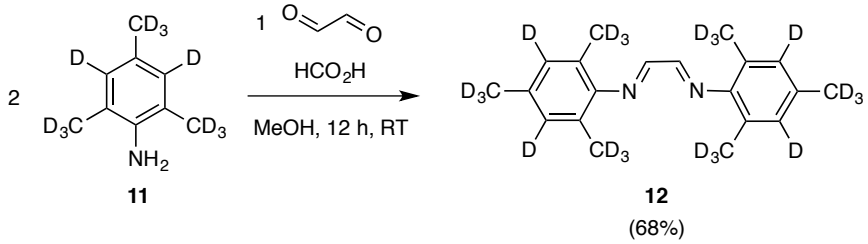

Scheme 4.4 Synthesis of d_{22}-glyoxal-bis(2,4,6-trimethylphenyl)imine 12.

4.2.2 Synthesis of d_{22}-1,3-bis(2,4,6-trimethyphenyl)imidazolinium chloride 14

Synthesis of the labelled imidazolinium chloride **14** was carried using the method for the non-labelled isotopologue (Scheme 4.5).[35] Reduction of diimine **12** to the corresponding diamine **13** (Scheme 4.5) was effected by stirring with sodium borohydride in THF/methanol for 4 h. Quenching with ice water and acidifying with 3M HCl caused the product to precipitate as the dihydrochloride salt **13**. Filtration yielded white **13** in 60% yield. To convert **13** to heterocyclic **14**, a suspension of the diamine in neat triethylorthoformate was heated at 135 °C with a catalytic amount of formic acid, and the ethanol by-product from the cyclization reaction was distilled off as it formed, under a gentle aspirator vacuum. Once evolution of ethanol ceased, the solution was cooled in an ice bath to precipitate the product. This was filtered off and washed with petroleum ether to deliver white **14** in 81% yield.

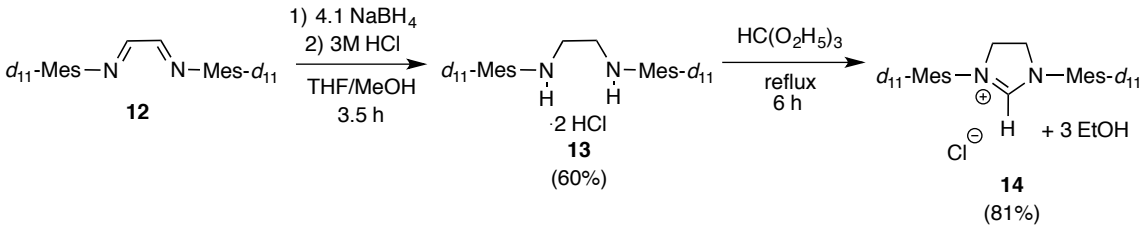

12 → **13** (60%) → **14** (81%)

Scheme 4.5 Synthetic route to d_{22}-1,3-bis(2,4,6-trimethyphenyl)imidazolinium chloride 14.

4.2.3 Synthesis of free d_{22}-H_2IMes

In the Piers route to ***d*$_{22}$-Ru-2a**, the free carbene was generated in situ by deprotecting the imidazolinium chloride **14** with potassium bis(trimethylsilyl)amide (KHMDS; Scheme 4.6).[21] Although widely used to prepare NHC complexes, this procedure suffers from a number of disadvantages, which have been outlined elsewhere.[36] Briefly, excess base is required to ensure complete consumption of the imidazolinium salt. This can cause side-reactions, including unintended loss of catalyst, during metathesis reactions.[30] Washing out the unreacted base with methanol, however, can generate methoxide ion, which is even more aggressive in triggering catalyst decomposition.[37]

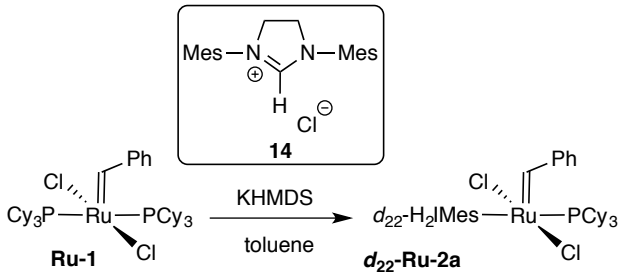

Scheme 4.6 Synthesis of the second-generation Grubbs catalyst via in situ liberation of the free NHC.

Ligand exchange of **Ru-1** with the free carbene, in comparison, was shown to offer rigorously clean **Ru-2a**.[36] This approach (Scheme 4.7) was therefore used to prepare free d_{22}-H_2IMes. Specifically, hydrochloride salt **14** was converted into the corresponding tetrafluoroborate **15** via salt metathesis with aqueous HBF_4. While the HCl salt **14** can

itself be used to access the free carbene directly, yields are consistently lower due to the lower purity of **14** relative to the tetrafluoroborate salt **15**. Nolan's 2010 report, for example, shows a ca. 10% increase in yield for deprotection of **15** compared to **14**.[35,38] While quantitative yields were reported for non-labelled [H_2IMes]•BF_4, yields of labelled **15** were limited to 78%. The difference in reaction scale (50 g vs. 1 g) undoubtedly contributes.

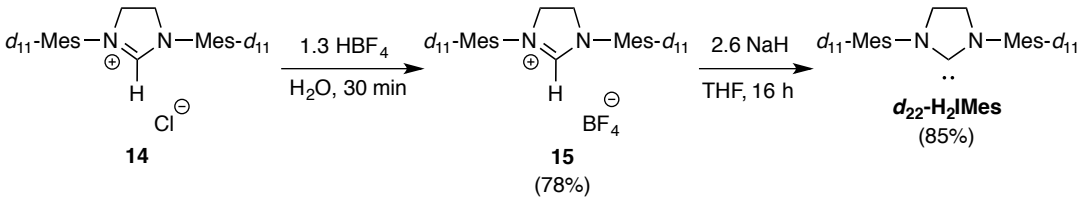

Scheme 4.7 Synthetic route to free d_{22}-H_2IMes from chloride salt 14.

Deprotection of **15** with NaH was then carried out to obtain free d_{22}-H_2IMes (Scheme 4.7).[35,38] In an initial attempt, failure to completely remove residual water from the BF_4 salt **15** caused competing hydrolysis of the free carbene, resulting in loss of material as formamide **17**, and affording the desired product in only 30% yield. The high sensitivity of free H_2IMes to water was described in earlier work from our group.[36] Treatment of a benzene solution of H_2IMes with just one equivalent of water caused complete hydrolysis within minutes (Scheme 4.8). The initial product **16** slowly converted into formamide **17** in benzene, but was formed essentially immediately in THF.

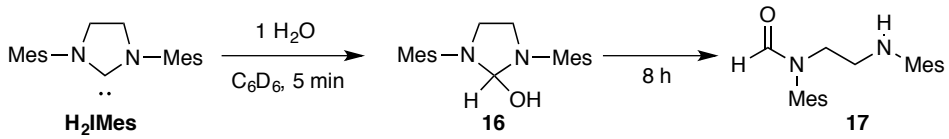

Scheme 4.8 Room-temperature hydrolysis of H_2IMes by added water in C_6D_6.

Given the low yield encountered in the first attempt to access d_{22}-H_2IMes, more rigorous efforts to remove water were undertaken. These involved stirring **15** in THF and removing the solvent under vacuum to effect azeotropic removal of residual water, and

heating solid **15** at 50 ºC under vacuum overnight. The water content in the THF from the solvent purification system (SPS) was also checked by Dr. Emma Davy using Karl-Fischer titration. As a value of >10 ppm H_2O was measured, the THF obtained from the SPS was dried for 16 h over freshly activated molecular sieves prior to use. It should be noted that the common, convenient method of assessing water content by testing with sodium benzophenone ketyl is not a reliable gauge. Ultimately, however, these improved procedures gave the free labelled d_{22}-H_2IMes in 85% yield.

4.2.4 Synthesis of d_{22}-H_2IMes labelled catalysts

Synthesis of the labelled Grubbs methylidene ***d*$_{22}$-Ru-4a** (Scheme 4.9) was achieved by the established ligand exchange method, but using d_{22}-H_2IMes.[34] (The corresponding labelled Grubbs catalyst, ***d*$_{22}$-Ru-2a**, was also prepared by Ms. Gwendolyn Bailey using this d_{22}-H_2IMes material). Accordingly, the first-generation methylidene complex **Ru-6** was treated with d_{22}-H_2IMes, and heated for 45 min in benzene at 60 ºC. The solvent was then removed under vacuum, and the brown residue was washed with cold pentane to extract free PCy_3 and Ru decomposition products, yielding the product as a fine yellow powder.

Critical to the planned use of the product is complete removal of any phosphonium salt formed by thermal decomposition of the starting methylidene complex, **Ru-6**. This is essential, to ensure that *non-labelled* [$MePCy_3$]Cl **2** (anticipated to be generated by deprotonation of PCy_3) is not present. The presence of the phosphonium salt is indicated by observation of a ^{31}P NMR singlet at 34.2 ppm in C_6D_6. To ensure the purity of the ***d*$_{22}$-**

Ru-4a product, it was extracted with degassed water to remove [$MePCy_3$]Cl **2**. Clean ***d*$_{22}$-Ru-4a** was obtained in 70% yield.

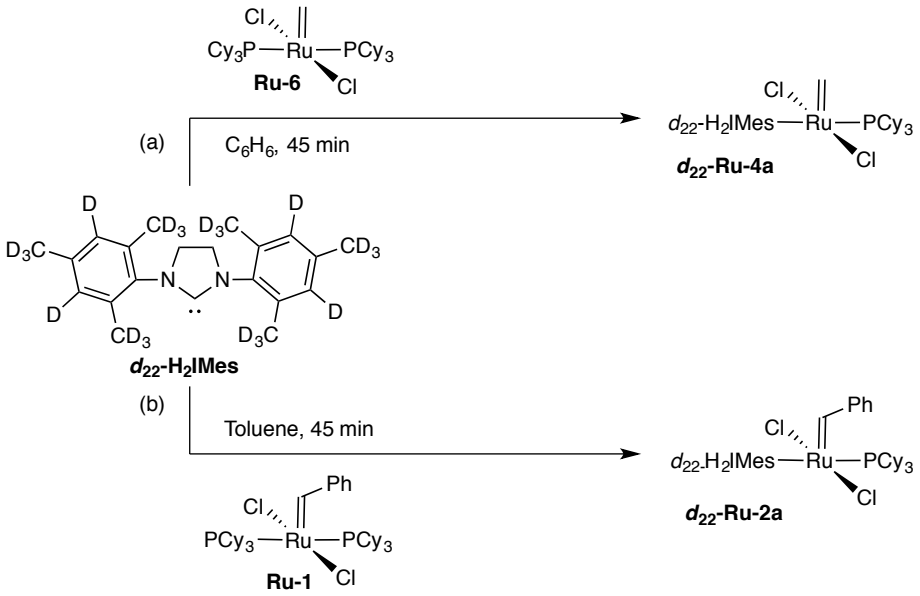

Scheme 4.9 Synthesis of *d*$_{22}$-H_2IMes labelled catalysts.

4.2.5 Rate-determining step in donor-accelerated deactivation of Ru-4a

These deuterium-labelled catalysts were used to probe the donor-accelerated methylidene abstraction pathway described in Chapter 3. To sum up, this is a multi-step reaction (Scheme 4.10) involving:

(1) donor binding to the metal center,

(2) displacement of the phosphine ligand,

(3) nucleophilic attack on the methylidene (observed for the first-generation system), and

(4) rapid C-H activation of the σ-alkyl species, resulting in liberation of [$MePCy_3$]Cl **2** and unknown Ru decomposition products.

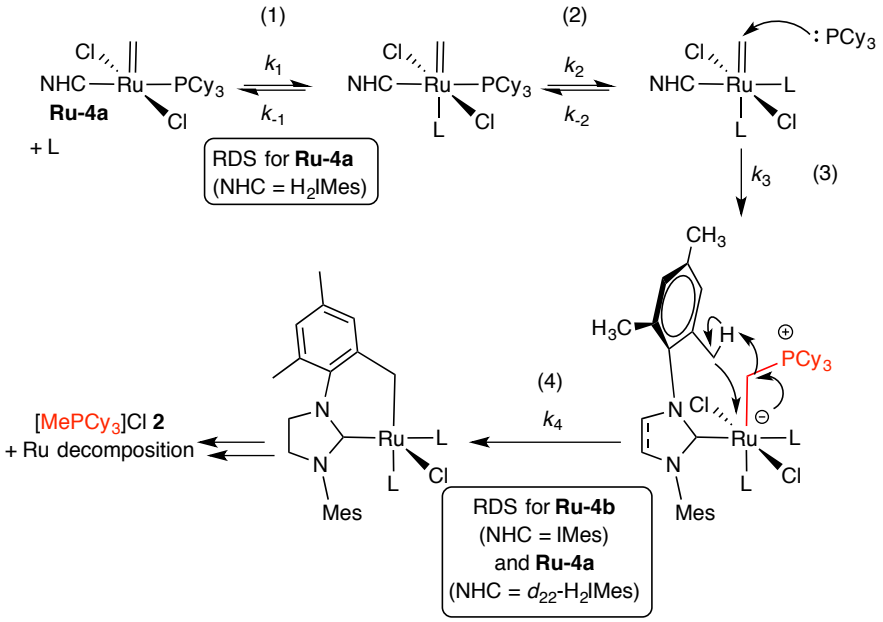

Scheme 4.10 Donor-accelerated decomposition mechanism of Grubbs catalysts.

The transience of the intermediates in Steps 1–4 makes mechanistic aspects of the net transformation difficult to probe. Within the H_2IMes system, the rapidity of the C-H activation step (k_4, Scheme 4.10) means that only the starting methylidene complex **Ru-4a** and the decomposition product [MePCy$_3$]Cl **2** are observed. This indicates that L-donor binding is rate-determining. This is not surprising, given the bulk of the NHC and PCy$_3$ ligands, which impose steric constraints on approach of L to five-coordinate **Ru-4a**. Of note, however, the rate-determining step for the IMes system **Ru-4b** switches to C-H activation, as inferred from the fact that the σ-alkyl intermediate is observable (Chapter 3). The energetic barriers to donor binding and to C-H activation are evidently very similar.

Corroboration of this point comes from deuterium-labelling studies with ***d*$_{22}$-Ru-4a**. On treating the labelled complex with pyridine, the σ-alkyl species **Ru-11a** could be observed at short reaction times (29% at 5 min, with essentially quantitative liberation of

the phosphonium salts $\mathbf{2^{Dn}}$ at 10 min) (Scheme 4.11). That is, deuteration is sufficient to change the rate-determining step from pyridine binding (step 1 in Scheme 4.10) to C–H activation (step 4).

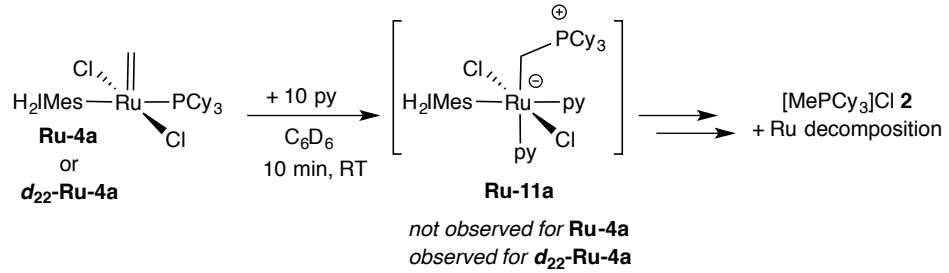

Scheme 4.11 Observation of a KIE in donor-accelerated decomposition.

A similar effect was evident with DMSO, with which decomposition was slower, and rate constants could be measured. Rate constants for disappearance of **Ru-4a** are collected in Table 4.1. The kinetic isotope effect, as judged from the k_H/k_D ratio, was 1.5. This is at the low end for a primary kinetic isotope effect,[4] perhaps indicating that C–H activation is only partially rate-determining. Competing H/D scrambling may also contribute, however. Scrambling is evident from the MALDI-MS spectrum of the decomposition products. Incorporation of a mesityl *o*-CD_3 deuteron into the phosphonium salt as $[CH_2DPCy_3]Cl$ $\mathbf{2^{D1}}$ was evident, but was accompanied by essentially equal amounts of non-labelled $[CH_3PCy_3]Cl$ **2** (Table 4.2). Consistent with H/D scrambling is the observation of the di- and tri-deutero isotopologues $\mathbf{2^{D2}}$ and $\mathbf{2^{D3}}$ (22% and 8%, respectively). $^{31}P\{^1H\}$ NMR analysis likewise showed a broad multiplet instead of the expected triplet for $[CH_2DPCy_3]Cl$.

Table 4.1 Kinetic isotope effect in the DMSO-induced decomposition of d-labelled and non-labelled Grubbs methylidene complexes

Catalyst	L-donor	k_{obs} (% loss **Ru-4a**)	k_H/k_D
Ru-4a	DMSO	0.003	1.5
***d*$_{22}$-Ru-4a**	DMSO	0.002	

Table 4.2 % [MePCy$_3$]Cl isotopomers detected by MALDI-MS

[MePCy$_3$]Cl **2**	% isotopomer[a]
[CH$_3$PCy$_3$]Cl **2**	38
[CH$_2$DPCy$_3$]Cl **2^{D1}**	32
[CHD$_2$PCy$_3$]Cl **2^{D2}**	22
[CD$_3$PCy$_3$]Cl **2^{D3}**	8

[a] % isotopomers are corrected for their natural isotopic distribution.

Observation of H/D scrambling could have multiple causes. As judged from the first-generation system, in which C-H bond is retarded following replacement of PCy_3 by pyridine, but still occurs, C-H activation of pyridine could also contribute to scrambling.[39,40] Proton abstraction from a minor contaminant such as water or non-silanized glassware could also be a factor. Most intriguing, however, is the possibility that C-H activation is reversible. Leitao and Piers proposed such an explanation step to account for H/D scrambling into the phosphonium salts liberated during decomposition of **Ru-16**.[21]

4.3 Conclusions and future work

The foregoing describes the synthesis of labelled **Ru-4a**, in which the mesityl groups on the H_2IMes are fully deuterated. Decomposition of ***d*$_{22}$-Ru-4a** by added pyridine revealed

a kinetic isotope effect, indicating that C-H activation of an *o*-methyl C–H bond is involved in the rate-determining step in donor-accelerated deactivation.

Other deactivation pathways in which the deuterium-labelled H_2IMes ligand could provide insight can be readily envisaged. For example, Gwen Bailey of the Fogg group recently examined the basis of the superior performance of the Hoveyda catalyst **Ru-15** over the Grubbs catalyst **Ru-2a** in acrylate metathesis (Scheme 4.12).[41] Based on observation of phosphonium salts **19** (Scheme 4.12), decomposition of **Ru-2a** was proposed to occur via attack of PCy_3 on the electron-deficient olefin **18**. The resulting basic phosphonium enolate was postulated to abstract a proton from the metallacyclobutane intermediate **MCB**.[41] If this is the case, no deuterium uptake should be seen on use of ***d*$_{22}$-Ru-2a** in this reaction, and indeed Ms. Bailey has recently demonstrated that this is the case, using *d*-labelled H_2IMes prepared by the author.

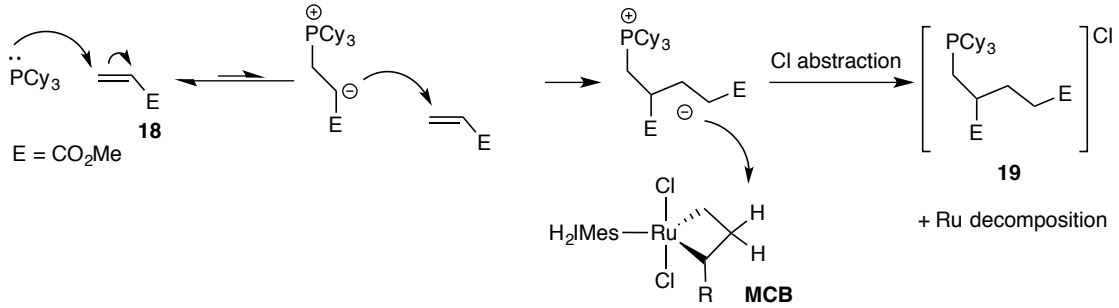

Scheme 4.12 Proposed decomposition pathway during acrylate metathesis with Ru-2a

MCB deprotonation was similarly proposed by Mr. Benjamin Ireland of this research group, to account for liberation of organic products such as **20** (containing the three **MCB** carbons; Scheme 4.13) during amine-mediated decomposition of **Ru-15** during metathesis.[42] Again, the **MCB** was proposed as the site of deprotonation. However, the *o*-mesityl substituent on the H_2IMes ligand is a plausible alternative, given the precedents

for such C-H activation noted above. Labelling studies using d_{22}-H_2IMes could aid in distinguishing between the two sites of deprotonation by tracking incorporation into the organic decomposition products.

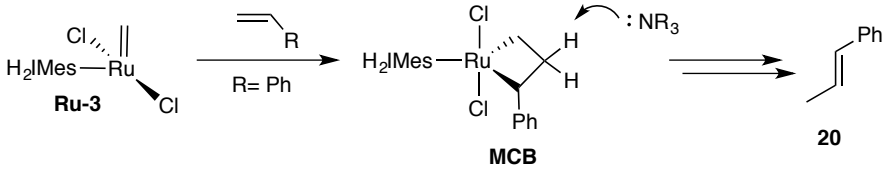

Scheme 4.13 Proposed decomposition pathways of active species Ru-3 by added base during styrene cross-metathesis.

4.4 References

(1) Lloyd-Jones, G. C.; Munoz, M. P. *J. Labelled Compd. Radiopharm.* **2007**, *50*, 1072–1087.
(2) Schroder, D. *Acc. Chem. Res.* **2012**, *45*, 1521-1532.
(3) Adlhart, C.; Hinderling, C.; Baumann, H.; Chen, P. *J. Am. Chem. Soc.* **2000**, *122*, 8204–8214.
(4) Gomez-Gallego, M.; Sierra, M. A. *Chem. Rev.* **2011**, *111*, 4857–4963.
(5) Marciniec, B.; Rogalski, S.; Potrzebowski, M. J.; Pietraszuk, C. *ChemCatChem* **2011**, *3*, 904–910.
(6) Lummiss, J. A. M.; Botti, A. G. G.; Fogg, D. E. *Catal. Sci. Technol.* **2014**, *4*, 4210–4218.
(7) Bates, J. M.; Lummiss, J. A. M.; Bailey, G. A.; Fogg, D. E. *ACS Catal.* **2014**, *4*, 2387−2394.
(8) Bieniek, M.; Michrowska, A.; Usanov, D. L.; Grela, K. *Chem. Eur. J.* **2008**, *14*, 806–818.
(9) Eelman, M. D.; Blacquiere, J. M.; Moriarty, M. M.; Fogg, D. E. *Angew. Chem. Int. Ed.* **2008**, *47*, 303–306.
(10) Henderson, W.; McIndoe, J. S., *Mass Spectrometry of Inorganic and Organometallic Compounds*. Wiley: Hoboken, N.J., 2005.
(11) Vikse, K. L.; Ahmadi, Z.; McIndoe, J. S. *Coord. Chem. Rev.* **2014**, *279*, 96–114.
(12) Jirasko, R.; Holcapek, M. *Mass Spectrometry Reviews - Billy look up teh CASSI abbreviation* **2011**, *30*, 1013– 1036.
(13) Bailey, G. A.; Fogg, D. E. *ACS Catal.* **2016**, *6*, 4962–4971.
(14) Grubbs, R. H.; Carr, D. D.; Hoppin, C.; Burk, P. L. *J. Am. Chem. Soc.* **1976**, *98*, 3478–3483.
(15) Pietraszuk, C.; Fischer, H.; Rogalski, S.; Marciniec, B. *J. Organomet. Chem.* **2005**, *690*, 5912–5921.
(16) Grubbs, R. H.; Burk, P. L.; Carr, D. D. *J. Am. Chem. Soc.* **1975**, *97*, 3265-3267.
(17) Kingsbury, J. S.; Harrity, J. P. A.; Bonitatebus, P. J.; Hoveyda, A. H. *J. Am. Chem. Soc.* **1999**, *121*, 791–799.
(18) Kingsbury, J. S.; Hoveyda, A. H. *J. Am. Chem. Soc.* **2005**, *127*, 4510–4517.

(19) Vorfalt, T.; Wannowius, K. J.; Thiel, V.; Plenio, H. *Chem. Eur. J.* **2010**, *16*, 12312–12315.
(20) Núñez-Zarur, F.; Solans-Monfort, X.; Pleixats, R.; Rodríguez-Santiago, L.; Sodupe, M. *Chem. Eur. J.* **2013**, *19*, 14553-14565.
(21) Leitao, E. M.; Dubberley, S. R.; Piers, W. E.; Wu, Q.; McDonald, R. *Chem. Eur. J.* **2008**, *14*, 11565–11572.
(22) Casey, C. P.; Tuinstra, H. E. *J. Am. Chem. Soc.* **1978**, *100*, 2270-2272.
(23) Stewart, I. C.; Keitz, B. K.; Kuhn, K. M.; Thomas, R. M.; Grubbs, R. H. *J. Am. Chem. Soc.* **2010**, *132*, 8534–8535.
(24) Fürstner, A.; Ackermann, L.; Beck, K.; Hori, H.; Koch, D.; Langemann, K.; Liebl, M.; Six, C.; Leitner, W. *J. Am. Chem. Soc.* **2001**, *123*, 9000–9006.
(25) van der Eide, E. F.; Piers, W. E. *Nature Chem.* **2010**, *2*, 571–576.
(26) McGinnis, J.; Katz, T. J.; Hurwitz, S. *J. Am. Chem. Soc.* **1976**, *98*, 605-606.
(27) Tanaka, K.; Tanaka, K.-I.; Takeo, H.; Matsumura, C. *J. Am. Chem. Soc.* **1987**, *109*, 2422-2425.
(28) Courchay, F. C.; Sworen, J. C.; Ghiviriga, I.; Abboud, K. A.; Wagener, K. B. *Organometallics* **2006**, *25*, 6074–6086.
(29) Pucino, M.; Mougel, V.; Schowner, R.; Fedorov, A.; Buchmeiser, M. R.; Copéret, C. *Angew. Chem. Int. Ed.* **2016**, *55*, 4300–4302.
(30) Trnka, T. M.; Morgan, J. P.; Sanford, M. S.; Wilhelm, T. E.; Scholl, M.; Choi, T.-L.; Ding, S.; Day, M. W.; Grubbs, R. H. *J. Am. Chem. Soc.* **2003**, *125*, 2546–2558.
(31) Abdur-Rashid, K.; Fedorkiw, T.; Lough, A. J.; Morris, R. H. *Organometallics* **2004**, *23*, 86–94.
(32) Endo, K.; Grubbs, R. H. *J. Am. Chem. Soc.* **2011**, *133*, 8525–8527.
(33) Endo, K.; Herbert, M. B.; Grubbs, R. H. *Organometallics* **2013**, *32*, 5128-5135.
(34) Lummiss, J. A. M.; Beach, N. J.; Smith, J. C.; Fogg, D. E. *Catal. Sci. Technol.* **2012**, *2*, 1630–1632.
(35) Arduengo, A. J.; Krafczyk, R.; Schmutzler, R.; Craig, H. A.; Goerlich, J. R.; Marshall, W. J.; Unverzagt, M. *Tetrahedron* **1999**, *55*, 14523–14534.
(36) van Lierop, B. J.; Reckling, A. M.; Lummiss, J. A. M.; Fogg, D. E. *ChemCatChem* **2012**, *4*, 2020–2025.
(37) Beach, N. J.; Lummiss, J. A. M.; Bates, J. M.; Fogg, D. E. *Organometallics* **2012**, *31*, 2349–2356.
(38) Bantreil, X.; Nolan, S. P. *Nature Protoc.* **2011**, *6*, 69–77.
(39) Johnson, D. G.; Lynam, J. M.; Mistry, N. S.; Slattery, J. M.; Thatcher, R. J.; Whitwood, A. C. *J. Am. Chem. Soc.* **2013**, *135*, 2222–2234.
(40) Bajo, S.; Esteruelas, M. A.; López, A. M.; Oñate, E. *Organometallics* **2014**, *33*, 1851–1858.
(41) Bailey, G. A.; Fogg, D. E. *J. Am. Chem. Soc.* **2015**, *137*, 7318–7321.
(42) Ireland, B. J.; Dobigny, B. T.; Fogg, D. E. *ACS Catal.* **2015**, *5*, 4690−4698.

Chapter 5. Conclusions and future work

Over the past 20 years, olefin metathesis has transformed the way synthetic chemists assemble new carbon skeletons. While metathesis has long been used in petrochemicals processing, implementation into the pharmaceutical and specialty chemical sectors has taken almost 60 years, with examples only emerging in the past 3 years. Even with industrial applications coming online, however, reports are prevalent of poor selectivities and isolated yields in pharmaceutical process chemistry, often arising from unknown catalyst decomposition pathways. Use of high-purity reagents and solvents is standard operating procedure during discovery-stage metathesis aimed at preparing active pharmaceutical ingredients. High catalyst loadings are also utilized, if required. In manufacturing, these are unaffordable luxuries, and catalyst decomposition is therefore a major challenge (particularly where this leads to poor process reproducibility). A fundamental problem is that catalyst decomposition processes cannot realistically be examined in industry. While such studies are not yet common in academia, they have an important potential role to play in improving fundamental understanding, while facilitating expanded industrial applications and catalyst redesign.

Phosphine-stabilized ruthenium catalysts are the most widely used catalysts in olefin metathesis. Chapter 3 focuses on a key pathway by which such Grubbs-class ruthenium catalysts decompose. In earlier work, the Fogg group showed that amine donors accelerate abstraction of the methylidene ligand, and catalyst decomposition. This thesis work shows that such "donor-accelerated decomposition" is general over a wide range of phosphine-stabilized ruthenium catalysts. Moreover, even weak Lewis donors, such as

water, ethers, alcohols, and nitriles – widespread among contaminants and and/or "green solvents" proposed for metathesis, and commonplace as functional groups – accelerate methylidene abstraction, with severely detrimental consequences for metathesis yields even for facile ring-closing reactions. Because of the associative nature of this mechanism, increasing donor concentration will result in faster catalyst decomposition while metathesis yields decrease. The deleterious impact of weak donors has gone widely unrecognized. This work gives the first mechanistic insights into the origin of this behaviour, which has profound implications for catalyst choice and use. Also presented is the first mechanistic understanding of the improved catalyst performance that results from replacing α-olefins by β-methyl olefins as metathesis substrates.

Presented in Chapter 4 is the synthesis and use of a deuterium-functionalized *N*-heterocyclic carbene ligand, with the aim of clarifying the source of the proton required to complete donor-accelerated decomposition of the Grubbs catalysts. This pathway is a multi-step mechanism involving transient intermediates. The rate-determining step was identified as C-H activation of a *o*-mesityl substituent on the H_2IMes ligand by *d*-labelling. These insights have important implications for catalyst redesign. They emphasize the need to hinder C-H activation of the carbene ligand to increase catalyst stability.

Our group has recently reported mechanistic details of many deactivation pathways in olefin metathesis. A better understanding of catalyst decomposition pathways positions the field for informed catalyst redesign. Design alternatives must consider ways to

eliminate alkylidene / methylidene abstraction. Among the enormous range of NHC substituents, examples that impede C-H activation warrant further investigation. Also of merit are methods to amplify steric bulk around the methylidene to hinder attack by the phosphine or other nucleophiles.

Appendix 1. Supplementary data for Chapter 3

A1.1 NMR spectra for new compounds

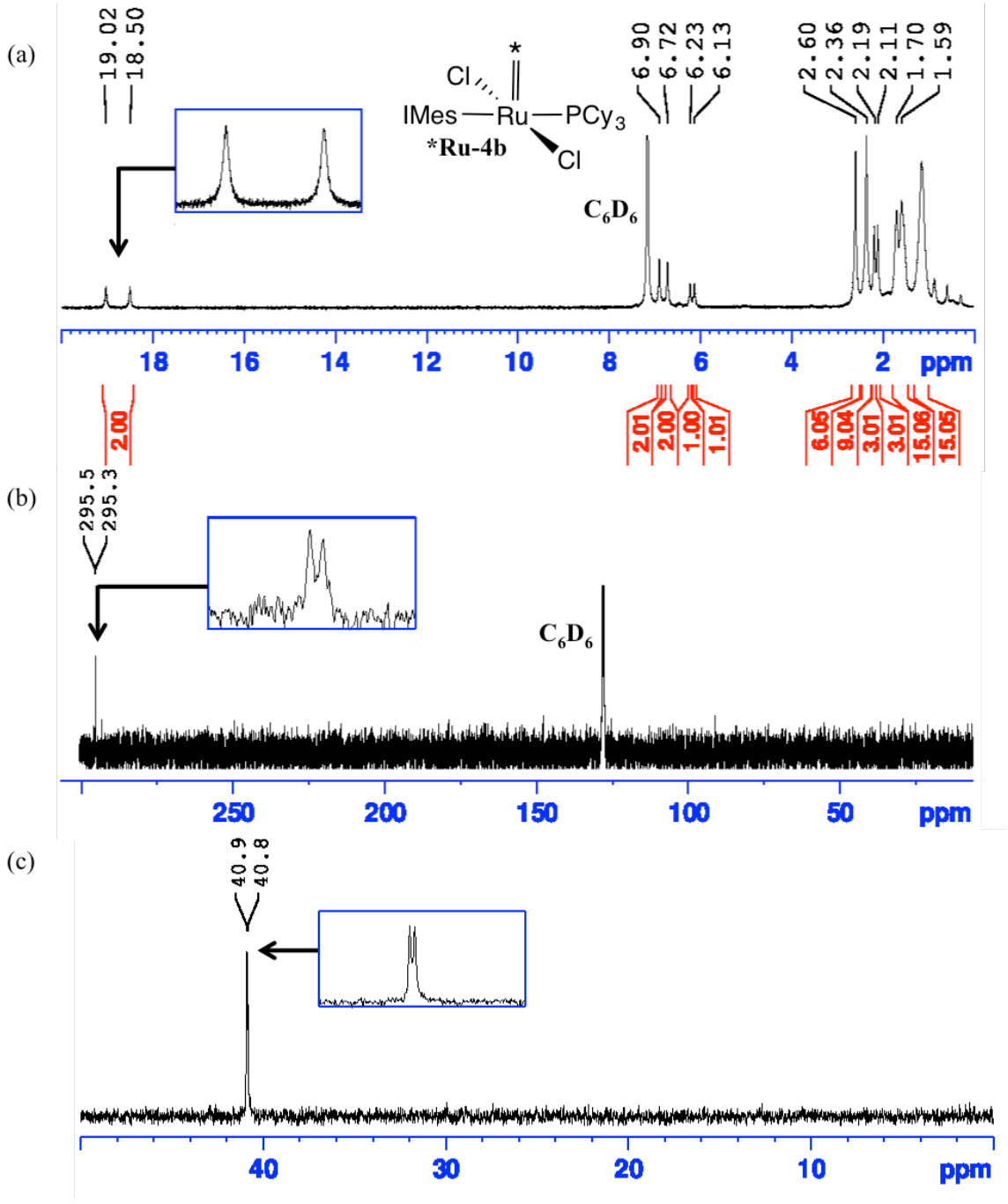

Figure A1.1. Characterization of $RuCl_2(IMes)(PCy_3)(=^{13}CH_2)$, ***Ru-4b**. (a) ^1H NMR spectrum (300 MHz, C_6D_6). (b) $^{13}C\{^1H\}$ NMR spectrum (75 MHz, C_6D_6), showing methylidene signal. (c) $^{31}P\{^1H\}$ NMR spectrum (121 MHz, C_6D_6).

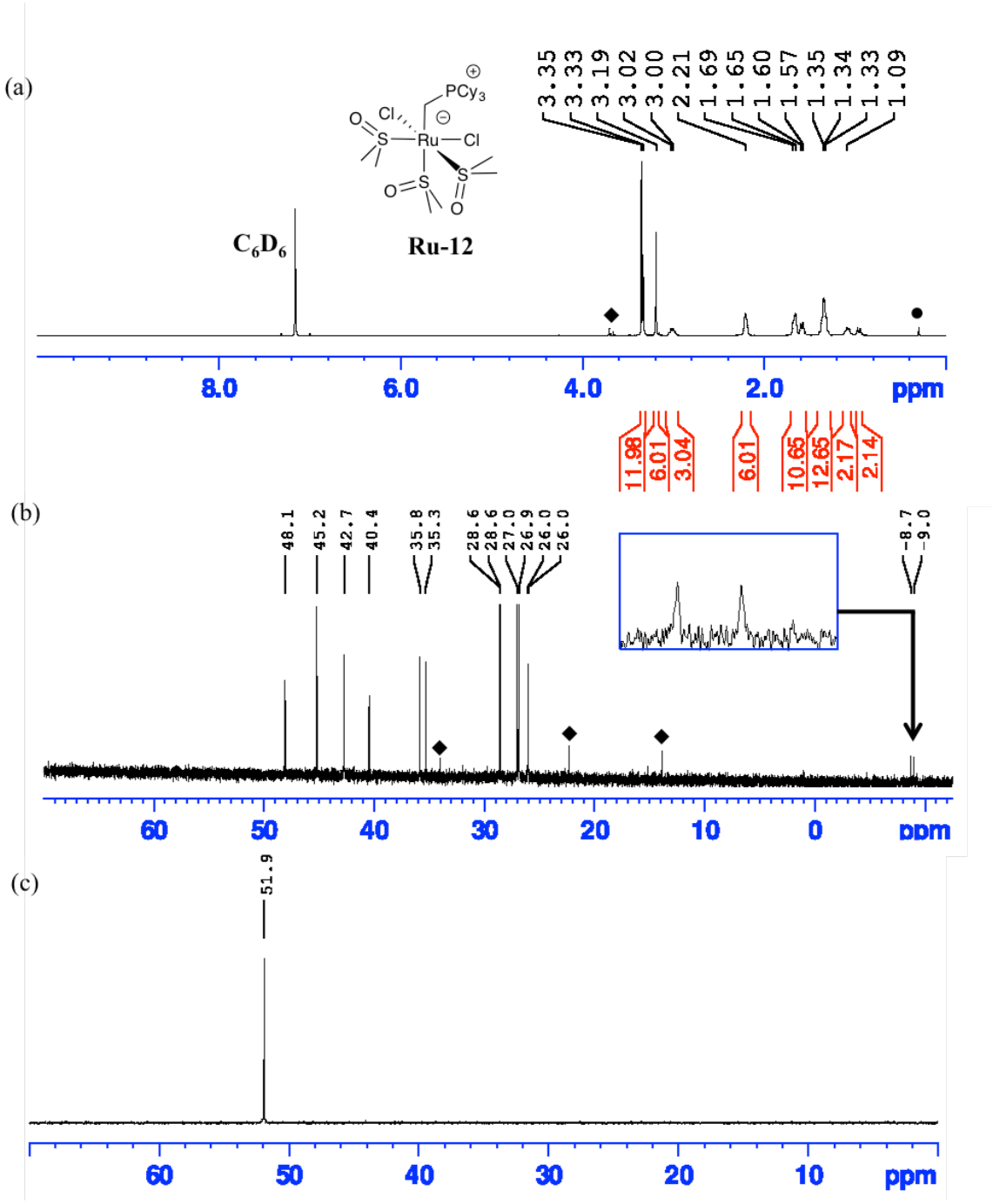

Figure A1.2. Characterization of $RuCl_2(\sigma\text{-}CH_2PCy_3)(DMSO)_3$ **Ru-12**. (a) ^1H NMR spectrum (300 MHz, C_6D_6). (b) $^{13}C\{^1H\}$ NMR spectrum (75 MHz, C_6D_6). (c) $^{31}P\{^1H\}$

NMR spectrum (121 MHz, C_6D_6). (•) Represents minor amount of pentane from workup. (⬥) Represents minor impurities.

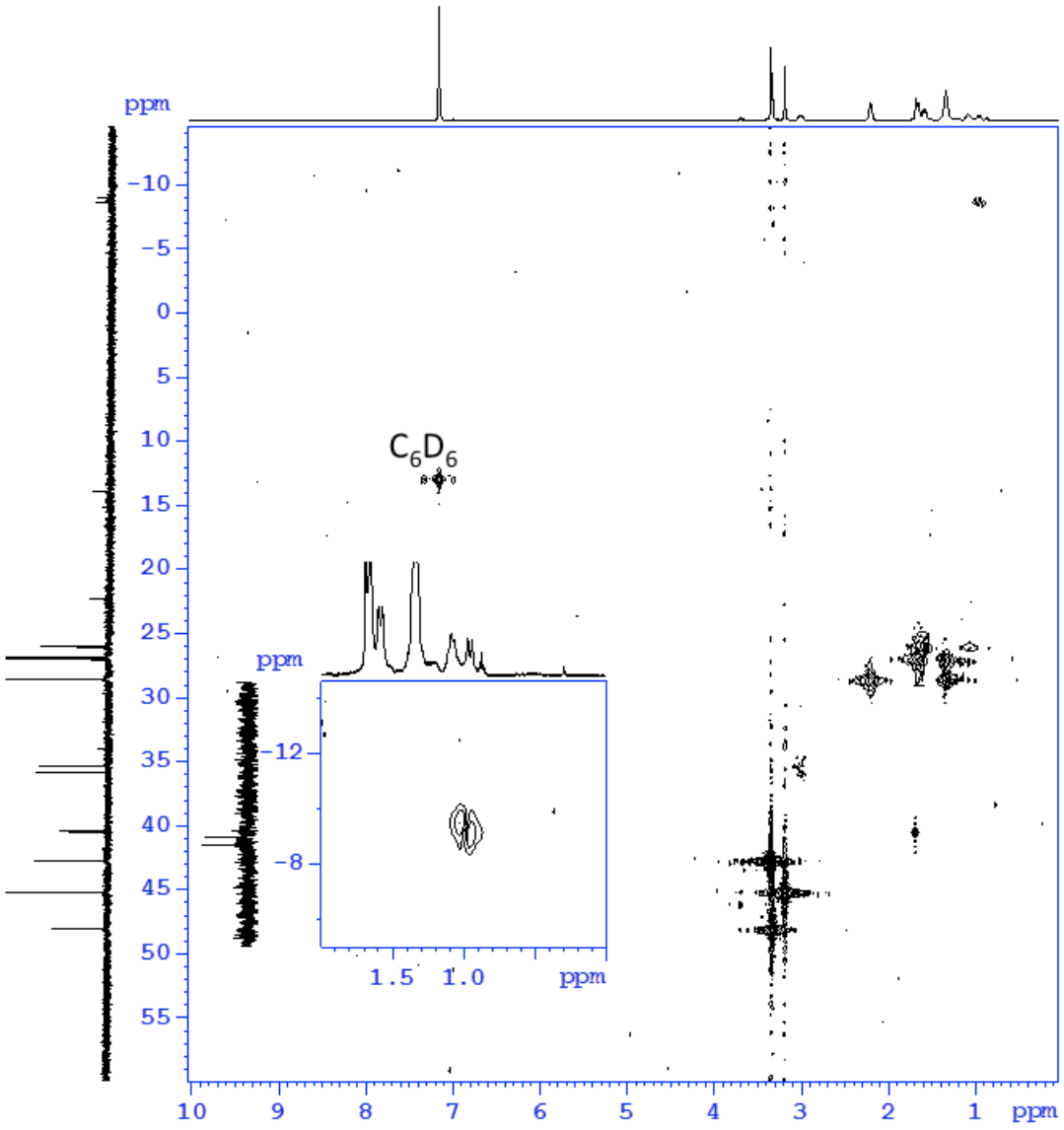

Figure A1.3. $^{1}H-^{13}C$ HMQC spectrum (C_6D_6) for $RuCl_2(\sigma\text{-}CH_2PCy_3)(DMSO)_3$ **Ru-12**. Inset shows C-H correlations within the Ru–CH_2 group.

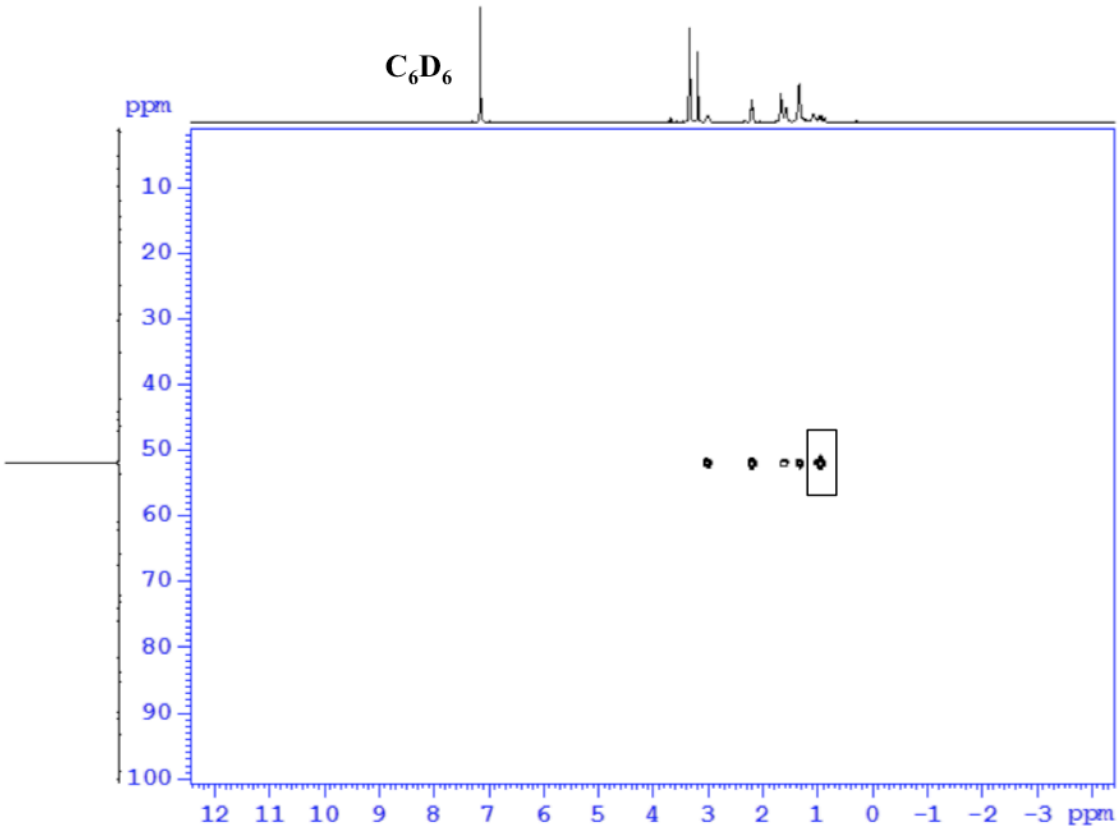

Figure A1.4. $^{1}H-^{31}P$ HMQC (C_6D_6) spectrum of $RuCl_2(\sigma\text{-}CH_2PCy_3)(DMSO)_3$ **Ru-12**. Box shows 2 bond H-P correlation within the Ru-CH_2PCy_3 group.

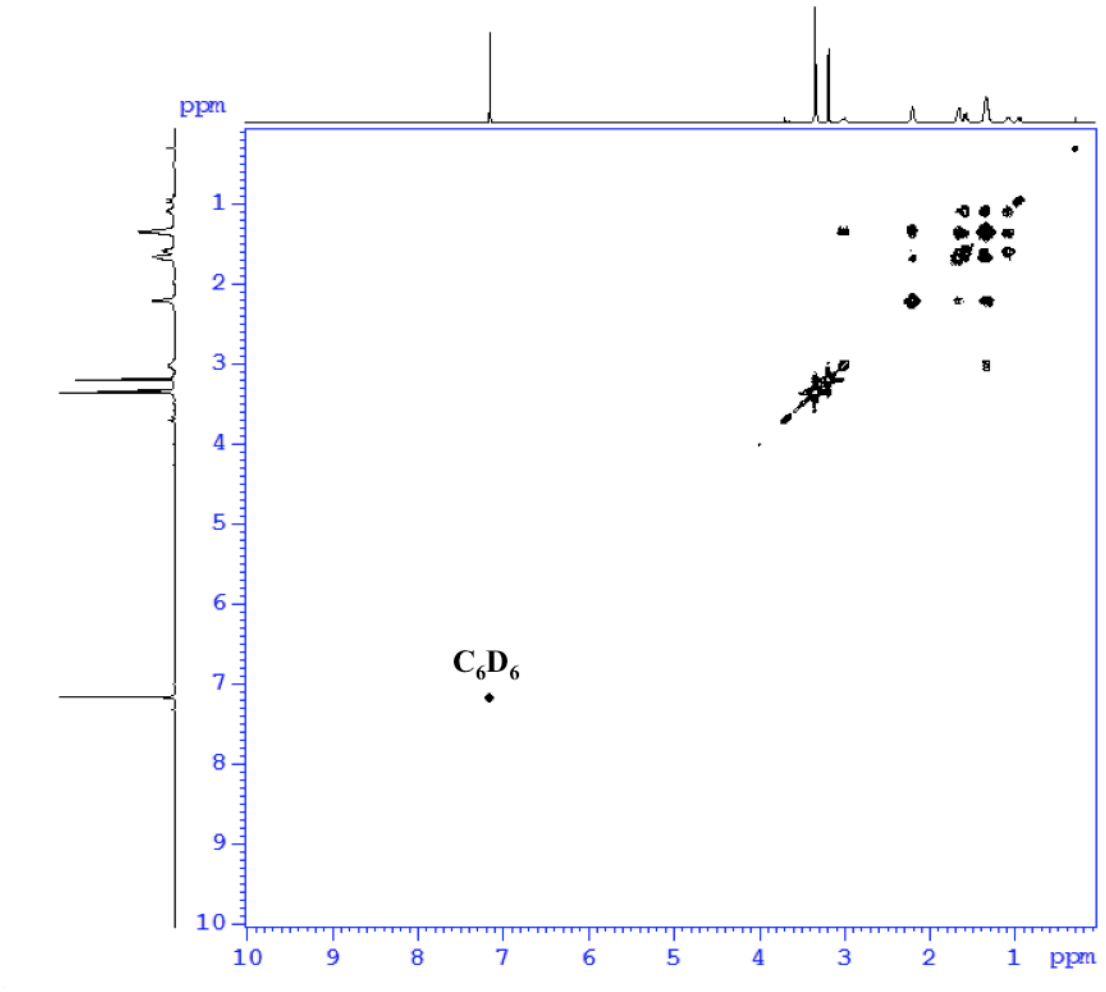

Figure A1.5. $^{1}H–^{1}H$ COSY (300 MHz, C_6D_6) spectrum of $RuCl_2(\sigma\text{-}CH_2PCy_3)(DMSO)_3$ **Ru-12**.

A1.2 Representative NMR spectra and tabulated data for transient σ-alkyl species

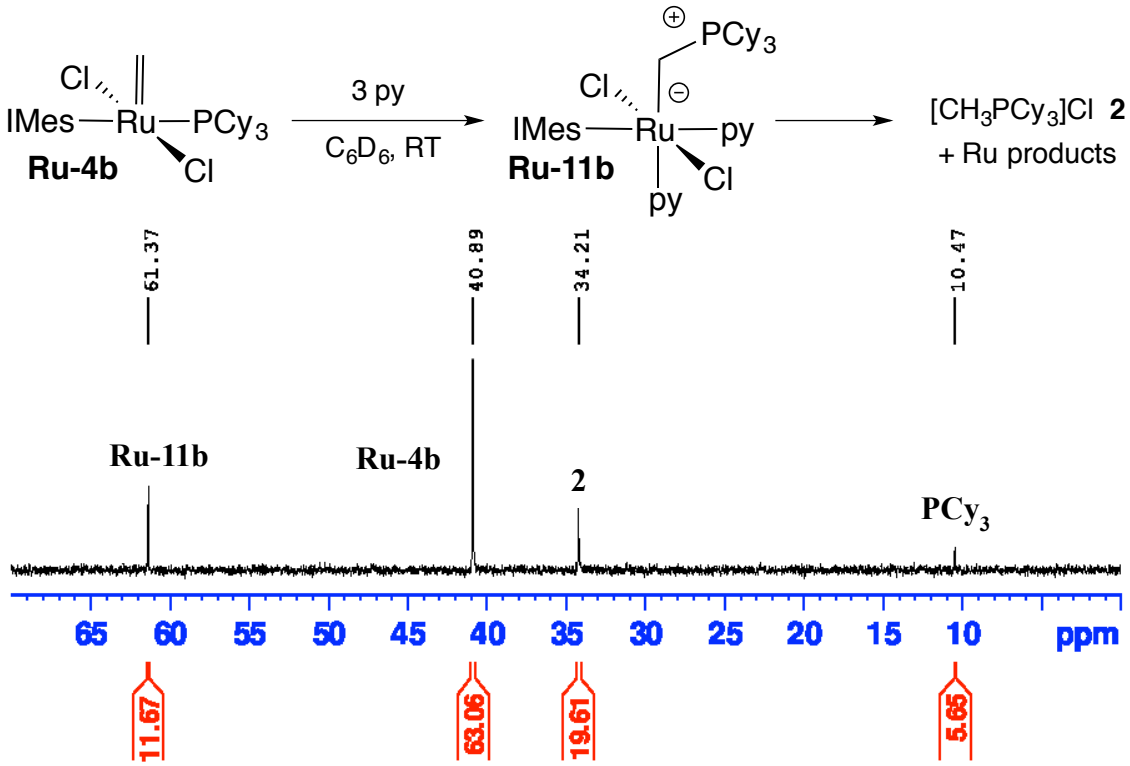

Figure A1.6. $^{31}P\{^{1}H\}$ NMR spectrum (121 MHz, C_6D_6) obtained on reaction of **Ru-4b** with 3 equiv pyridine, showing signal for transient **Ru-11b** (t = 5 min).

Table A1.1. Tabulated $^{31}P\{^{1}H\}$ data (121 MHz, C_6D_6) for Figure 3.3 in Chapter 3: observation of **Ru-11b** on treatment of **Ru-4b** with 3 equiv pyridine

time (min)	% **Ru-4b** (δ_P 40.9)	% **Ru-11b** (δ_P 61.3**)**	% [$MePCy_3$]Cl **2** (δ_P 34.2)	% free PCy_3 (δ_P 10.5)
0	100	0	0	0
3	75	9	9	7
5	63	12	20	5
7	53	13	26	8
10	46	10	36	8
13	38	10	43	9
20	26	7	57	10
31	17	4	68	10
36	11	2	77	10
45	6	1	82	11
48	6	0	83	11
75	0	0	89	11

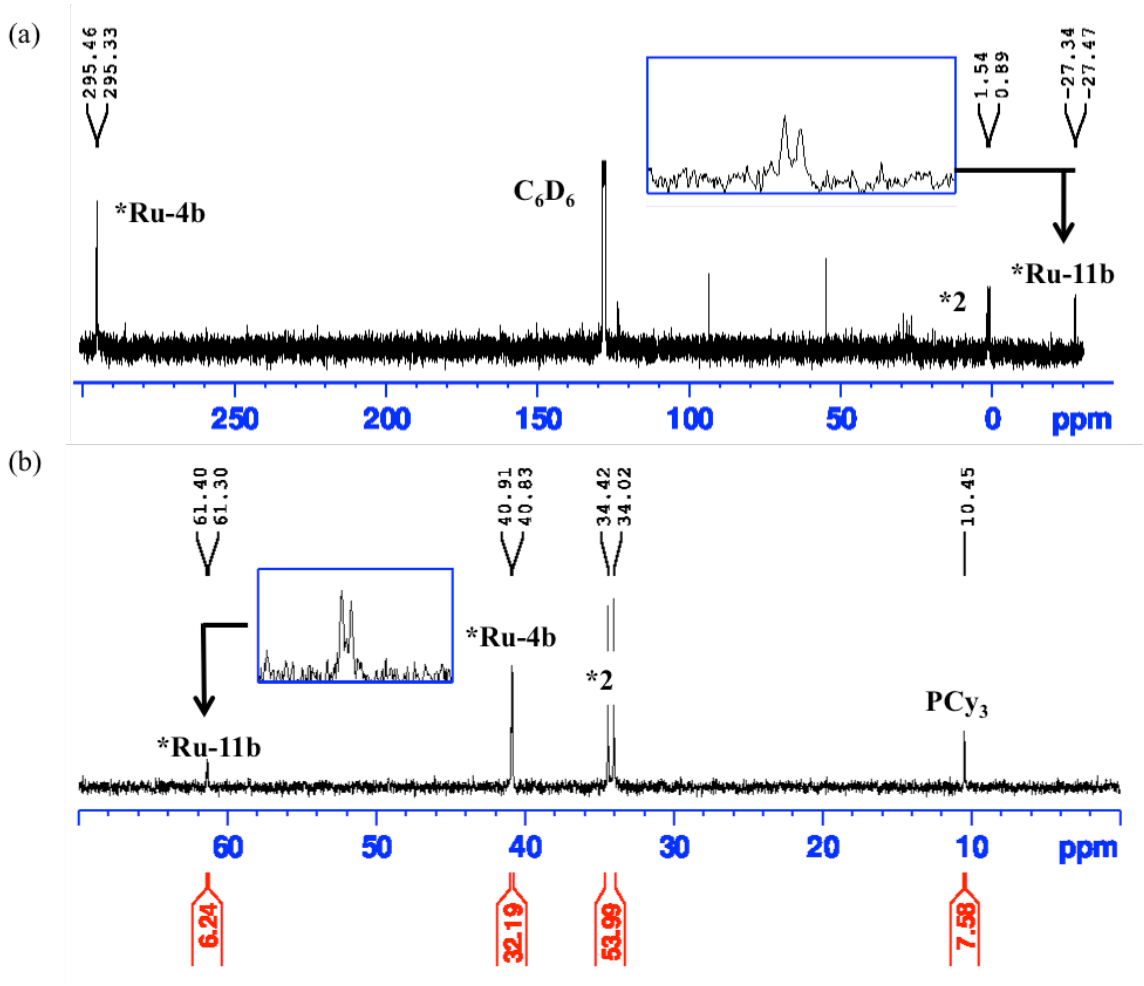

Figure A1.7. NMR spectra obtained on treating ^{13}C-labelled ***Ru-4b** with 3 equiv pyridine, showing transient ***Ru-11b**. (a) $^{13}C\{^1H\}$ NMR spectrum (75 MHz, C_6D_6), key signals only (400 scans, 2-16 min). (b) $^{31}P\{^1H\}$ NMR spectrum (121 MHz, C_6D_6) (16-22 min).

A1.3 Representative NMR spectra and tabulated data for catalyst scope studies

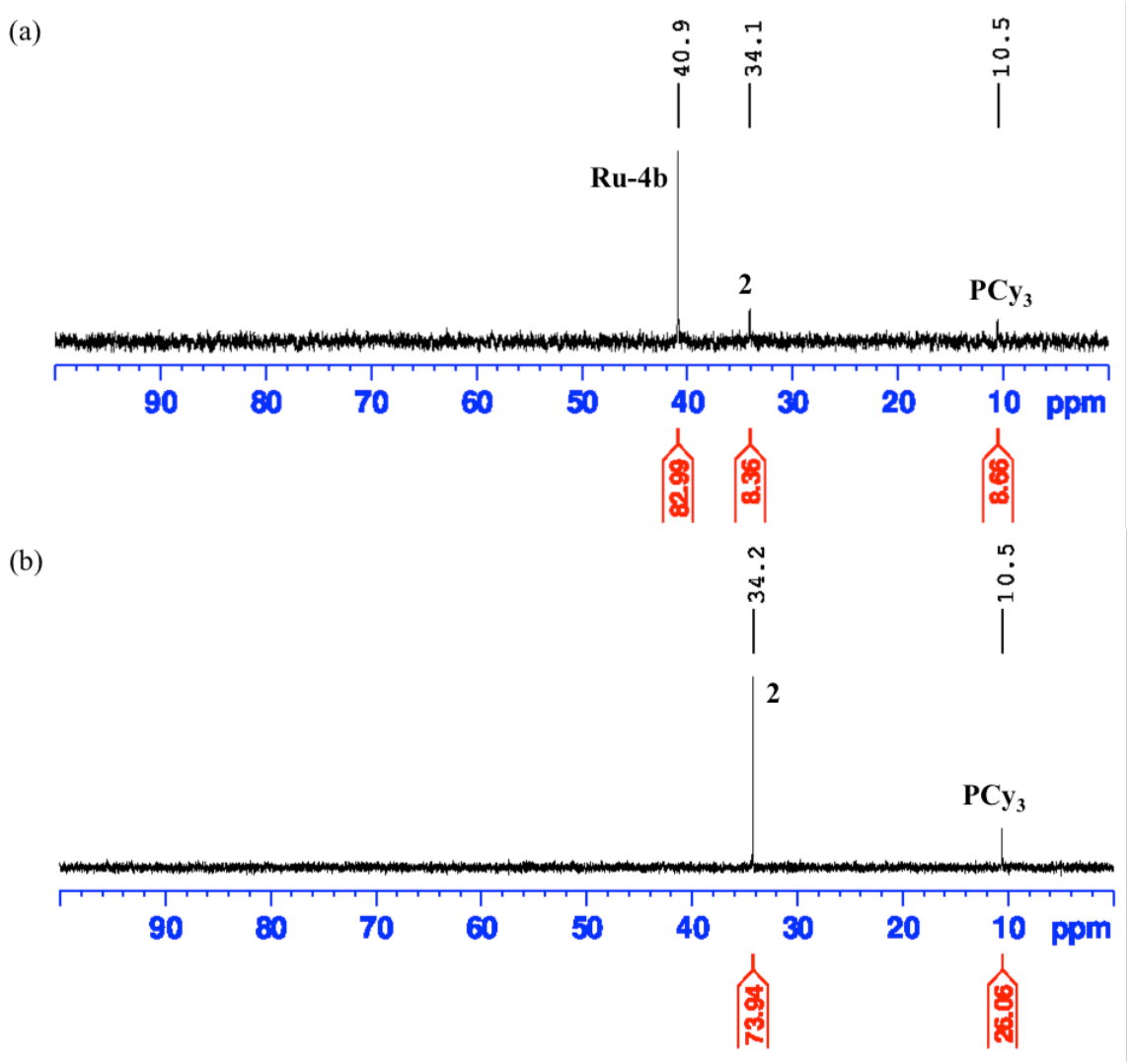

Figure A1.8. Representative $^{31}P\{^{1}H\}$ NMR spectra (121 MHz, C_6D_6) showing the impact of pyridine on the proportion of decomposition present at 2 h, for in situ-generated methylidene species (Figure 3.5 in Chapter 3). (a) **Ru-2b** under ethylene; no added pyridine. (b) **Ru-2b** under ethylene with pyridine (10 equiv).

Table A1.2. Tabulated ^{31}P NMR data demonstrating the accelerating effect of pyridine (*n* equiv) on decomposition of phosphine-stabilized catalysts under ethylene (Figure 3.5 in Chapter 3)

System	*n*	% [Ru]=CHR (δ_P)		% **2**	% PCy_3
		R = Ph	R = H	(δ_P 34.2)	(δ_P 10.5)
Ru-2a	0	0	62 (38.2)	38	0
	10	0	0	100	0
Ru-2b	0	0	83 (40.9)	8	9
	10	0	0	74	26
Ru-2c	0	0	29 (38.4)	71	0
	10	0	0	100	0
Ru-2d	0	0	85 (40.4)	15	0
	10	0	0	100	0
Ru-2f	0	19 (26.5)	69 (38.2)	12	0
	10	0	0	91	9
Ru-2g	0	86 (28.1)	14 (40.9)	0	0
	10	0	0	82	18
Ru-2e[a]	0	0	0	51	0
	10	0	0	81	6

[a]For the reaction of **Ru-2e** with ethylene in the absence of py, three new, unidentified ^{31}P NMR singlets (55.5, 54.8 and 31.5 ppm) account for the mass balance. ^{1}H NMR analysis shows no alkylidene signals. In the presence of py, one unidentified singlet is apparent at 48.1 ppm; again, no alkylidene is evident.

A1.4 Representative NMR spectra for donor scope studies

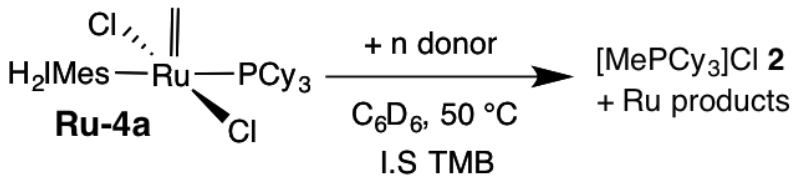

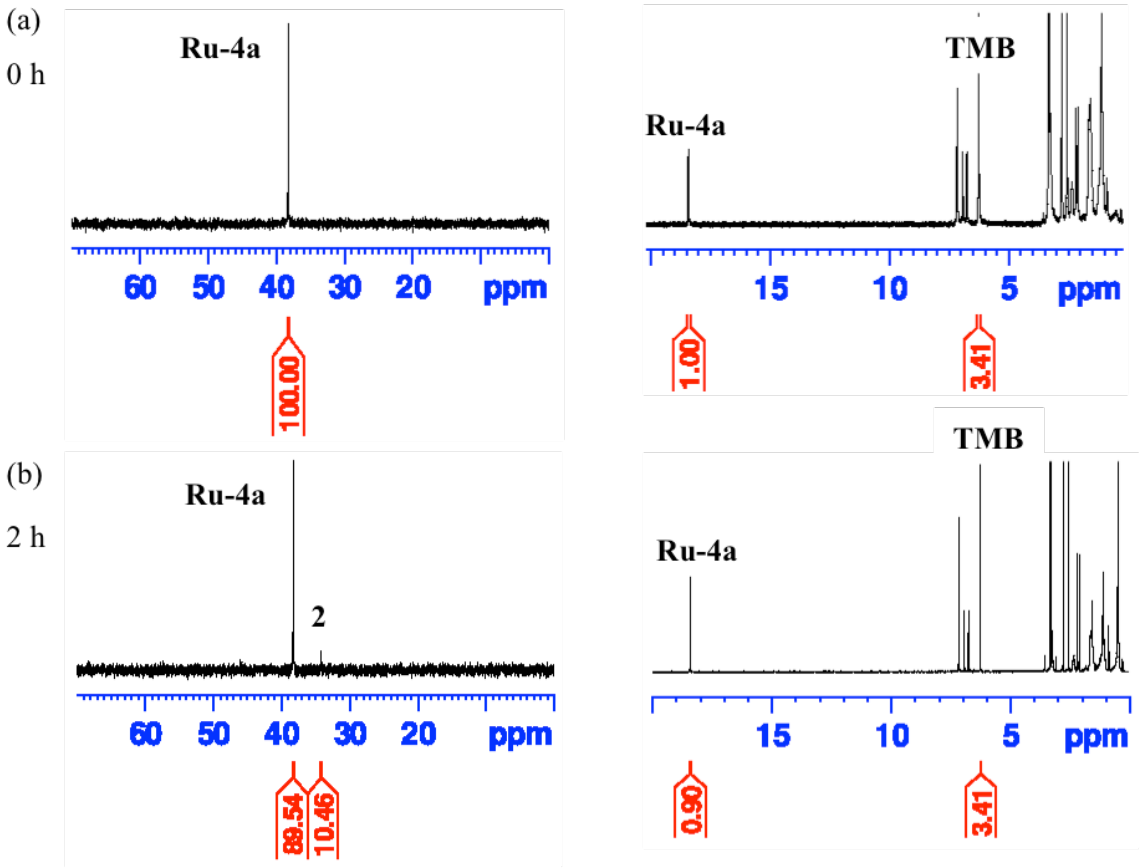

Figure A1.9. Representative NMR spectra (left, $^{31}P\{^{1}H\}$; right, ^{1}H) showing disappearance of a selected methylidene complex, **Ru-4a**, and formation of $[MePCy_3]Cl$ **2** in the absence of an added donor. (a) Spectra obtained immediately after making up the sample. (b) After 2 h at 50 °C. See Table 3.1 in Chapter 3.

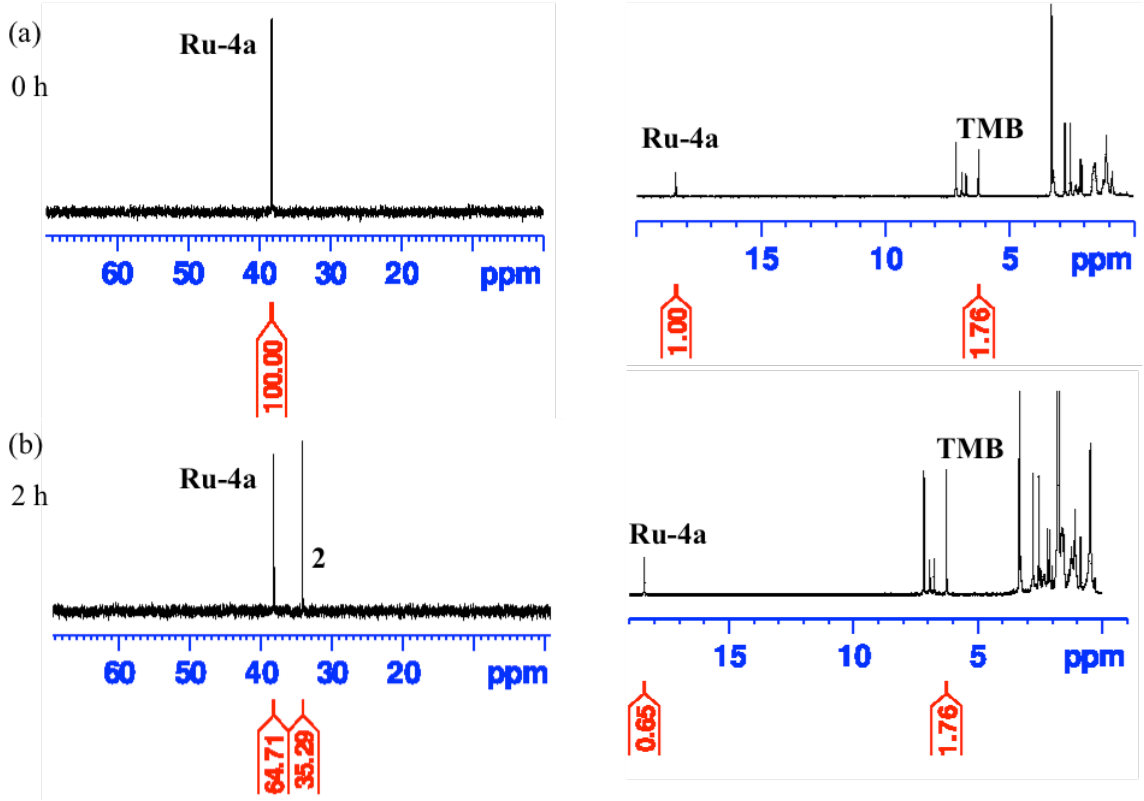

Figure A1.10. Representative NMR spectra showing disappearance of a selected methylidene complex, **Ru-4a**, and formation of [$MePCy_3$]Cl **2** on addition of *n* equiv donor (here DMSO, *n* = 10 at 50 °C. (a) Immediate. (b) After 2 h. See Table 3.1 in Chapter 3.

A1.5 Kinetics data for decomposition of methylidene complexes

Table A1.3. Kinetics data showing disappearance of methylidene species on reaction with DMSO at 25 °C. See Figure 3.6b in Chapter 3

n equiv	time (h)	% **Ru-6**[a]	% **Ru-4a**[a]
10	0	100	100
	1	81	99
	2	72	97
	4	53	93
	6	43	90
	27	9	64
33	0	100	100
	1	53	92
	2	33	91
	4	17	87
	6	9	81
	24	0	57
55	0	100	100
	1	44	78
	2	24	76
	4	2	64
	6	0	60
	27	0	21
78	0	100	100
	1	49	77
	2	14	73
	4	5	58
	6	0	48
	27	0	13
100	0	100	100
	1	30	77
	2	5	71
	4	0	56
	6	0	36
	27	0	6

[a] Integrated ^{1}H NMR analysis vs. TMB.

Table A1.4. Half-lives (min) and rate constants (min^{-1}) for kinetics data in Table A1.3, showing decomposition of **Ru-6** and **Ru-4a** by DMSO

	Ru-6	**Ru-4a**
equiv DMSO	$t_{1/2}$ (k_{obs})	$t_{1/2}$ (k_{obs})
10	250 (0.0016)	1800 (0.0003)
33	70 (0.0062)	1700 (0.0004)
55	50 (0.011)	420 (0.0009)
78	40 (0.014)	330 (0.0012)
100	30 (0.017)	270 (0.0015)

A1.6 NMR spectra of commercially available compounds relating to points discussed in text

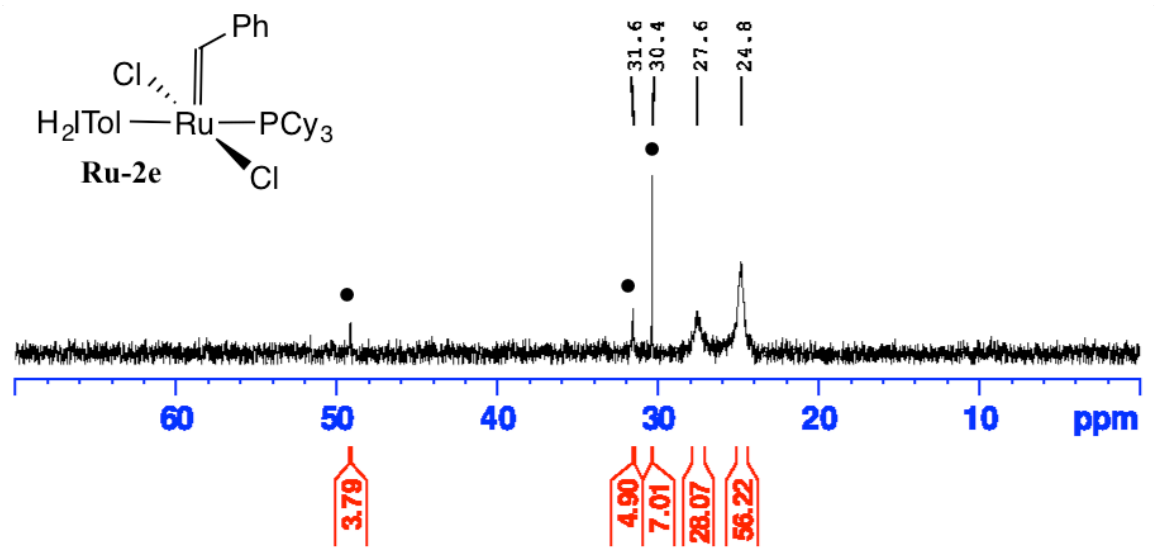

Figure A1.11. $^{31}P\{^{1}H\}$ NMR spectrum (121 MHz, C_6D_6) of commercial H_2ITol complex **Ru-2e**, showing unidentified impurities (•). See Figure 3.5 and accompanying discussion in Chapter 3

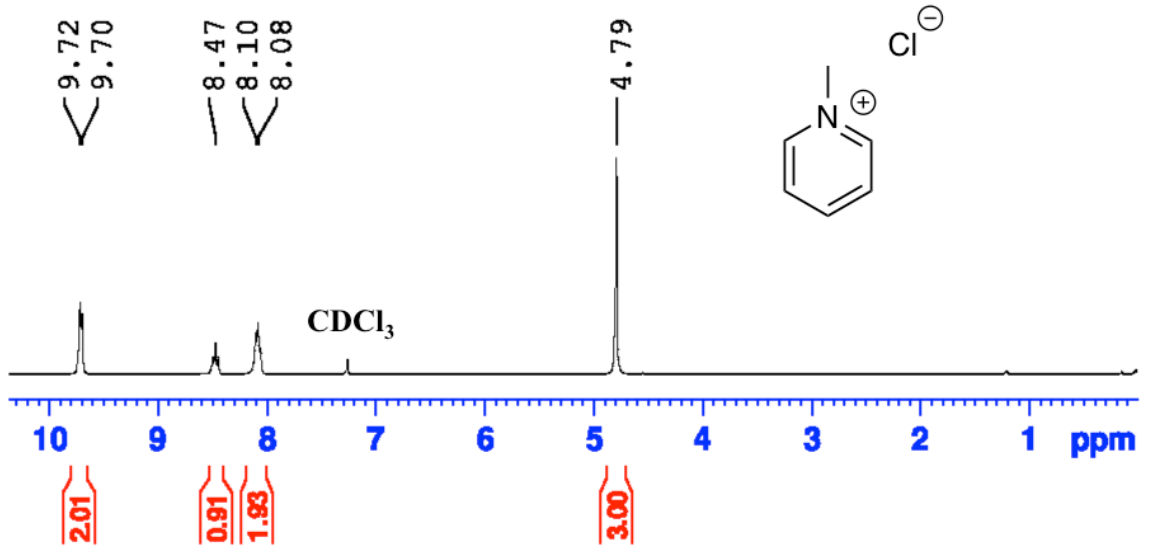

Figure A1.12. ^{1}H NMR (300 MHz, $CDCl_3$) spectrum of commercially available $[MeNC_5H_5]Cl$. See Ref. 31 in Chapter 3, and associated discussion.

A1.7 Representative GC data

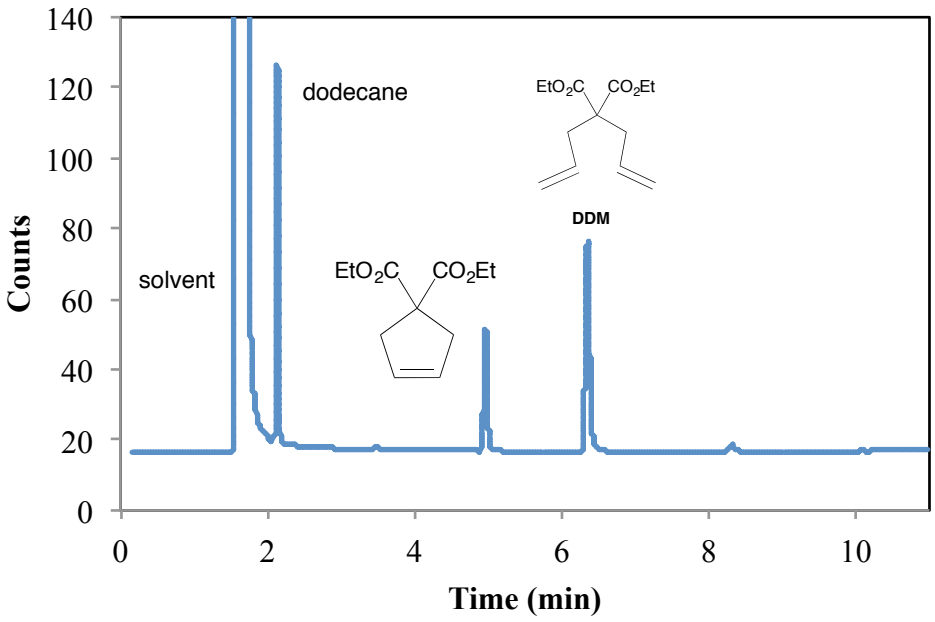

Figure A1.13. GC-FID trace for RCM of DDM by **Ru-2a** in the presence of 90 μL water at 2 h.

A1.8 NMR spectra for generation and attempted decomposition of ethylidene complexes

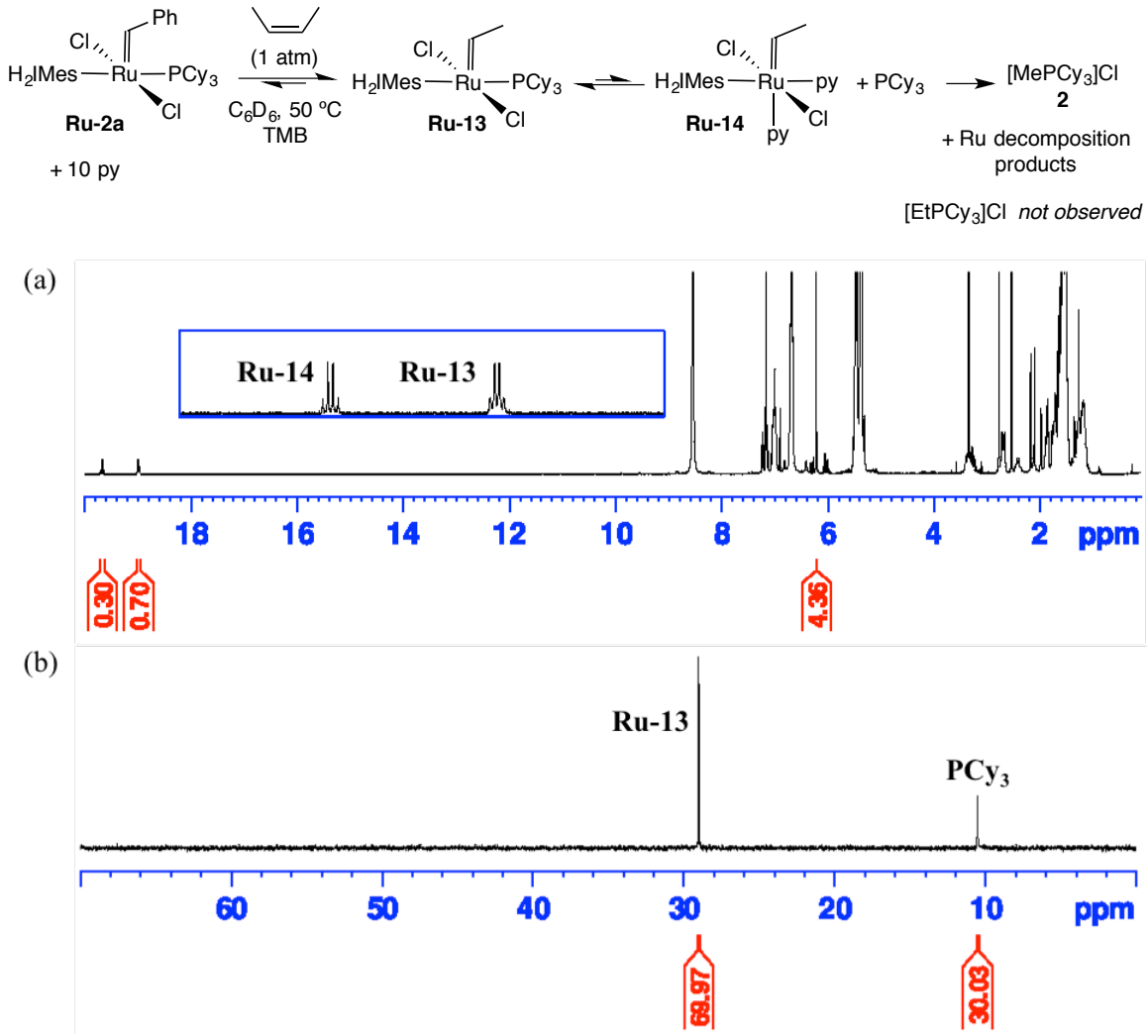

Figure A1.14. In situ formation of ethylidene species after 1 h at 50 °C (see Scheme 3.4 in Chapter 3). (a) ^{1}H NMR spectrum (300 MHz, C_6D_6), showing **Ru-13** and **Ru-14**. (b) $^{31}P\{^{1}H\}$ NMR spectrum (121 MHz, C_6D_6) showing **Ru-13** and free PCy_3.

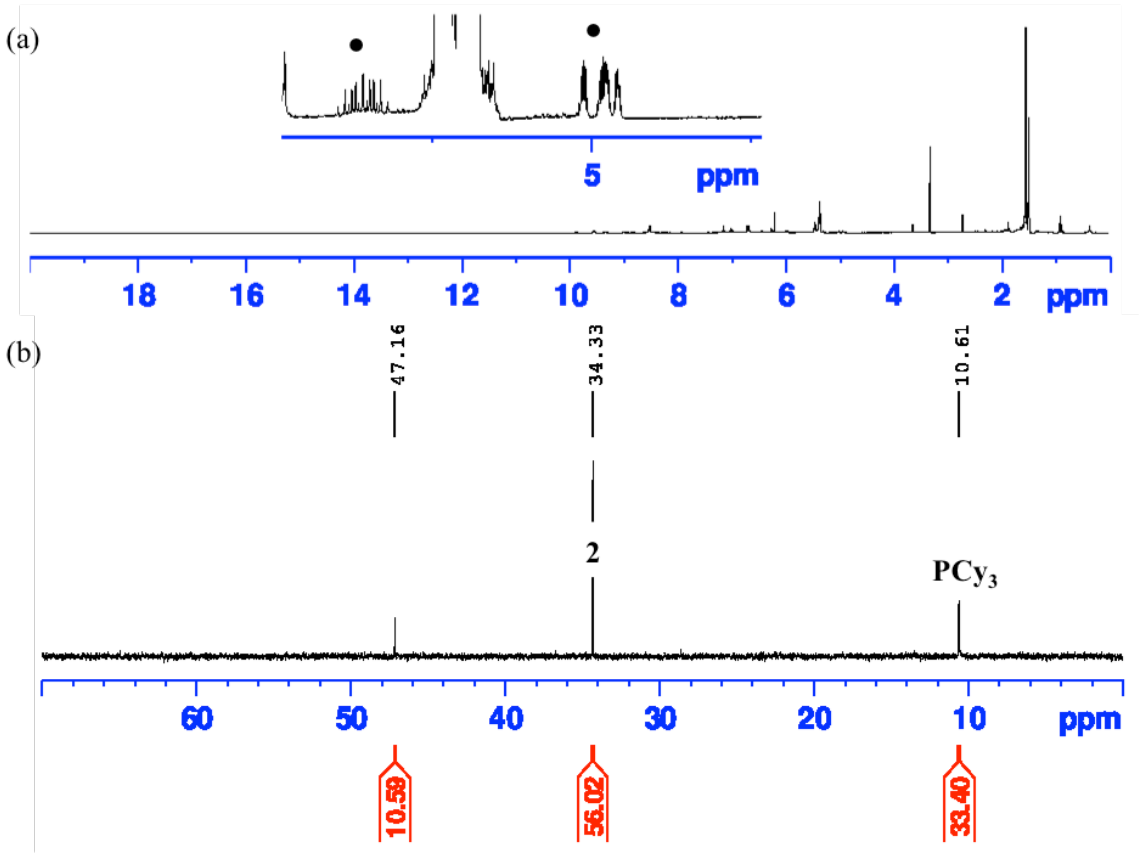

Figure A1.15. NMR spectra for reaction shown in Figure A1.14, after 48 h in the presence of pyridine and 2-butene (see Scheme 3.4 in Chapter 3). (a) ^{1}H NMR spectrum (300 MHz, C_6D_6) showing complete loss of [Ru]=CHR species. Chemical shifts for 1-butene are labelled (•). (b) $^{31}P\{^{1}H\}$ NMR spectrum (121 MHz, C_6D_6) showing a single peak in the phosphonium salt region (ca. 34.3 ppm). Assignment as [$MePCy_3$]Cl **2** confirmed by MALDI-TOF MS. The signal at 47.2 ppm is unassigned.

Appendix 2. Supplementary data for Chapter 4

A2.1 NMR spectra for labelled compounds and experiments

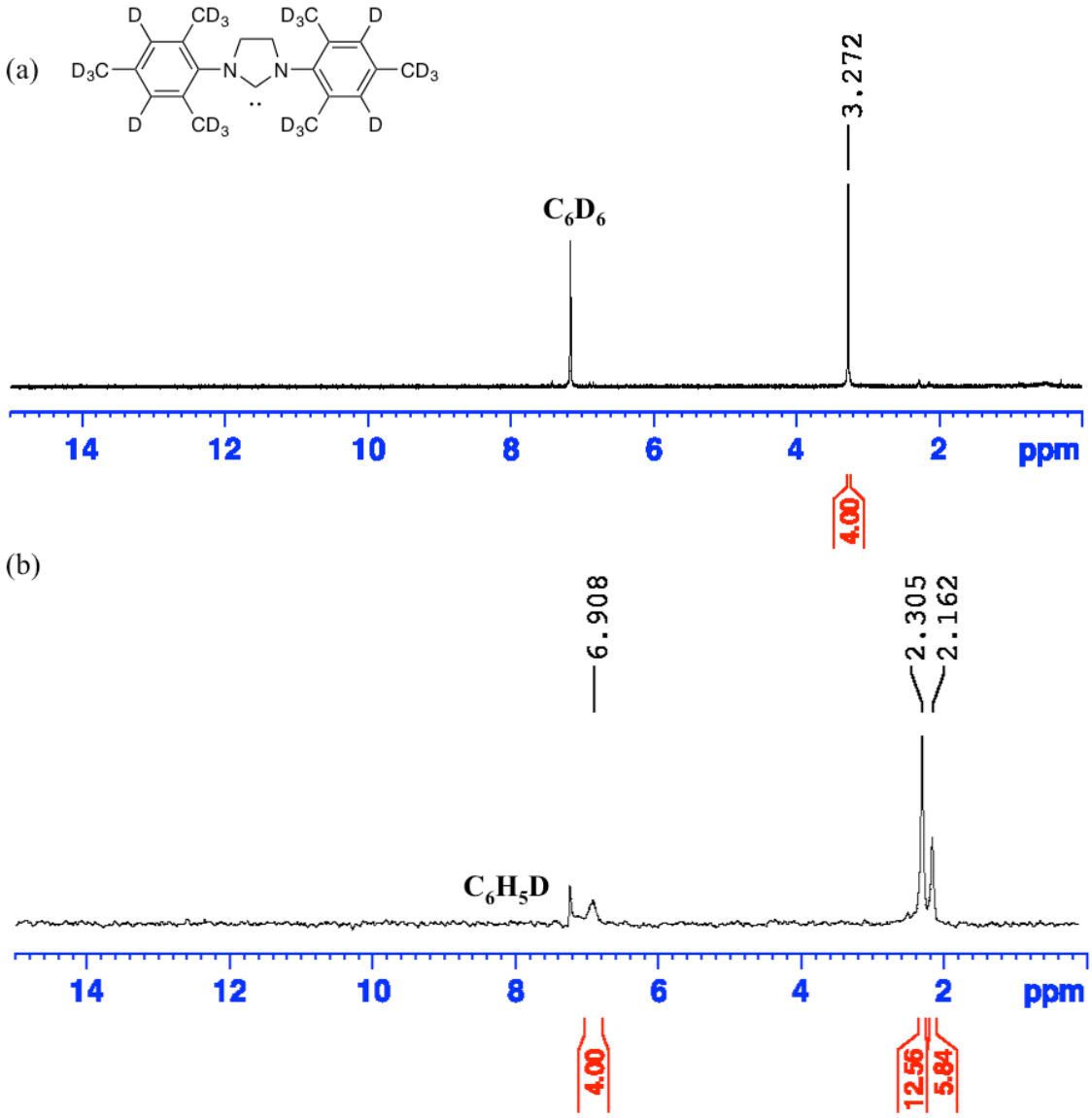

Figure A2.1. NMR spectra for d_{22}-H_2IMes. (a) ^{1}H NMR spectrum (300 MHz, C_6D_6). (b) ^{2}H NMR spectrum (46 MHz, C_6H_6).

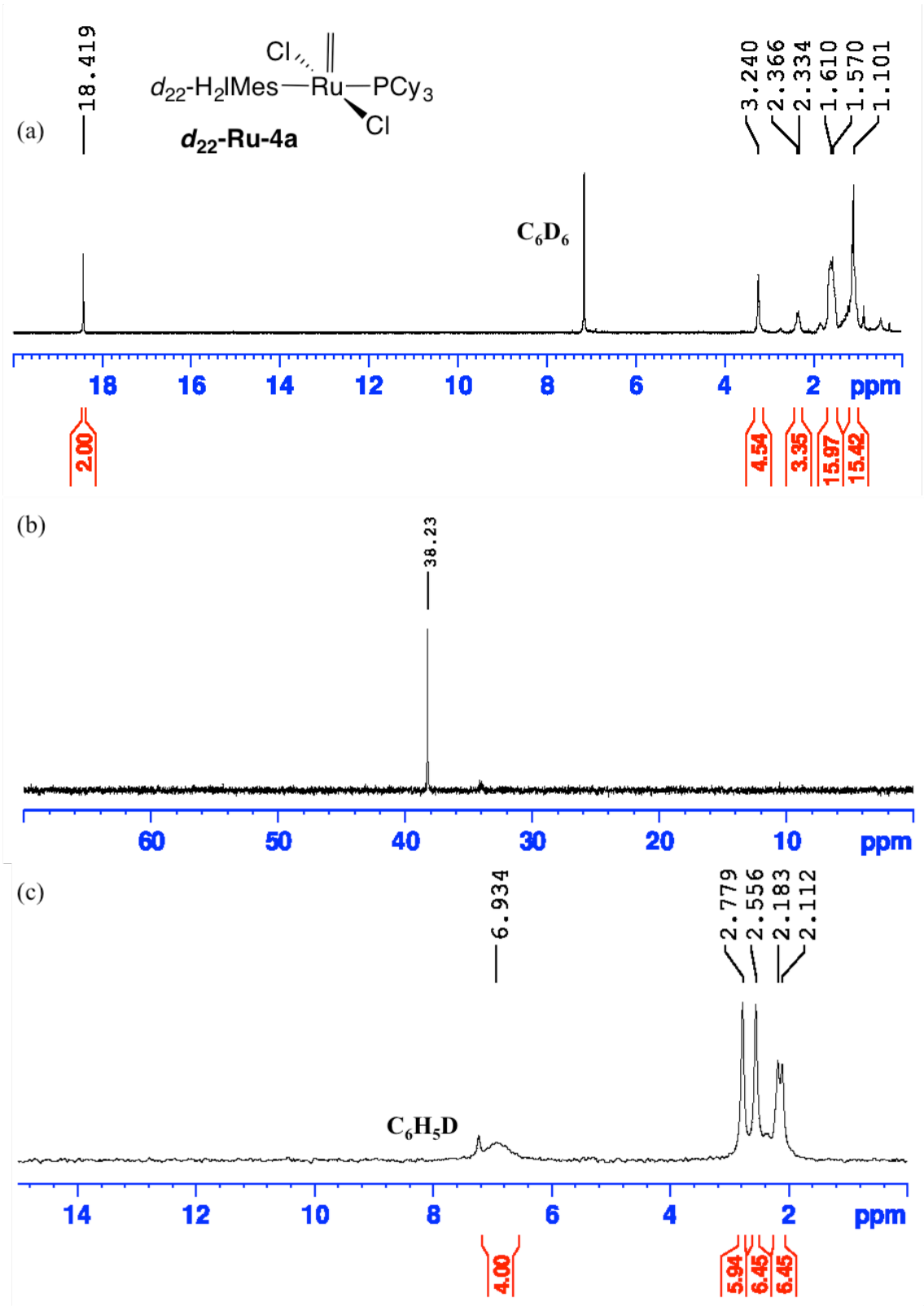
(a)
18.419
Cl
d_{22}-H_2IMes—Ru—PCy$_3$
Cl
d_{22}-Ru-4a
3.240
2.366
2.334
1.610
1.570
1.101
C_6D_6
18
16
14
12
10
8
6
4
2
ppm
2.00
4.54
3.35
15.97
15.42
(b)
38.23
60
50
40
30
20
10
ppm
(c)
6.934
2.779
2.556
2.183
2.112
C_6H_5D
14
12
10
8
6
4
2
ppm
4.00
5.94
6.45
6.45

Figure A2.2. NMR spectra for ***d*$_{22}$-Ru-4a**. (a) ^{1}H NMR spectrum (300 MHz, C_6D_6). (b) ^{31}P{^{1}H} NMR spectrum (121 MHz, C_6D_6). (c) ^{2}H NMR spectrum (46 MHz, C_6H_6).

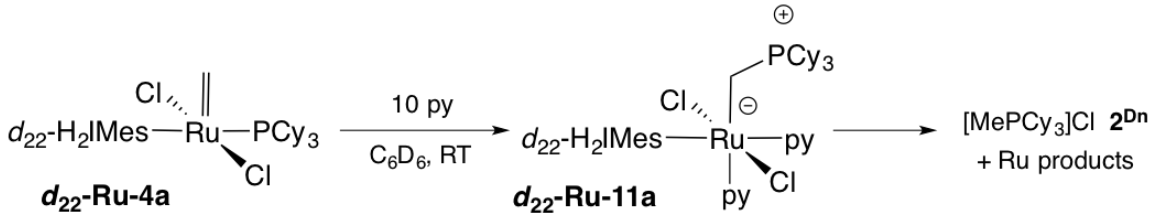

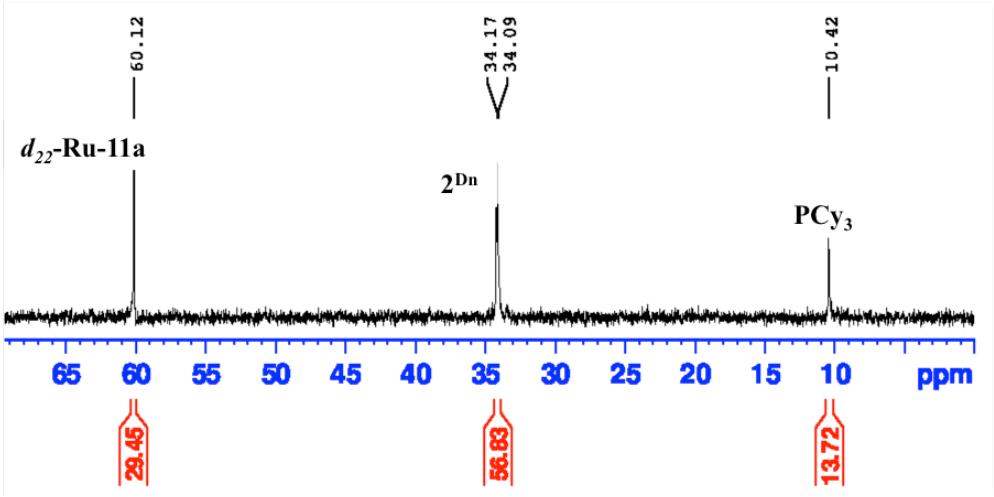

Figure A2.3. ^{31}P{^{1}H} NMR spectrum (121 MHz, C_6D_6) obtained on treating ***d*$_{22}$-Ru-4a** with 10 equiv pyridine, showing signal for transient ***d*$_{22}$-Ru-11a** (t = 5 min). The signal for the phosphonium salt at ca. 34.2 ppm shows H–D scrambling.

Appendix 3. Published contributions

1. "Donor-Induced Decomposition of the Grubbs Catalysts: An Intercepted Intermediate." J. A. M. Lummiss, **W. L. McClennan**, R. McDonald, D. E. Fogg*, *Organometallics*, **2014**, 33, 6738-6741
2. "A General Decomposition Pathway for Phosphine-Stabilized Metathesis Catalysts: Lewis Donors Accelerate Methylidene Abstraction." **W. L. McClennan**, S. A. Rufh, J. A. M. Lummiss, D. E. Fogg.* *J. Am. Chem. Soc.*, **2016**, 138, 14668-14677

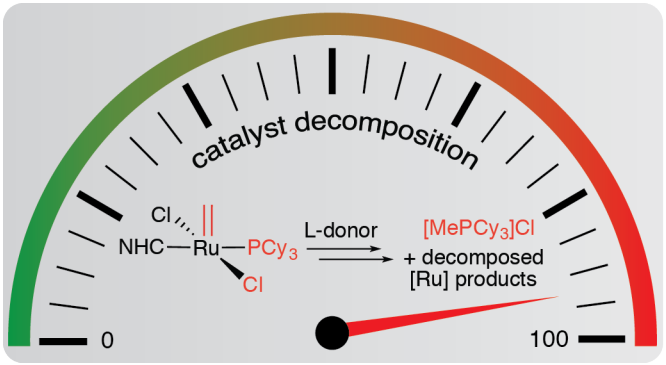

Abstract: Sterically accessible Lewis donors are shown to accelerate decomposition for a broad range of Grubbs-class metathesis catalysts, including benzylidene derivatives $RuCl_2(NHC)(PCy_3)(=CHPh)$ (**Ru-2**: NHC = H_2IMes, **a**; IMes, **b**; H_2IPr, **c**; IPr, **d**; H_2ITol, **e**) and indenylidene complexes $RuCl_2(NHC)(PCy_3)(=C_{15}H_{10})$ (NHC = H_2IMes, **Ru-2f**; IMes, **Ru-2g**). All of these precatalysts form methylidene complex $RuCl_2(NHC)(=CH_2)$ **Ru-3** as the active species in metathesis of terminal olefins, and generate $RuCl_2(NHC)(PCy_3)(=CH_2)$ **Ru-4** as the catalyst resting state. On treatment with a tenfold excess of pyridine, **Ru-4a** and **Ru-4b** decomposed within minutes in solution at RT, eliminating $[MePCy_3]Cl$ **A** by net loss of three ligands (PCy_3, methylidene, and one chloride), and a mesityl proton. In comparison, loss of **A** from **Ru-4a** in the absence of a donor requires up to 3 days at 55 °C. The σ-alkyl intermediate $RuCl_2(^{13}CH_2PCy_3)(NHC)(py)_2$ resulting from nucleophilic attack of free PCy_3 on the methylidene ligand was undetectable for the H_2IMes system, but was spectroscopically observable for the IMes system. The relevance of this pathway to decomposition of catalysts **Ru-2a–g** was demonstrated by assessing the impact of pyridine on the in situ-generated methylidene species. Slow initiation (as observed for the indenylidene catalysts) did not protect against methylidene abstraction. Importantly, studies with **Ru-4a** and **Ru-4b** indicated that weaker donors (L = THF, MeCN, DMSO, MeOH, and even H_2O) likewise promote this pathway, at rates that increase with donor concentration, and severely degrade catalyst productivity in RCM, even for a readily-cyclized substrate. In all cases, **A** was the sole or major ^{31}P-containing product. For DMSO, a first-order dependence of decomposition rates on DMSO concentration was established. This behaviour sends a warning about the use of phosphine-stabilized metathesis catalysts in donor solvents, or with substrates bearing readily accessible donor sites. Addition of pyridine to $RuCl_2(H_2IMes)(PCy_3)(=CHMe)$ did not result in ethylidene abstraction, indicating that this decomposition pathway can be inhibited by use of substrates in which the olefin bears a β-methyl group.